



Splitting schemes and unfitted mesh methods for the coupling of an incompressible fluid with a thin-walled structure

Miguel Angel Fernández, Mikel Landajuela

► To cite this version:

Miguel Angel Fernández, Mikel Landajuela. Splitting schemes and unfitted mesh methods for the coupling of an incompressible fluid with a thin-walled structure. IMA Journal of Numerical Analysis, 2020, 40 (2), pp.1407-1453. 10.1093/imanum/dry098 . hal-01309462v2

HAL Id: hal-01309462

<https://inria.hal.science/hal-01309462v2>

Submitted on 3 May 2016 (v2), last revised 3 May 2020 (v3)

HAL is a multi-disciplinary open access archive for the deposit and dissemination of scientific research documents, whether they are published or not. The documents may come from teaching and research institutions in France or abroad, or from public or private research centers.

L'archive ouverte pluridisciplinaire **HAL**, est destinée au dépôt et à la diffusion de documents scientifiques de niveau recherche, publiés ou non, émanant des établissements d'enseignement et de recherche français ou étrangers, des laboratoires publics ou privés.



Unfitted mesh formulations and splitting schemes for incompressible fluid/thin-walled structure interaction

Miguel A. Fernández, Mikel Landajuela

**RESEARCH
REPORT**

N° 8908

April 2016

Project-Team REO



Unfitted mesh formulations and splitting schemes for incompressible fluid/thin-walled structure interaction

Miguel A. Fernández^{*†}, Mikel Landajuela^{*†}

Project-Team REO

Research Report n° 8908 — April 2016 — 45 pages

Abstract: This paper presents two new numerical methods for incompressible fluid/thin-walled structure interaction problems using unfitted meshes. The spatial discretization is based on different variants of Nitsche's method with cut elements. The degree of fluid-solid splitting (semi-implicit or explicit) is given by the order in which the space and time discretizations are performed. For the semi-implicit schemes, energy-based stability and a priori error estimates are derived and which guarantee the unconditional stability and optimal accuracy in the energy-norm of one the methods. Stability and a priori error estimates are also derived for one of the explicit schemes. Numerical experiments in a benchmark illustrate the performance of the different methods proposed.

Key-words: fluid–structure interaction, incompressible fluid, thin-walled solid, unfitted meshes, fictitious domain method, Nitsche method, splitting schemes

^{*} Inria, 75012 Paris, France

[†] Sorbonne Universités, UPMC Université Paris 6, Laboratoire Jacques-Louis Lions, 75005 Paris, France

**RESEARCH CENTRE
PARIS – ROCQUENCOURT**

Domaine de Voluceau, - Rocquencourt
B.P. 105 - 78153 Le Chesnay Cedex

Méthodes de maillages non compatibles et schémas de couplage pour l'interaction d'un fluide incompressible avec une structure mince

Résumé : Cet article présente deux nouvelles méthodes numériques avec des maillages non compatibles pour la simulation de l'interaction d'un fluide incompressible avec une structure mince. La discrétisation spatiale est basée sur des variantes de la méthode de Nitsche avec des éléments coupés. Le caractère semi-implicite ou explicite du couplage en temps est donnée par l'ordre dans lequel les discrétisations spatiale et temporelle sont effectuées. Pour les schémas semi-implicites, nous établissons des estimations d'énergie et d'erreur a priori qui garantissent la stabilité inconditionnelle et la précision optimale d'une des méthodes. Des estimations d'énergie et d'erreur a priori sont également établies pour l'un des schémas explicites. Le comportement des différentes méthodes proposées est illustré par des expériences numériques.

Mots-clés : interaction fluide–structure, fluide incompressible, structure mince, maillages non compatibles, méthode de domaines fictifs, méthode de Nitsche, schéma de couplage.

1 Introduction

The numerical simulation of multi-physic systems involving the interaction of an incompressible fluid with a deformable thin-walled solid is of great importance in many engineering fields: from aeroelasticity to bio-mechanics (see, e.g., [44, 53, 22, 48, 50, 36]). A major difficulty that has to be faced when solving this kind of coupled problems is the *stiffness* of the *kinematic-dynamic* interface coupling, which is known to lead to severe numerical issues (see, e.g., [42, 16, 31, 54]). For instance, the stability of naive fluid-solid splitting schemes is driven by the amount of *added-mass* in the system, rather than by the discretization parameters. A natural way of bypassing these difficulties is to consider *strong coupling* (i.e., a fully implicit treatment of the interface coupling). This guarantees stability and accuracy, but at the price of solving a computationally demanding heterogeneous system at each time-step.

Over the last decade, significant advances have been achieved on the development and the analysis of splitting schemes that avoid *strong coupling* without compromising stability and accuracy. In most of these studies, the discretization in space is based on fitted fluid and solid meshes (see, e.g., [27, 51, 4, 12, 33, 11, 45, 26, 30, 5, 25, 29, 40]). Such a fitted mesh framework is very appealing in practice because it enables a simple and accurate prescription of the interface conditions. However, it rapidly becomes cumbersome or unfeasible in the presence of large interface deflections and of topological changes (e.g., due to contacting or fracturing solids). The alternative in this case is to consider an unfitted mesh formulation, in which the fluid-structure interface is independent of the background fluid mesh (see, e.g., [49, 43, 55, 32, 52, 18, 2, 7, 13, 39, 8]).

Within the unfitted mesh framework, splitting schemes which avoid strong coupling are rare in the literature. In fact, we are only aware of the schemes reported and analyzed in [7], using the finite element immersed boundary method, and in [13], for an unfitted Nitsche method with cut elements. The fundamental drawback of these two approaches is that either stability or accuracy demands severe time-step restrictions (e.g., parabolic-CFL) and/or correction iterations.

In this paper, we introduce and analyze two new classes of numerical methods which simultaneously overcome strong coupling and the above mentioned stability/accuracy issues. To this purpose, a representative linearized model problem (static interface) is considered. The methods proposed generalize, for the first time, the Robin-Neumann splitting paradigm introduced in [26, 30] to the case of unfitted meshes. For the spatial discretization we consider the robust Nitsche's method reported in [13] and a new variant which builds on arguments from [15, 38]. A salient difference with respect to the fitted mesh framework is that the semi-implicit or explicit nature of the splitting is driven by the order in which the spatial and time discretizations are performed. In [26, 30], both approaches commute and lead to the same explicit scheme.

Robust *a priori* energy and error estimates are derived for all the semi-implicit schemes and for the simplest explicit scheme (without extrapolation). The analysis shows, in particular, that the semi-implicit scheme with first-order extrapolation delivers unconditional stability and optimal (first-order) accuracy in the energy-norm. Previous studies devoted to the numerical analysis of linear incompressible fluid-structure interaction problems can be found in [41, 20, 3, 26, 30, 13, 24, 9]. To the best of our knowledge, this is the first time that the convergence analysis addresses the case of unfitted meshes without strong coupling.

The theoretical findings and the performance of the methods proposed are illustrated through numerical experiments in a well-known benchmark. Some preliminary results of the present work have been announced, without proof, in [28].

The rest of the paper is organized as follows. In Section 2 we present the linear continuous setting. Section 3 is devoted to the case in which the space discretization is performed in the first place. The resulting semi-implicit schemes are introduced in Section 3.2, and their stability and

convergence analysis is reported in Section 3.3. The alternative approach which consists in first performing the discretization in time is addressed in Section 4. The resulting explicit schemes are presented in Section 4.2. The simplest variant is analyzed in Section 4.3. The numerical experiments are reported and discussed in Section 5. Finally, a summary of the conclusions is given in Section 6.

2 Linear model problem

Let Ω be a polyhedral bounded domain in \mathbb{R}^d ($d = 2, 3$) with boundary partitioned as $\partial\Omega = \Gamma \cup \Sigma$. The outward unit normal to $\partial\Omega$ is denoted by \mathbf{n} . We consider a fluid-structure interaction problem in which the fluid is described by the Stokes equations in Ω and the structure by a linear thin membrane or shell with mid-surface given by Σ . The coupled linear problem reads: find the fluid velocity $\mathbf{u} : \Omega \times \mathbb{R}^+ \rightarrow \mathbb{R}^d$, the fluid pressure $p : \Omega \times \mathbb{R}^+ \rightarrow \mathbb{R}$, the solid displacement $\mathbf{d} : \Sigma \times \mathbb{R}^+ \rightarrow \mathbb{R}^d$ and the solid velocity $\dot{\mathbf{d}} : \Sigma \times \mathbb{R}^+ \rightarrow \mathbb{R}^d$ such that

$$\begin{cases} \rho^f \partial_t \mathbf{u} - \operatorname{div} \boldsymbol{\sigma}(\mathbf{u}, p) = \mathbf{0} & \text{in } \Omega \times \mathbb{R}^+, \\ \operatorname{div} \mathbf{u} = 0 & \text{in } \Omega \times \mathbb{R}^+, \\ \mathbf{u} = \mathbf{0} & \text{on } \Gamma \times \mathbb{R}^+, \end{cases} \quad (1)$$

$$\begin{cases} \mathbf{u} = \dot{\mathbf{d}} & \text{on } \Sigma \times \mathbb{R}^+, \\ \rho^s \epsilon \partial_t \dot{\mathbf{d}} + \mathbf{L} \mathbf{d} = -\boldsymbol{\sigma}(\mathbf{u}, p) \mathbf{n} & \text{in } \Sigma \times \mathbb{R}^+, \\ \dot{\mathbf{d}} = \partial_t \mathbf{d} & \text{in } \Sigma \times \mathbb{R}^+, \\ \mathbf{d} = \mathbf{0} & \text{on } \partial\Sigma \times \mathbb{R}^+, \end{cases} \quad (2)$$

complemented with the initial conditions $\mathbf{u}(0) = \mathbf{u}_0$, $\mathbf{d}(0) = \mathbf{d}_0$ and $\dot{\mathbf{d}}(0) = \dot{\mathbf{d}}_0$. Here, ρ^f and ρ^s denote the fluid and solid densities and ϵ the solid thickness. The strain rate and Cauchy-stress tensors are defined by

$$\boldsymbol{\varepsilon}(\mathbf{u}) \stackrel{\text{def}}{=} \frac{1}{2} (\nabla \mathbf{u} + \nabla \mathbf{u}^T), \quad \boldsymbol{\sigma}(\mathbf{u}, p) \stackrel{\text{def}}{=} -p \mathbf{I} + 2\mu \boldsymbol{\varepsilon}(\mathbf{u}),$$

where μ denotes the fluid dynamic viscosity and \mathbf{I} is the identity matrix in $\mathbb{R}^{d \times d}$. The abstract differential surface operator \mathbf{L} describes the solid elastic effects. Equations (2)_{1,2} enforce the so-called kinematic and dynamic coupling conditions. Note that, due to the thin-walled nature of the structure, the latter also represents the momentum equilibrium in the solid.

In the following, we consider the usual Sobolev spaces $H^m(\omega)$ ($m \geq 0$), with norm $\|\cdot\|_{m,\omega}$ and semi-norm $|\cdot|_{m,\omega}$. The closed subspace consisting of functions in $H^1(\omega)$ with zero trace on $\gamma \subset \partial\omega$ is denoted by $H_\gamma^1(\omega)$. The L^2 -scalar product on ω is denoted by $(\cdot, \cdot)_\omega$ and its associated norm by $\|\cdot\|_{0,\omega}$.

We consider $\mathbf{V} = [H_\Gamma^1(\Omega)]^d$ and $Q = L^2(\Omega)$ as the fluid velocity and pressure functional spaces, respectively. The standard Stokes bi-linear forms are given by

$$a(\mathbf{u}, \mathbf{v}) \stackrel{\text{def}}{=} 2\mu (\boldsymbol{\varepsilon}(\mathbf{u}), \boldsymbol{\varepsilon}(\mathbf{v}))_\Omega, \quad b(q, \mathbf{v}) \stackrel{\text{def}}{=} -(q, \operatorname{div} \mathbf{v})_\Omega, \quad a^f((\mathbf{u}, p), (\mathbf{v}, q)) \stackrel{\text{def}}{=} a(\mathbf{u}, \mathbf{v}) + b(p, \mathbf{v}) - b(q, \mathbf{u}).$$

We assume that the unbounded linear operator surface operator $\mathbf{L} : \mathbf{D} \subset [L^2(\Sigma)]^d \rightarrow [L^2(\Sigma)]^d$ is densely defined and self-adjoint. Associated to this operator, we define the elastic bilinear form

$$a^s(\mathbf{d}, \mathbf{w}) \stackrel{\text{def}}{=} (\mathbf{L} \mathbf{d}, \mathbf{w})_\Sigma$$

for all $\mathbf{d} \in \mathbf{D}$ and $\mathbf{w} \in \mathbf{W}$, where $\mathbf{W} \subset [H_{\partial\Sigma}^1(\Sigma)]^d$ is the space of admissible displacements. We further assume that a^s and $\|\cdot\|_s \stackrel{\text{def}}{=} a^s(\cdot, \cdot)^{\frac{1}{2}}$ are, respectively, an inner-product and a norm into \mathbf{W} . The following continuity estimate is also assumed,

$$\|\mathbf{w}\|_s^2 \leq \beta^s \|\mathbf{w}\|_{1,\Sigma}^2 \quad (3)$$

for all $\mathbf{w} \in \mathbf{W}$, with $\beta^s > 0$.

Theoretical results on the well-posedness of (1)–(2) can be found in [41] (see also [19]). Sections 3–4 below are devoted to the numerical approximation of (1)–(2), using unfitted meshes in space and splitting schemes in time.

3 First discretize in space and then in time: semi-implicit schemes

The first class of methods is derived by applying the time splitting of [26, 30] to the unfitted mesh spatial approximation of (1)–(2) introduced in [13]. In this section, we present the method and address its stability and convergence analysis. In particular, optimal first-order accuracy is shown for some of the variants considered.

3.1 Unfitted mesh spatial semi-discretization

Standard finite element approximations of (1)–(2) are often constructed with fitted fluid and solid meshes (see Figure 1(a)). In this work, we assume that they are not necessarily fitted (see Figure 1(b)). To this purpose, we consider two families of quasi-uniform fluid and solid triangulations $\{\mathcal{T}_h^f\}_{0 < h \leq 1}$ and $\{\mathcal{T}_h^s\}_{0 < h \leq 1}$, respectively, such that:

- $\Sigma = \bigcup_{K \in \mathcal{T}_h^s} K$ for every \mathcal{T}_h^s ;
- $\bar{\Omega} \subsetneq \bigcup_{K \in \mathcal{T}_h^f} K$ for every \mathcal{T}_h^f , but for every simplex $K \in \mathcal{T}_h^f$ it holds $K \cap \Omega \neq \emptyset$;
- Every \mathcal{T}_h^f is fitted to Γ but, in general, not to Σ .

The subscript $h \in (0, 1]$ in the above triangulations refers to the level of refinement, which is defined, for a generic fluid or solid triangulation \mathcal{T}_h , by $h \stackrel{\text{def}}{=} \max_{K \in \mathcal{T}_h} h_K$, with h_K the diameter of a simplex $K \in \mathcal{T}_h$.

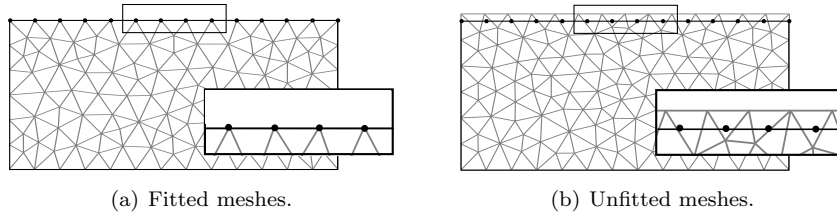


Figure 1: Examples of fluid and solid meshes.

We denote by Ω_h the domain covered by \mathcal{T}_h^f (i.e., the fluid computational domain), by \mathcal{G}_h the set of elements in \mathcal{T}_h^f that are intersected by Σ and by $\mathcal{F}_{\mathcal{G}_h}$ the set of edges or faces of elements in \mathcal{G}_h that do not belong to $\partial\Omega_h$, that is,

$$\Omega_h \stackrel{\text{def}}{=} \text{int}(\cup_{K \in \mathcal{T}_h^f} K), \quad \mathcal{G}_h \stackrel{\text{def}}{=} \{K \in \mathcal{T}_h^f / K \cap \Sigma \neq \emptyset\}, \quad \mathcal{F}_{\mathcal{G}_h} \stackrel{\text{def}}{=} \{F \in \partial K / K \in \mathcal{G}_h, F \cap \partial\Omega_h \neq F\}.$$

The standard spaces of continuous piecewise affine functions associated to \mathcal{T}_h^s and \mathcal{T}_h^f are given, respectively, by

$$X_h^f \stackrel{\text{def}}{=} \{v_h \in C^0(\overline{\Omega_h}) / v_h|_K \in \mathbb{P}_1(K) \quad \forall K \in \mathcal{T}_h^f\}, \quad X_h^s \stackrel{\text{def}}{=} \{w_h \in C^0(\Sigma) / w_h|_K \in \mathbb{P}_1(K) \quad \forall K \in \mathcal{T}_h^s\}. \quad (4)$$

For the approximation of the fluid and solid unknowns, we consider the following spaces

$$\mathbf{V}_h \stackrel{\text{def}}{=} \{\mathbf{v}_h \in [X_h^f]^d / \mathbf{v}_h|_\Gamma = \mathbf{0}\}, \quad Q_h \stackrel{\text{def}}{=} X_h^f, \quad \mathbf{W}_h \stackrel{\text{def}}{=} \{\mathbf{w}_h \in [X_h^s]^d / \mathbf{w}_h|_{\partial\Sigma} = \mathbf{0}\}.$$

In a standard conforming discretization of problem (1)–(2) based on fitted meshes (see Figure 1(a)), the kinematic condition (2)₁ is strongly enforced. In the unfitted mesh setting described above, the strong imposition of (2)₁ is no longer possible. In this section, we adopt the unfitted mesh method proposed in [13], where the interface fluid-solid coupling is treated in a consistent fashion via Nitsche's method. Thus, problem (1)–(2) is approximated in space as follows: for $t > 0$, find $(\mathbf{u}_h(t), p_h(t), \dot{\mathbf{d}}_h(t), \mathbf{d}_h(t)) \in \mathbf{V}_h \times Q_h \times \mathbf{W}_h \times \mathbf{W}_h$, such that $\dot{\mathbf{d}}_h = \partial_t \mathbf{d}_h$ and

$$\begin{cases} \rho^f(\partial_t \mathbf{u}_h, \mathbf{v}_h)_\Omega + a_h^f((\mathbf{u}_h, p_h), (\mathbf{v}_h, q_h)) + \rho^s \epsilon(\partial_t \dot{\mathbf{d}}_h, \mathbf{w}_h)_\Sigma + a^s(\mathbf{d}_h, \mathbf{w}_h) \\ - (\boldsymbol{\sigma}(\mathbf{u}_h, p_h) \mathbf{n}, \mathbf{v}_h - \mathbf{w}_h)_\Sigma - (\mathbf{u}_h - \dot{\mathbf{d}}_h, \boldsymbol{\sigma}(\mathbf{v}_h, -q_h) \mathbf{n})_\Sigma + \frac{\gamma\mu}{h}(\mathbf{u}_h - \dot{\mathbf{d}}_h, \mathbf{v}_h - \mathbf{w}_h)_\Sigma = 0 \end{cases} \quad (5)$$

for all $(\mathbf{v}_h, q_h, \mathbf{w}_h) \in \mathbf{V}_h \times Q_h \times \mathbf{W}_h$. Here, $\gamma > 0$ denotes the Nitsche's penalty parameter and the discrete bilinear form a_h^f is given by

$$a_h^f((\mathbf{u}_h, p_h), (\mathbf{v}_h, q_h)) \stackrel{\text{def}}{=} a^f((\mathbf{u}_h, p_h), (\mathbf{v}_h, q_h)) + S_h((\mathbf{u}_h, p_h), (\mathbf{v}_h, q_h)),$$

where the definition of the stabilization operator S_h is detailed in Section 3.1.1 below. The unfitted space semi-discrete formulation (5) is stable and delivers optimal first-order accuracy in the energy-norm (see [13]).

Remark 3.1. *Note that the fluid's bulk terms in (5) are integrated only over the physical domain Ω . This guarantees consistency but, from the implementation standpoint, it requires non-standard quadrature techniques for the evaluation of the integrals over the cut elements (see, e.g., [46, 1]).*

3.1.1 The stabilization operator S_h

Two sources of stabilization are included in the operator S_h , which is defined as

$$S_h((\mathbf{u}_h, p_h), (\mathbf{v}_h, q_h)) \stackrel{\text{def}}{=} s_h(p_h, q_h) + g_h(\mathbf{u}_h, \mathbf{v}_h). \quad (6)$$

The term $s_h : Q_h \times Q_h \rightarrow \mathbb{R}$ in (6) represents a pressure stabilization operator. It is introduced to cure the instabilities related to the inf-sup incompatible choice of the velocity and pressure discrete spaces. We assume that the following lower and upper bounds hold

$$C_1 \mu^{-1} h^2 |q_h|_{1, \Omega_h}^2 \leq s_h(q_h, q_h) \leq C_2 \mu^{-1} h^2 |q_h|_{1, \Omega_h}^2 \quad (7)$$

with $C_1, C_2 > 0$, for all $q_h \in Q_h$. Note that in (7) the H^1 -seminorm is taken over the whole computation domain Ω_h . As an example of such an operator, we may consider the classical Brezzi-Pitkäranta stabilisation (see [10]):

$$s_h(p_h, q_h) \stackrel{\text{def}}{=} \frac{\gamma_p h^2}{\mu} (\nabla p_h, \nabla q_h)_{\Omega_h}, \quad (8)$$

with $\gamma_p > 0$.

The term $g_h : \mathbf{V}_h \times \mathbf{V}_h \rightarrow \mathbb{R}$ in (6) represents the so-called ghost-penalty stabilization (see [14]). This operator is assumed to bring additional control over the velocity ghost values so that the following strengthened stability holds

$$\tilde{c}_g (\mu \|\boldsymbol{\varepsilon}(\mathbf{v}_h)\|_{0,\Omega_h}^2 + g_h(\mathbf{v}_h, \mathbf{v}_h)) \leq \mu \|\boldsymbol{\varepsilon}(\mathbf{v}_h)\|_{0,\Omega}^2 + g_h(\mathbf{v}_h, \mathbf{v}_h), \quad (9)$$

with $\tilde{c}_g > 0$, for all $\mathbf{v}_h \in \mathbf{V}_h$. It guarantees the robustness of the methods irrespectively of the way Σ intersects the fluid mesh (see Section 3.3 below). As an example of such an operator, we have (see [14]):

$$g_h(\mathbf{u}_h, \mathbf{v}_h) \stackrel{\text{def}}{=} \gamma_g \mu h \sum_{F \in \mathcal{F}_{\mathcal{G}_h}} (\llbracket \nabla \mathbf{u}_h \rrbracket_F, \llbracket \nabla \mathbf{v}_h \rrbracket_F)_F, \quad (10)$$

where the symbol $\llbracket \cdot \rrbracket_F$ denotes the jump of a given quantity across the edge or face F .

Finally, associated to the overall stabilization operator S_h we define the semi-norm

$$|(u_h, p_h)|_S \stackrel{\text{def}}{=} S_h((\mathbf{u}_h, p_h), (\mathbf{v}_h, q_h))^{\frac{1}{2}}.$$

Remark 3.2. *The assumption that all the elements of the computational domain Ω_h intersect the physical domain Ω can be relaxed in practice (see Section 5). It suffices, for instance, to extend the ghost-penalty operator (10) to all the internal edges or faces of \mathcal{T}_h^f , i.e.,*

$$g_h(\mathbf{u}_h, \mathbf{v}_h) \stackrel{\text{def}}{=} \gamma_g \mu h \sum_{F \in \mathcal{F}_h} (\llbracket \nabla \mathbf{u}_h \rrbracket_F, \llbracket \nabla \mathbf{v}_h \rrbracket_F)_F, \quad (11)$$

with $\mathcal{F}_h \stackrel{\text{def}}{=} \{F \in \partial K / K \in \mathcal{T}_h^f, \quad F \cap \partial\Omega_h \neq F\}$. This guarantees the invertibility of the stiffness matrix associated to the discrete bilinear form $a_h^f(\cdot, \cdot)$. Moreover, since the relation (9) holds true with $\tilde{\Omega}_h \stackrel{\text{def}}{=} \text{int}(\cup_{K \in \mathcal{T}_h^f, K \cap \Omega \neq \emptyset} K)$ instead of Ω_h , the stability and convergence results of Sections 3.3 and 4.3 below remain valid.

3.2 Fully discrete formulation: semi-implicit coupling scheme with unfitted meshes

In the following, $\tau > 0$ denotes the time-step length, $t_n \stackrel{\text{def}}{=} n\tau$ for $n \in \mathbb{N}$, and $\partial_\tau x^n \stackrel{\text{def}}{=} \frac{1}{\tau}(x^n - x^{n-1})$ stands for the first-order backward difference. The superscript n, \star denotes the r -th order explicit extrapolations to x^n , namely,

$$x^{n,\star} \stackrel{\text{def}}{=} \begin{cases} 0 & \text{if } r = 0, \\ x^{n-1} & \text{if } r = 1, \\ 2x^{n-1} - x^{n-2} & \text{if } r = 2. \end{cases} \quad (12)$$

As mentioned above, a natural approach to guarantee stability in the simulation of the stiff problem (1)–(2) is to resort to a fully implicit time discretization. For problem (5), this approach leads to Algorithm 1. As a matter of fact, this method is unconditionally stable and delivers optimal first-order accuracy in the energy norm (see Remark 3.6 and Corollary 3.2 below). This is however achieved at the price of solving system (13) at each time-step, which can be computationally demanding. Besides, general thin-walled solid models are known to yield ill-conditioned stiffness matrices, requiring specific solvers.

In a fitted mesh framework (see Figure 1(a)), an alternative to avoid implicit coupling without compromising stability an optimal accuracy is given by the Robin-Neumann coupling schemes

Algorithm 1 Implicit coupling scheme.

For $n \geq 1$, find $(\mathbf{u}_h^n, p_h^n, \dot{\mathbf{d}}_h^n, \mathbf{d}_h^n) \in \mathbf{V}_h \times Q_h \times \mathbf{W}_h \times \mathbf{W}_h$, such that $\dot{\mathbf{d}}_h = \partial_\tau \mathbf{d}_h^n$ and

$$\begin{cases} \rho^f (\partial_\tau \mathbf{u}_h^n, \mathbf{v}_h)_\Omega + a_h^f((\mathbf{u}_h^n, p_h^n), (\mathbf{v}_h, q_h)) + \rho^s \epsilon (\partial_\tau \dot{\mathbf{d}}_h^n, \mathbf{w}_h)_\Sigma + a^s(\mathbf{d}_h^n, \mathbf{w}_h) \\ - (\boldsymbol{\sigma}(\mathbf{u}_h^n, p_h^n) \mathbf{n}, \mathbf{v}_h - \mathbf{w}_h)_\Sigma - (\mathbf{u}_h^n - \dot{\mathbf{d}}_h^n, \boldsymbol{\sigma}(\mathbf{v}_h, -q_h) \mathbf{n})_\Sigma + \frac{\gamma \mu}{h} (\mathbf{u}_h^n - \dot{\mathbf{d}}_h^n, \mathbf{v}_h - \mathbf{w}_h)_\Sigma = 0 \end{cases} \quad (13)$$

for all $(\mathbf{v}_h, q_h, \mathbf{w}_h) \in \mathbf{V}_h \times Q_h \times \mathbf{W}_h$.

introduced in [26, 30]. These schemes are based on a specific fractional-step time-marching of the solid subproblem. Applied to (5), this approach leads to the following incremental displacement-correction scheme, for $n > 0$ if $r = 0, 1$ or for $n > 1$ if $r = 2$:

1. Fluid with solid inertia substep: find $(\mathbf{u}_h^n, p_h^n, \dot{\mathbf{d}}_h^{n-\frac{1}{2}}) \in \mathbf{V}_h \times Q_h \times \mathbf{W}_h$ such that

$$\begin{cases} \rho^f (\partial_\tau \mathbf{u}_h^n, \mathbf{v}_h)_\Omega + a_h^f((\mathbf{u}_h^n, p_h^n), (\mathbf{v}_h, q_h)) + \frac{\rho^s \epsilon}{\tau} (\dot{\mathbf{d}}_h^{n-\frac{1}{2}} - \dot{\mathbf{d}}_h^{n-1}, \mathbf{w}_h)_\Sigma + a^s(\mathbf{d}_h^{n,*}, \mathbf{w}_h) \\ - (\boldsymbol{\sigma}(\mathbf{u}_h^n, p_h^n) \mathbf{n}, \mathbf{v}_h - \mathbf{w}_h)_\Sigma - (\mathbf{u}_h^n - \dot{\mathbf{d}}_h^{n-\frac{1}{2}}, \boldsymbol{\sigma}(\mathbf{v}_h, -q_h) \mathbf{n})_\Sigma + \frac{\gamma \mu}{h} (\mathbf{u}_h^n - \dot{\mathbf{d}}_h^{n-\frac{1}{2}}, \mathbf{v}_h - \mathbf{w}_h)_\Sigma = 0 \end{cases} \quad (14)$$

for all $(\mathbf{v}_h, q_h, \mathbf{w}_h) \in \mathbf{V}_h \times Q_h \times \mathbf{W}_h$.

2. Solid substep: find $(\dot{\mathbf{d}}_h^n, \mathbf{d}_h^n) \in \mathbf{W}_h \times \mathbf{W}_h$ such that $\dot{\mathbf{d}}_h^n = \partial_\tau \mathbf{d}_h^n$ and

$$\frac{\rho^s \epsilon}{\tau} (\dot{\mathbf{d}}_h^n - \dot{\mathbf{d}}_h^{n-\frac{1}{2}}, \mathbf{w}_h)_\Sigma + a^s(\mathbf{d}_h^n - \mathbf{d}_h^{n,*}, \mathbf{w}_h) = 0 \quad (15)$$

for all $\mathbf{w}_h \in \mathbf{W}_h$.

Steps (14)-(15) give a partially segregated solution of problem (5). Note that in (14), the intermediate solid velocity $\dot{\mathbf{d}}_h^{n-\frac{1}{2}}$ is implicitly coupled to the fluid through the solid inertial term. The remaining solid elastic contributions are treated explicitly (or ignored) in (14) via extrapolation. This level of fluid-solid coupling is enough to guarantee (added-mass free) stability (see Section 3.3.1 below), while enabling a significant degree of fluid-solid splitting (i.e., with respect to the strong coupling of Algorithm 1). The end-of-step solid velocity $\dot{\mathbf{d}}_h^n$ is retrieved by solving the solid correction step (15).

Remark 3.3. *It should be noted that the intermediate solid-velocity $\dot{\mathbf{d}}_h^{n-\frac{1}{2}}$ cannot be eliminated in (14) and, hence, the coupling scheme is not explicit. This is a major difference with respect to the case of fitted meshes and conformal discretizations considered in [26, 30]. In that case, we can take $\dot{\mathbf{d}}_h^{n-\frac{1}{2}} = \mathbf{u}_h^n|_\Sigma$ and $\mathbf{w}_h = \mathbf{v}_h|_\Sigma$ in (14), which yields a standard fluid problem with an explicit Robin condition on the interface Σ .*

In practice, it is convenient to reformulate the solid correction step (15) as a traction problem, by eliminating the quantities $\dot{\mathbf{d}}_h^{n-\frac{1}{2}}$ and $\mathbf{d}_h^{n,*}$ in (15). To this purpose, we observe that testing (14) with $\mathbf{v}_h = \mathbf{0}$ and $q_h = 0$ yields

$$\frac{\rho^s \epsilon}{\tau} (\dot{\mathbf{d}}_h^{n-\frac{1}{2}} - \dot{\mathbf{d}}_h^{n-1}, \mathbf{w}_h)_\Sigma + a^s(\mathbf{d}_h^{n,*}, \mathbf{w}_h) = -(\boldsymbol{\sigma}(\mathbf{u}_h^n, p_h^n) \mathbf{n}, \mathbf{w}_h)_\Sigma + \frac{\gamma \mu}{h} (\mathbf{u}_h^n - \dot{\mathbf{d}}_h^{n-\frac{1}{2}}, \mathbf{w}_h)_\Sigma$$

for all $\mathbf{w}_h \in \mathbf{W}_h$. Hence, by adding this expression to (15) we get the standard solid problem

$$\rho^s \epsilon(\partial_\tau \dot{\mathbf{d}}_h^n, \mathbf{w}_h)_\Sigma + a^s(\mathbf{d}_h^n, \mathbf{w}_h) = -(\boldsymbol{\sigma}(\mathbf{u}_h^n, p_h^n) \mathbf{n}, \mathbf{w}_h)_\Sigma + \frac{\gamma\mu}{h}(\mathbf{u}_h^n - \dot{\mathbf{d}}_h^{n-\frac{1}{2}}, \mathbf{w}_h)_\Sigma$$

for all $\mathbf{w}_h \in \mathbf{W}_h$. On the other hand, for $n > r$, it follows that

$$a^s(\mathbf{d}_h^{n,*}, \mathbf{w}_h) = -\rho^s \epsilon(\partial_\tau \dot{\mathbf{d}}_h^{n,*}, \mathbf{w}_h)_\Sigma - (\boldsymbol{\sigma}(\mathbf{u}_h^{n,*}, p_h^{n,*}) \mathbf{n}, \mathbf{w}_h)_\Sigma + \frac{\gamma\mu}{h}(\mathbf{u}_h^{n,*} - \dot{\mathbf{d}}_h^{n-\frac{1}{2},*}, \mathbf{w}_h)_\Sigma$$

for all $\mathbf{w}_h \in \mathbf{W}_h$. This relation gives an (intrinsic) expression of the elastic extrapolations in (14), exclusively in terms of interface fluid quantities and solid velocities. Owing to these observations, the numerical method (14)–(15) is reformulated as given in Algorithm 2.

Algorithm 2 Semi-implicit coupling schemes.

For $n > r$:

1. Fluid with solid inertia substep: find $(\mathbf{u}_h^n, p_h^n, \dot{\mathbf{d}}_h^{n-\frac{1}{2}}) \in \mathbf{V}_h \times Q_h \times \mathbf{W}_h$ such that

$$\begin{cases} \rho^f(\partial_\tau \mathbf{u}_h^n, \mathbf{v}_h)_\Omega + a_h^f((\mathbf{u}_h^n, p_h^n), (\mathbf{v}_h, q_h)) + \frac{\rho^s \epsilon}{\tau}(\dot{\mathbf{d}}_h^{n-\frac{1}{2}}, \mathbf{w}_h)_\Sigma \\ - (\boldsymbol{\sigma}(\mathbf{u}_h^n, p_h^n) \mathbf{n}, \mathbf{v}_h - \mathbf{w}_h)_\Sigma - (\mathbf{u}_h^n - \dot{\mathbf{d}}_h^{n-\frac{1}{2}}, \boldsymbol{\sigma}(\mathbf{v}_h, -q_h) \mathbf{n})_\Sigma + \frac{\gamma\mu}{h}(\mathbf{u}_h^n - \dot{\mathbf{d}}_h^{n-\frac{1}{2}}, \mathbf{v}_h - \mathbf{w}_h)_\Sigma \\ = \frac{\rho^s \epsilon}{\tau}(\dot{\mathbf{d}}_h^{n-1} + \tau \partial_\tau \dot{\mathbf{d}}_h^{n,*}, \mathbf{w}_h)_\Sigma + (\boldsymbol{\sigma}(\mathbf{u}_h^{n,*}, p_h^{n,*}) \mathbf{n}, \mathbf{w}_h)_\Sigma - \frac{\gamma\mu}{h}(\mathbf{u}_h^{n,*} - \dot{\mathbf{d}}_h^{n-\frac{1}{2},*}, \mathbf{w}_h)_\Sigma \end{cases} \quad (16)$$

for all $(\mathbf{v}_h, q_h, \mathbf{w}_h) \in \mathbf{V}_h \times Q_h \times \mathbf{W}_h$.

2. Solid substep: find $(\dot{\mathbf{d}}_h^n, \mathbf{d}_h^n) \in \mathbf{W}_h \times \mathbf{W}_h$ such that $\dot{\mathbf{d}}_h^n = \partial_\tau \mathbf{d}_h^n$ and

$$\frac{\rho^s \epsilon}{\tau}(\partial_\tau \dot{\mathbf{d}}_h^n, \mathbf{w}_h)_\Sigma + a^s(\mathbf{d}_h^n, \mathbf{w}_h) = -(\boldsymbol{\sigma}(\mathbf{u}_h^n, p_h^n) \mathbf{n}, \mathbf{w}_h)_\Sigma + \frac{\gamma\mu}{h}(\mathbf{u}_h^n - \dot{\mathbf{d}}_h^{n-\frac{1}{2}}, \mathbf{w}_h)_\Sigma$$

for all $\mathbf{w}_h \in \mathbf{W}_h$.

Remark 3.4. *It should be noted that for $r = 1, 2$ additional data is needed to start the time-marching in Algorithm 2. In practice, this data can be obtained by performing one step of the scheme with $r = 0$, this yields $(\mathbf{u}_h^1, p_h^1, \dot{\mathbf{d}}_h^1)$, and then one step of the scheme with $r = 1$, which gives $(\mathbf{u}_h^2, p_h^2, \dot{\mathbf{d}}_h^2)$.*

The semi-implicit coupling scheme provided by Algorithm 2 has a reduced computational complexity with respect to Algorithm 1. Indeed, the solid contribution to (16) reduces to a simple interface mass-matrix, which does not degrade the conditioning of the system matrix. This reduction in the coupling complexity is particularly important when considering general shell models (see, e.g., [17]), whose elastic contributions incorporate additional unknowns (e.g., rotations).

In the following sections, we show that Algorithm 2 preserves the stability and accuracy properties of the explicit coupling schemes introduced in [26, 30] with fitted meshes. In particular, it overcomes the severe stability restrictions observed in [7] for the traditional time-marching schemes of the immersed boundary method. It is worth noting that these stability conditions have been recently overcome in [8] by resorting to a full implicit treatment of the kinematic-dynamic coupling (in the spirit of Algorithm 1), which yields a solution procedure much more

computationally demanding than Algorithm 2. On the other hand, Algorithm 2 with $r = 1$ delivers optimal first-order accuracy. This is also significant progress with respect to the stabilized explicit scheme of [13], whose accuracy is non-uniform in h .

Remark 3.5. *Algorithm 2 has been extended in [1] to address the case in which the solid is immersed within the fluid. In this framework, fluid (weak and strong) discontinuities across the interface are captured using a XFEM local enrichment. The following analysis can be straightforwardly adapted to this further involved situation.*

3.2.1 Kinematic perturbation of implicit coupling.

We conclude this section by pointing out a fundamental property of Algorithm 2. To this purpose, we will make use of the discrete reconstruction $\mathbf{L}_h : \mathbf{W} \rightarrow \mathbf{W}_h$ of the elastic solid operator, defined by the relation

$$(\mathbf{L}_h \mathbf{w}, \mathbf{w}_h)_\Sigma = a^s(\mathbf{w}, \mathbf{w}_h) \quad (17)$$

for all $(\mathbf{w}, \mathbf{w}_h) \in \mathbf{W} \times \mathbf{W}_h$. Owing to (17) and (15), we get that

$$\dot{\mathbf{d}}_h^{n-\frac{1}{2}} = \dot{\mathbf{d}}_h^n + \frac{\tau}{\rho^s \epsilon} \mathbf{L}_h(\mathbf{d}_h^n - \mathbf{d}_h^{n,*}) \quad (18)$$

for $n > r$. On the other hand, adding (14) and (15) yields

$$\begin{cases} \rho^f (\partial_\tau \mathbf{u}_h^n, \mathbf{v}_h)_\Omega + a_h^f((\mathbf{u}_h^n, p_h^n), (\mathbf{v}_h, q_h)) + \rho^s \epsilon (\partial_\tau \dot{\mathbf{d}}_h^n, \mathbf{w}_h)_\Sigma + a^s(\mathbf{d}_h^n, \mathbf{w}_h) \\ - (\boldsymbol{\sigma}(\mathbf{u}_h^n, p_h^n) \mathbf{n}, \mathbf{v}_h - \mathbf{w}_h)_\Sigma - (\mathbf{u}_h^n - \dot{\mathbf{d}}_h^{n-\frac{1}{2}}, \boldsymbol{\sigma}(\mathbf{v}_h, -q_h) \mathbf{n})_\Sigma + \frac{\gamma \mu}{h} (\mathbf{u}_h^n - \dot{\mathbf{d}}_h^{n-\frac{1}{2}}, \mathbf{v}_h - \mathbf{w}_h)_\Sigma = 0 \end{cases} \quad (19)$$

for all $(\mathbf{v}_h, q_h, \mathbf{w}_h) \in \mathbf{V}_h \times Q_h \times \mathbf{W}_h$ and $n > r$. Thus, Algorithm 2 can be regarded as a kinematic perturbation of the fully implicit time discretization given by Algorithm 1. As a matter of fact, Algorithm 1 formally enforces (through Nitsche's method) the interface condition $\mathbf{u}_h^n \simeq \dot{\mathbf{d}}_h^n$, whereas (18)-(19) imposes

$$\mathbf{u}_h^n \simeq \dot{\mathbf{d}}_h^n + \frac{\tau}{\rho^s \epsilon} \mathbf{L}_h(\mathbf{d}_h^n - \mathbf{d}_h^{n,*}).$$

Note that the size of the perturbation depends on the extrapolation order r . The basic idea in the forthcoming analysis is to investigate how the kinematic perturbation (18) affects the stability and convergence of the underlying implicit coupling scheme (Algorithm 1).

3.3 Stability and convergence analysis

We consider the following mesh-dependent semi-norms for functions f defined on the interface Σ ,

$$\|f\|_{\frac{1}{2}, h, \Sigma}^2 = \sum_{K \in \mathcal{G}_h} h_K^{-1} \|f\|_{0, \Sigma_K}^2, \quad \|f\|_{-\frac{1}{2}, h, \Sigma}^2 = \sum_{K \in \mathcal{G}_h} h_K \|f\|_{0, \Sigma_K}^2,$$

where Σ_K denotes the part of the interface intersecting the simplex K , i.e., $\Sigma_K \stackrel{\text{def}}{=} \Sigma \cap K$. The following estimates involving the solid elastic operator will be used,

$$\|\mathbf{L}_h \mathbf{d}\|_{0,\Sigma} \leq \|\mathbf{L} \mathbf{d}\|_{0,\Sigma}, \quad (20)$$

$$\|\mathbf{w}_h\|_s^2 \leq \frac{\beta^s C_I^2}{h^2} \|\mathbf{w}_h\|_{0,\Sigma}^2, \quad (21)$$

$$\|\mathbf{L}_h \mathbf{w}_h\|_s \leq \frac{\beta^s C_I^2}{h^2} \|\mathbf{w}_h\|_s, \quad (22)$$

$$\|\mathbf{L}_h \mathbf{w}_h\|_{0,\Sigma} \leq \frac{(\beta^s)^{\frac{1}{2}} C_I}{h} \|\mathbf{w}_h\|_s \quad (23)$$

for all $\mathbf{d} \in \mathbf{D}$ and $\mathbf{w}_h \in \mathbf{W}_h$ and with $C_I > 0$ the constant of a discrete inverse inequality. Estimates (20)–(23) follow readily from application of the Cauchy-Schwarz inequality, the definition (17) and the continuity estimate (3) (see [26, Appendix A] for the details). We will also make use of the discrete Gronwall lemma (see, e.g., [37]), which we collect here without a proof.

Lemma 3.1. *Let τ , B and a_m , b_m , c_m , η_m (for integers $m \geq 1$) be nonnegative numbers such that*

$$a_n + \tau \sum_{m=1}^n b_m \leq \tau \sum_{m=1}^n \eta_m a_m + \tau \sum_{m=1}^n c_m + B$$

for $n \geq 1$. Suppose that $\tau \eta_m < 1$ for all $m \geq 1$. Then, there holds

$$a_n + \tau \sum_{m=1}^n b_m \leq \exp \left(\tau \sum_{m=1}^n \frac{\eta_m}{1 - \tau \eta_m} \right) \left(\tau \sum_{m=1}^n c_m + B \right)$$

for $n \geq 1$.

For the purpose of the analysis, we will assume that Σ is well resolved by \mathcal{T}_h^f (see, e.g., [14]), so that the following trace inequality holds for functions in $H^1(K)$, for all $K \in \mathcal{T}_h^f$: there exists a constant $C_T > 0$, depending only on Σ , such that

$$\|v\|_{0,\Sigma \cap K} \leq C_T (h_K^{-\frac{1}{2}} \|v\|_{0,K} + h_K^{\frac{1}{2}} \|\nabla v\|_{0,K}) \quad (24)$$

for all $v \in H^1(K)$. The proof for this result follows from [34, Lemma 3]. In particular, using (24) with a discrete inverse inequality, it follows

$$h \|\boldsymbol{\varepsilon}(\mathbf{v}_h) \mathbf{n}\|_{0,\Sigma}^2 \leq C_{TI} \|\boldsymbol{\varepsilon}(\mathbf{v}_h)\|_{0,\Omega_h}^2 \quad (25)$$

for all $\mathbf{v}_h \in \mathbf{V}_h$. Note that (25) holds irrespectively of the interface position because the norm on the right-hand side is taken over the whole computational domain Ω_h . However, this control on the interfacial viscous flux can not be bounded by the natural viscous dissipation of the fluid, which is only available in the physical domain $\Omega \subset \Omega_h$. The strengthened stability (9) provided by the ghost-penalty operator, allows to extend to Ω_h the coercivity of the spatial discrete Stokes-Nitsche operator. This is stated in the following lemma from [13], whose proof is presented here for completeness.

Lemma 3.2. *For $\gamma > 0$ sufficiently large, there exists a constant $c_g > 0$ such that*

$$\begin{aligned} c_g \left(\mu \|\nabla \mathbf{v}_h\|_{0,\Omega_h}^2 + \gamma \mu \|\mathbf{v}_h - \mathbf{w}_h\|_{\frac{1}{2},h,\Sigma}^2 + |(\mathbf{v}_h, q_h)|_S^2 \right) \leq \\ a_h^f((\mathbf{v}_h, q_h), (\mathbf{v}_h, q_h)) - (\boldsymbol{\sigma}(\mathbf{v}_h, q_h) \mathbf{n}, \mathbf{v}_h - \mathbf{w}_h)_\Sigma \\ - (\mathbf{v}_h - \mathbf{w}_h, \boldsymbol{\sigma}(\mathbf{v}_h, -q_h) \mathbf{n})_\Sigma + \frac{\gamma \mu}{h} (\mathbf{v}_h - \mathbf{w}_h, \mathbf{v}_h - \mathbf{w}_h)_\Sigma \end{aligned}$$

for all $(\mathbf{v}_h, q_h) \in \mathbf{V}_h \times Q_h$ and $\mathbf{w}_h \in \mathbf{W}_h$.

Proof. First, we have

$$\begin{aligned} a_h^f((\mathbf{v}_h, q_h), (\mathbf{v}_h, q_h)) - (\boldsymbol{\sigma}(\mathbf{v}_h, q_h) \mathbf{n}, \mathbf{v}_h - \mathbf{w}_h)_\Sigma \\ - (\mathbf{v}_h - \mathbf{w}_h, \boldsymbol{\sigma}(\mathbf{v}_h, -q_h) \mathbf{n})_\Sigma + \frac{\gamma\mu}{h} (\mathbf{v}_h - \mathbf{w}_h, \mathbf{v}_h - \mathbf{w}_h)_\Sigma + |(\mathbf{v}_h, q_h)|_S^2 \\ = 2\mu \|\boldsymbol{\varepsilon}(\mathbf{v}_h)\|_{0,\Omega}^2 - 2(\boldsymbol{\sigma}(\mathbf{v}_h, 0) \mathbf{n}, \mathbf{v}_h - \mathbf{w}_h)_\Sigma + \gamma\mu \|\mathbf{v}_h - \mathbf{w}_h\|_{\frac{1}{2},h,\Sigma}^2 + |(\mathbf{v}_h, q_h)|_S^2. \end{aligned}$$

Combining the Cauchy-Schwarz inequality with (25), we have

$$\begin{aligned} (2\boldsymbol{\sigma}(\mathbf{v}_h, 0) \mathbf{n}, \mathbf{v}_h - \mathbf{w}_h)_\Sigma &\leq 2\left(\frac{h\mu}{\gamma}\right)^{\frac{1}{2}} \|\boldsymbol{\varepsilon}(\mathbf{v}_h) \mathbf{n}\|_{0,\Sigma} \left(\frac{\gamma\mu}{h}\right)^{\frac{1}{2}} \|\mathbf{v}_h - \mathbf{w}_h\|_{0,\Sigma} \\ &\leq \frac{8C_{\text{TI}}}{\gamma} \mu \|\boldsymbol{\varepsilon}(\mathbf{v}_h)\|_{0,\Omega_h}^2 + \frac{1}{2} \gamma\mu \|\mathbf{v}_h - \mathbf{w}_h\|_{\frac{1}{2},h,\Sigma}^2. \end{aligned}$$

We conclude by using (9), taking

$$\gamma > \frac{8C_{\text{TI}}}{\tilde{c}_g} \quad (26)$$

and using Korn's inequality. \square

3.3.1 Stability analysis

At time-step t_n , we define the total discrete energy by

$$E_h^n \stackrel{\text{def}}{=} \rho^f \|\mathbf{u}_h^n\|_{0,\Omega}^2 + \rho^s \epsilon \|\dot{\mathbf{d}}_h^n\|_{0,\Sigma}^2 + \|\mathbf{d}_h^n\|_s^2, \quad (27)$$

and the dissipation as

$$\begin{aligned} D_h^n &\stackrel{\text{def}}{=} \frac{\rho^f}{\tau} \|\mathbf{u}_h^n - \mathbf{u}_h^{n-1}\|_{0,\Omega}^2 + \frac{\rho^s \epsilon}{\tau} \|\dot{\mathbf{d}}_h^n - \dot{\mathbf{d}}_h^{n-1}\|_{0,\Sigma}^2 + \frac{1}{\tau} \|\mathbf{d}_h^n - \mathbf{d}_h^{n-1}\|_s^2 \\ &\quad + c_g \left(\mu \|\nabla \mathbf{u}_h^n\|_{0,\Omega_h}^2 + \gamma\mu \|\mathbf{u}_h^n - \dot{\mathbf{d}}_h^{n-\frac{1}{2}}\|_{\frac{1}{2},h,\Sigma}^2 + |(\mathbf{u}_h^n, p_h^n)|_S^2 \right). \end{aligned}$$

The following result states the energy stability of the semi-implicit schemes reported in Algorithm 2. In the succeeding text, the symbol \lesssim indicates an inequality up to a multiplicative constant (independent of the physical and discretization parameters and of the fluid-interface intersection).

Theorem 3.1. *Let $\{(\mathbf{u}_h^n, p_h^n, \dot{\mathbf{d}}_h^{n-\frac{1}{2}}, \mathbf{d}_h^n, \dot{\mathbf{d}}_h^n)\}_{n>r}$ be the sequence given by Algorithm 2, with the initialization procedure of Remark 3.4 for $r = 1, 2$. Assume that $\gamma > 0$ is given by Lemma 3.2. Then, we have the following a priori energy estimates:*

- For $r = 0, 1$ and $n > r$, there holds

$$E_h^n + \tau \sum_{m=r+1}^n D_h^m \lesssim E_h^0, \quad (28)$$

irrespectively of the discretization parameters.

- For $r = 2$ and $n > 2$, there holds

$$E_h^n + \tau \sum_{m=3}^n D_h^m \lesssim \exp\left(\frac{t_n \zeta}{1 - \tau \zeta}\right) E_h^0, \quad (29)$$

provided the following conditions hold

$$\tau(\omega^s)^{\frac{6}{5}} \leq \zeta h^{\frac{6}{5}}, \quad \tau\zeta < 1, \quad \zeta > 0, \quad (30)$$

with $\omega^s \stackrel{\text{def}}{=} C_I \sqrt{\beta^s / (\rho^s \epsilon)}$.

Proof. The proof follows by combining arguments from [13, 26]. We first test (19) with

$$(\mathbf{v}_h, q_h, \mathbf{w}_h) = \tau(\mathbf{u}_h^n, p_h^n, \dot{\mathbf{d}}_h^{n-\frac{1}{2}})$$

for $n > r$. This yields the following discrete energy equation,

$$\begin{aligned} & \frac{\rho^f}{2} (\tau \partial_\tau \|\mathbf{u}_h^n\|_{0,\Omega}^2 + \|\mathbf{u}_h^n - \mathbf{u}_h^{n-1}\|_{0,\Omega}^2) + 2\mu\tau \|\boldsymbol{\varepsilon}(\mathbf{u}_h^n)\|_{0,\Omega}^2 + \tau |(\mathbf{u}_h^n, p_h^n)|_S^2 \\ & + \rho^s \epsilon \tau (\partial_\tau \dot{\mathbf{d}}_h^n, \dot{\mathbf{d}}_h^{n-\frac{1}{2}})_\Sigma + \tau a^s (\mathbf{d}_h^n, \dot{\mathbf{d}}_h^{n-\frac{1}{2}}) + 2\tau (\boldsymbol{\sigma}(\mathbf{u}_h^n, 0) \mathbf{n}, \mathbf{u}_h^n - \dot{\mathbf{d}}_h^{n-\frac{1}{2}})_\Sigma + \gamma\mu\tau \|\mathbf{u}_h^n - \dot{\mathbf{d}}_h^{n-\frac{1}{2}}\|_{\frac{1}{2},h,\Sigma}^2 = 0 \end{aligned}$$

for $n > r$. Hence, from Lemma 3.2, we have that

$$\begin{aligned} & \frac{\rho^f}{2} (\tau \partial_\tau \|\mathbf{u}_h^n\|_{0,\Omega}^2 + \|\mathbf{u}_h^n - \mathbf{u}_h^{n-1}\|_{0,\Omega}^2) + c_g \tau \left(\mu \|\nabla \mathbf{u}_h^n\|_{0,\Omega_h}^2 + \gamma\mu \|\mathbf{u}_h^n - \dot{\mathbf{d}}_h^{n-\frac{1}{2}}\|_{\frac{1}{2},h,\Sigma}^2 + |(\mathbf{u}_h^n, p_h^n)|_S^2 \right) \\ & + \rho^s \epsilon \tau (\partial_\tau \dot{\mathbf{d}}_h^n, \dot{\mathbf{d}}_h^{n-\frac{1}{2}})_\Sigma + \tau a^s (\mathbf{d}_h^n, \dot{\mathbf{d}}_h^{n-\frac{1}{2}}) \leq 0. \end{aligned}$$

Hence, using the perturbed kinematic relation (18), we get the following fundamental energy inequality

$$\begin{aligned} & \frac{\rho^f}{2} (\tau \partial_\tau \|\mathbf{u}_h^n\|_{0,\Omega}^2 + \|\mathbf{u}_h^n - \mathbf{u}_h^{n-1}\|_{0,\Omega}^2) + c_g \tau \left(\mu \|\nabla \mathbf{u}_h^n\|_{0,\Omega_h}^2 + \gamma\mu \|\mathbf{u}_h^n - \dot{\mathbf{d}}_h^{n-\frac{1}{2}}\|_{\frac{1}{2},h,\Sigma}^2 + |(\mathbf{u}_h^n, p_h^n)|_S^2 \right) \\ & + \frac{\rho^s \epsilon}{2} \left(\tau \partial_\tau \|\dot{\mathbf{d}}_h^n\|_{0,\Sigma}^2 + \|\dot{\mathbf{d}}_h^n - \dot{\mathbf{d}}_h^{n-1}\|_{0,\Sigma}^2 \right) + \frac{1}{2} \left(\tau \partial_\tau \|\mathbf{d}_h^n\|_s^2 + \|\mathbf{d}_h^n - \mathbf{d}_h^{n-1}\|_s^2 \right) \\ & + \underbrace{\tau^2 (\partial_\tau \dot{\mathbf{d}}_h^n, \mathbf{L}_h(\mathbf{d}_h^n - \mathbf{d}_h^{n,*}))_\Sigma}_{T_1} + \underbrace{\frac{\tau^2}{\rho^s \epsilon} (\mathbf{L}_h \mathbf{d}_h^n, \mathbf{L}_h(\mathbf{d}_h^n - \mathbf{d}_h^{n,*}))_\Sigma}_{T_2} \lesssim 0 \quad (31) \end{aligned}$$

for $n > r$. The terms T_1 and T_2 , introduced by (18), can be controlled as in [26, Theorem 1] for each extrapolation order $r = 0, 1, 2$. For the sake of completeness, the different estimates are briefly recalled below.

Algorithm 2 with $r = 0$. In this case, using Young's inequality, we have

$$T_1 + T_2 \geq -\frac{\rho^s \epsilon}{3} \|\dot{\mathbf{d}}_h^n - \dot{\mathbf{d}}_h^{n-1}\|_{0,\Sigma}^2 + \frac{\tau^2}{4\rho^s \epsilon} \|\mathbf{L}_h \mathbf{d}_h^n\|_{0,\Sigma}^2 \quad (32)$$

for $n > 0$. Hence, the estimate (28) follows by inserting this expression into (31) and summing over $m = 1, \dots, n$.

Algorithm 2 with $r = 1$. In this case we have

$$T_1 = \frac{\tau^2}{2} \left(\tau \partial_\tau \|\dot{\mathbf{d}}_h^n\|_s^2 + \|\dot{\mathbf{d}}_h^n - \dot{\mathbf{d}}_h^{n-1}\|_s^2 \right) \quad (33)$$

and

$$T_2 = \frac{\tau^2}{2\rho^s \epsilon} \left(\tau \partial_\tau \|\mathbf{L}_h \mathbf{d}_h^n\|_{0,\Sigma}^2 + \|\mathbf{L}_h(\mathbf{d}_h^n - \mathbf{d}_h^{n-1})\|_{0,\Sigma}^2 \right) \quad (34)$$

for $n > 1$. Hence, by inserting this expression into (31) and summing over $m = 2, \dots, n$ we get the estimate

$$E_h^n + \tau \sum_{m=2}^n D_h^m \lesssim E_h^1 + \frac{\tau^2}{2} \|\dot{\mathbf{d}}_h^1\|_s^2 + \frac{\tau^2}{2\rho^s \epsilon} \|\mathbf{L}_h \mathbf{d}_h^1\|_{0,\Sigma}^2.$$

The last two terms, related to the initialization of the scheme (see Remark 3.4), can be bounded using (28) with $r = 0$, $n = 1$ and the additional control given by (32). This yields the estimate (28) in the case $r = 1$.

Algorithm 2 with $r = 2$. In this case, the term T_1 in (31) reduces simply to

$$T_1 = \tau \left(\dot{\mathbf{d}}_h^n - \dot{\mathbf{d}}_h^{n-1}, \mathbf{L}^e(\mathbf{d}_h^n - 2\mathbf{d}_h^{n-1} + \mathbf{d}_h^{n-2}) \right)_\Sigma = \tau^2 \|\dot{\mathbf{d}}_h^n - \dot{\mathbf{d}}_h^{n-1}\|_s^2. \quad (35)$$

The term T_2 , which reads as

$$T_2 = \frac{\tau^3}{\rho^s \epsilon} \left(\mathbf{L}_h \mathbf{d}_h^n, \mathbf{L}_h(\dot{\mathbf{d}}_h^n - \dot{\mathbf{d}}_h^{n-1}) \right)_\Sigma, \quad (36)$$

is treated as in [26, Page 38] using (21) and (22), which yields

$$T_2 \geq -\tau^6 \frac{(\omega^s)^6}{h^6} \|\mathbf{d}_h^n\|_s^2 - \frac{\rho^s \epsilon}{4} \|\dot{\mathbf{d}}_h^n - \dot{\mathbf{d}}_h^{n-1}\|_{0,\Sigma}^2. \quad (37)$$

We now proceed by inserting (35) and (37) into (31) and summing over $m = 3, \dots, n$. The last term of (37) is controlled by the numerical dissipation provided by (31), while the first is handled via Lemma 3.1 under condition (30). This yields the bound

$$E_h^n + \sum_{m=3}^n D_h^m \lesssim \exp\left(\frac{t_n \zeta}{1 - \tau \zeta}\right) E_h^2.$$

The estimate (29) for $r = 2$ then follows by using the energy estimate (28) with $r = 1$ and $n = 2$, the additional control provided by (33) and (34), and the stability condition (30). \square

Remark 3.6. Note that testing (13) with $(\mathbf{v}_h, q_h, \mathbf{w}_h) = \tau(\mathbf{u}_h^n, p_h^n, \dot{\mathbf{d}}_h^n)$ for $n > 0$, equation (31) holds with $\dot{\mathbf{d}}_h^{n-\frac{1}{2}} = \dot{\mathbf{d}}_h^n$ and $T_1 = T_2 = 0$. Thus, for Algorithm 1, the following energy estimate holds,

$$E_h^n + \tau \sum_{m=1}^n D_h^m \lesssim E_h^0$$

for $n > 0$ and $\gamma > 0$ given by Lemma 3.2, irrespectively of the discretization parameters.

3.3.2 Convergence analysis

In the following, we use the notation $f^n \stackrel{\text{def}}{=} f(t_n)$ for a given time dependent function f . We may then consider $\partial_\tau f^n$ and $f^{n,*}$, involving the quantities f^n , f^{n-1} and f^{n-2} . In the following, a slight abuse of notation will be committed by using $\partial_t f^n$ to denote $(\partial_t f)^n$.

For the the convergence analysis we assume that the interface Σ is flat. We also assume that the elements of \mathcal{T}_h^s can be grouped into disjoint $(d-1)$ -dimensional macropatches P_i , with $\text{meas}(P_i) = \mathcal{O}(h^{d-1})$. Each macropatch is assumed to contain at least one interior node and its union is assumed to cover Σ , i.e., $\cup_i P_i = \Sigma$.

Interpolation operators. Basically, the discrete interpolation operators are those used in [13, Section 3.3] for the error analysis of the space semi-discrete formulation (5). For the solid displacement, we consider the elastic Ritz-projection operator $\pi_h^s : \mathbf{W} \rightarrow \mathbf{W}_h$ defined by the relation

$$a^s(\mathbf{w} - \pi_h^s \mathbf{w}, \mathbf{w}_h) = 0$$

for all $\mathbf{w}_h \in \mathbf{W}_h$, and for which there holds

$$\|\mathbf{w} - \pi_h^s \mathbf{w}\|_{0,\Sigma} + h\|\nabla(\mathbf{w} - \pi_h^s \mathbf{w})\|_{0,\Sigma} \lesssim h^2|\mathbf{w}|_{2,\Sigma} \quad (38)$$

for all $\mathbf{w} \in [H^2(\Sigma)]^d \cap \mathbf{W}$. Note also that owing to definition (17), we have

$$(\mathbf{L}_h \pi_h^s \mathbf{w}, \mathbf{w}_h)_\Sigma = a^s(\pi_h^s \mathbf{w}, \mathbf{w}_h) = a^s(\mathbf{w}, \mathbf{w}_h) = (\mathbf{L}_h \mathbf{w}, \mathbf{w}_h)_\Sigma,$$

and thus

$$\mathbf{L}_h \pi_h^s = \mathbf{L}_h. \quad (39)$$

For the solid velocity, we consider the operator $\mathcal{I}_h : \mathbf{W} \rightarrow \mathbf{W}_h$ defined by the relation

$$\mathcal{I}_h \mathbf{w} \stackrel{\text{def}}{=} \pi_h^s \mathbf{w} + \sum_i \alpha_i \varphi_i,$$

with $\alpha_i \in \mathbb{R}$. The φ_i are functions with support in the macropatches P_i , such that

$$0 \leq \varphi_i \leq 1, \quad \|\varphi_i\|_{0,P_i} \lesssim h^{\frac{d-1}{2}}$$

and take the value 1, component-wise, in the interior nodes of the associated patch P_i . The scalars α_i are chosen so that the following orthogonality condition holds

$$\int_{P_i} (\mathbf{w} - \mathcal{I}_h \mathbf{w}) \cdot \mathbf{n} = 0. \quad (40)$$

We refer to [13, 6] for the detailed construction of such an operator. It can be shown (see [13, Lemma 3.3]) that

$$\|\mathbf{w} - \mathcal{I}_h \mathbf{w}\|_{0,\Sigma} + h\|\nabla(\mathbf{w} - \mathcal{I}_h \mathbf{w})\|_{0,\Sigma} \lesssim h^2|\mathbf{w}|_{2,\Sigma} \quad (41)$$

for all $\mathbf{w} \in [H^2(\Sigma)]^d \cap \mathbf{W}$.

Since the fluid physical solution is defined in Ω and the discrete one in Ω_h , with $\Omega \subset \Omega_h$, we consider two linear continuous lifting operators $E_2 : H^2(\Omega) \rightarrow H^2(\mathbb{R}^d)$ and $E_1 : H^1(\Omega) \rightarrow H^1(\mathbb{R}^d)$, satisfying the bounds $\|E_1 v\|_{H^1(\mathbb{R}^d)} \lesssim \|v\|_{H^1(\Omega)}$ and $\|E_2 v\|_{H^2(\mathbb{R}^d)} \lesssim \|v\|_{H^2(\Omega)}$ (see, e.g., [23]). To interpolate the resulting extended fluid solution we consider the Scott-Zhang operator i_{sz} (see, e.g., [21]). Then it holds (see [13, Lemma 3.3]),

$$\begin{aligned} \|\mathbf{v} - i_{sz} E_2 \mathbf{v}\|_{0,\Omega} + h\|\nabla(\mathbf{v} - i_{sz} E_2 \mathbf{v})\|_{0,\Omega} &\lesssim h^2|\mathbf{v}|_{2,\Omega}, \\ \|q - i_{sz} E_1 q\|_{0,\Omega} + h\|\nabla(q - i_{sz} E_1 q)\|_{0,\Omega} &\lesssim h|q|_{1,\Omega}, \\ \|\sigma(\mathbf{v} - i_{sz} E_2 \mathbf{v}, q - i_{sz} E_1 q) \mathbf{n}\|_{-\frac{1}{2},h,\Sigma} &\lesssim h(\|\mathbf{v}\|_{2,\Omega} + \|q\|_{1,\Omega}) \end{aligned} \quad (42)$$

for all $\mathbf{v} \in [H^2(\Omega)]^d$ and $q \in H^1(\Omega)$.

On the other hand, we assume that the stabilization operator (6) satisfies the following weak consistency relation

$$|(i_{sz} E_2 \mathbf{v}, i_{sz} E_1 q)|_S \lesssim h \left(\mu^{\frac{1}{2}} |\mathbf{v}|_{2,\Omega} + \mu^{-\frac{1}{2}} |q|_{1,\Omega} \right) \quad (43)$$

for all $\mathbf{v} \in [H^2(\Omega)]^d$ and $q \in H^1(\Omega)$. The pressure estimate follows readily from (7), the H^1 -stability of the Scott-Zhang interpolant and the stability of the extension operator (see [13]). For the estimate regarding the ghost-penalty operator (10) we refer to [14].

Finally, owing to (24), (42)₁ and (41), the following result involving both the fluid and solid velocity projections holds

$$\|\mathbf{v} - i_{\text{sz}} E_2 \mathbf{v}\|_{\frac{1}{2}, h, \Sigma} \lesssim h \|\mathbf{v}\|_{2, \Omega}, \quad \|\mathbf{w} - \mathcal{I}_h \mathbf{w}\|_{\frac{1}{2}, h, \Sigma} \lesssim h^{\frac{3}{2}} \|\mathbf{w}\|_{2, \Sigma} \quad (44)$$

for all $\mathbf{v} \in [H^2(\Omega)]^d$ and $\mathbf{w} \in [H^2(\Sigma)]^d \cap \mathbf{W}$ (see [13, Lemma 3.3]).

A priori error estimates. We assume that the exact solution of problem (1)-(2) has the following regularity, for a given final time $T \geq \tau$:

$$\begin{aligned} \mathbf{u} &\in [H^1(0, T; H^2(\Omega))]^d, \quad \mathbf{u}|_{\Sigma} \in [H^1(0, T; H^2(\Sigma))]^d, \\ \partial_{tt} \mathbf{u} &\in [L^2(0, T; L^2(\Omega))]^d, \quad \partial_{tt} \mathbf{u}|_{\Sigma} \in [L^2(0, T; L^2(\Sigma))]^d, \\ p &\in C^0([0, T]; H^1(\Omega)) \end{aligned} \quad (45)$$

and

$$\mathbf{L}^e \mathbf{d} \in \begin{cases} [C^0([0, T]; L^2(\Sigma))]^d & \text{if } r = 0, \\ [H^r(0, T; L^2(\Sigma))]^d & \text{if } r = 1, 2. \end{cases} \quad (46)$$

For the derivation of the error estimate, let us write the approximation errors for the fluid as,

$$\begin{aligned} E_2 \mathbf{u}^n - \mathbf{u}_h^n &= \underbrace{E_2 \mathbf{u}^n - i_{\text{sz}} E_2 \mathbf{u}^n}_{\stackrel{\text{def}}{=} \boldsymbol{\theta}_{\pi}^n} + \underbrace{i_{\text{sz}} E_2 \mathbf{u}^n - \mathbf{u}_h^n}_{\stackrel{\text{def}}{=} \boldsymbol{\theta}_h^n} \quad \text{in } \Omega_h, \\ E_1 p^n - p_h^n &= \underbrace{E_1 p^n - i_{\text{sz}} E_1 p^n}_{\stackrel{\text{def}}{=} y_{\pi}^n} + \underbrace{i_{\text{sz}} E_1 p^n - p_h^n}_{\stackrel{\text{def}}{=} y_h^n} \quad \text{in } \Omega_h. \end{aligned} \quad (47)$$

Similarly, for the solid we have

$$\begin{aligned} \mathbf{d}^n - \mathbf{d}_h^n &= \underbrace{\mathbf{d}^n - \pi_h^s \mathbf{d}^n}_{\stackrel{\text{def}}{=} \boldsymbol{\xi}_{\pi}^n} + \underbrace{\pi_h^s \mathbf{d}^n - \mathbf{d}_h^n}_{\stackrel{\text{def}}{=} \boldsymbol{\xi}_h^n} \quad \text{in } \Sigma, \\ \dot{\mathbf{d}}^n - \dot{\mathbf{d}}_h^n &= \underbrace{\dot{\mathbf{d}}^n - \mathcal{I}_h \dot{\mathbf{d}}^n}_{\stackrel{\text{def}}{=} \dot{\boldsymbol{\xi}}_{\pi}^n} + \underbrace{\mathcal{I}_h \dot{\mathbf{d}}^n - \dot{\mathbf{d}}_h^n}_{\stackrel{\text{def}}{=} \dot{\boldsymbol{\xi}}_h^n} \quad \text{in } \Sigma. \end{aligned} \quad (48)$$

Finally, the error in the intermediate solid velocity is split as

$$\dot{\mathbf{d}}^n - \dot{\mathbf{d}}_h^{n-\frac{1}{2}} = \underbrace{\dot{\mathbf{d}}^n - \mathcal{I}_h \dot{\mathbf{d}}^n}_{\stackrel{\text{def}}{=} \dot{\boldsymbol{\xi}}_{\pi}^n} + \underbrace{\mathcal{I}_h \dot{\mathbf{d}}^n - \dot{\mathbf{d}}_h^{n-\frac{1}{2}}}_{\stackrel{\text{def}}{=} \boldsymbol{\chi}_h^n} \quad \text{in } \Sigma. \quad (49)$$

In the sequel, the following equation, relating $\dot{\boldsymbol{\xi}}_h^n$ and $\partial_{\tau} \boldsymbol{\xi}_h^n$, will be used

$$\dot{\boldsymbol{\xi}}_h^n = \partial_{\tau} \boldsymbol{\xi}_h^n + \underbrace{\mathcal{I}_h \dot{\mathbf{d}}^n - \pi_h^s \partial_{\tau} \mathbf{d}^n}_{\stackrel{\text{def}}{=} \mathbf{z}_h^n}. \quad (50)$$

Similarly, the discrete error counterpart of (18) reads as

$$\chi_h^n = \mathcal{I}_h \dot{\mathbf{d}}^n - \dot{\mathbf{d}}_h^{n-\frac{1}{2}} = \mathcal{I}_h \dot{\mathbf{d}}^n - \dot{\mathbf{d}}_h^n - \frac{\tau}{\rho^s \epsilon} \mathbf{L}_h(\mathbf{d}_h^n - \mathbf{d}_h^*) = \dot{\xi}_h^n + \frac{\tau}{\rho^s \epsilon} \mathbf{L}_h(\xi_h^n - \xi_h^{n,*}) - \frac{\tau}{\rho^s \epsilon} \mathbf{L}_h(\mathbf{d}^n - \mathbf{d}^{n,*}) \quad (51)$$

for $n > r$, where we have used (39).

We first provide an a priori estimate for the discrete errors $(\theta_h^n, y_h^n, \xi_h^n, \dot{\xi}_h^n, \chi_h^n)$. We define the energy-norm of the discrete error at time step t_n , as

$$\begin{aligned} \mathcal{E}_h^n \stackrel{\text{def}}{=} & (\rho^f)^{\frac{1}{2}} \|\theta_h^n\|_{0,\Omega} + (\rho^s \epsilon)^{\frac{1}{2}} \|\xi_h^n\|_{0,\Sigma} + \|\xi_h^n\|_s + \left(\sum_{m=r+1}^n c_g \tau \mu \|\nabla \theta_h^m\|_{0,\Omega}^2 \right)^{\frac{1}{2}} \\ & + \left(\sum_{m=r+1}^n c_g \tau |(\theta_h^m, y_h^m)|_S^2 \right)^{\frac{1}{2}} + \left(\sum_{m=r+1}^n c_g \tau \gamma \mu \|\theta_h^m - \chi_h^m\|_{\frac{1}{2},h,\Sigma}^2 \right)^{\frac{1}{2}} \end{aligned}$$

for $n > r$.

Theorem 3.2. *Let $(\mathbf{u}, p, \mathbf{d}, \dot{\mathbf{d}})$ be the solution of the coupled problem (1)-(2) and $\{(\mathbf{u}_h^n, p_h^n, \dot{\mathbf{d}}_h^{n-\frac{1}{2}}, \mathbf{d}_h^n, \dot{\mathbf{d}}_h^n)\}_{n>r}$ be the approximation given by Algorithm 2 with initial data $(\mathbf{u}_h^0, \mathbf{d}_h^0, \dot{\mathbf{d}}_h^0) = (i_{sz} E_2 \mathbf{u}^0, \pi_h^s \mathbf{d}^0, \mathcal{I}_h \dot{\mathbf{d}}^0)$. The initialization procedure of Remark 3.4 is considered for the schemes with $r = 1, 2$. Suppose that the exact solution has the regularity (45)-(46). Assume that $\gamma > 0$ is given by Lemma 3.2. For the scheme with $r = 2$ we assume, in addition, that the stability condition (30) holds. Then, we have the following error estimates, for $n > r$ and $n\tau < T$:*

$$\mathcal{E}_h^n \lesssim c_1 h + c_2 \tau + c_3 \tau^{2^{r-1}}. \quad (52)$$

Here, the symbols $\{c_i\}_{i=1}^3$ denote positive constants independent of h and τ , but which depend on the physical parameters and on the regularity of $(\mathbf{u}, p, \mathbf{d}, \dot{\mathbf{d}})$.

Proof. The proof combines some of the arguments reported in [13, 26], with the following additional difficulties:

- Only the spatial semi-discrete case is considered in [13];
- The intermediate solid velocity $\dot{\mathbf{d}}_h^{n-\frac{1}{2}}$ cannot be eliminated in terms of \mathbf{u}_h^n , as in [26], which requires the control of an extrapolation dependent term $T_{2,r}$.

The spatial semi-discrete formulation (5) is weakly consistent with the coupled problem (1)-(2). In fact, if we multiply (1)₁ by $\mathbf{v}_h \in \mathbf{V}_h$, (1)₂ by $q_h \in Q_h$ and (2)₁ by $\mathbf{w}_h \in \mathbf{W}_h$, integrate by parts and add the resulting equations, we get

$$\begin{aligned} & \rho^f (\partial_t \mathbf{u}, \mathbf{v}_h)_\Omega + a^f((\mathbf{u}, p), (\mathbf{v}_h, q_h)) + \rho^s \epsilon (\partial_t \dot{\mathbf{d}}, \mathbf{w}_h)_\Sigma + a^s(\mathbf{d}, \mathbf{w}_h) \\ & - (\sigma(\mathbf{u}, p) \mathbf{n}, \mathbf{v}_h - \mathbf{w}_h)_\Sigma - (\mathbf{u} - \dot{\mathbf{d}}, \sigma(\mathbf{v}_h, -q_h) \mathbf{n})_\Sigma + \frac{\gamma \mu}{h} (\mathbf{u} - \dot{\mathbf{d}}, \mathbf{v}_h - \mathbf{w}_h)_\Sigma = 0 \end{aligned} \quad (53)$$

for all $\mathbf{v}_h, q_h, \mathbf{w}_h \in \mathbf{V}_h \times Q_h \times \mathbf{W}_h$. Taking the difference between the continuous problem (53) at time $t = t_n$ and the expression (19), we obtain, after adding and subtracting $\partial_\tau \mathbf{u}^n$ and $\partial_\tau \dot{\mathbf{d}}^n$, the following modified Galerkin orthogonality:

$$\begin{aligned} & \rho^f (\partial_\tau (\mathbf{u}^n - \mathbf{u}_h^n), \mathbf{v}_h)_\Omega + a^f((\mathbf{u}^n - \mathbf{u}_h^n, p^n - p_h^n), (\mathbf{v}_h, q_h)) \\ & + \rho^s \epsilon (\partial_\tau (\dot{\mathbf{d}}^n - \dot{\mathbf{d}}_h^n), \mathbf{w}_h)_\Sigma + a^s(\mathbf{d}^n - \mathbf{d}_h^n, \mathbf{w}_h) - (\sigma(\mathbf{u}^n - \mathbf{u}_h^n, p^n - p_h^n) \mathbf{n}, \mathbf{v}_h - \mathbf{w}_h)_\Sigma \\ & - ((\mathbf{u}^n - \mathbf{u}_h^n) - (\dot{\mathbf{d}}^n - \dot{\mathbf{d}}_h^{n-\frac{1}{2}}), \sigma(\mathbf{v}_h, -q_h) \mathbf{n})_\Sigma + \frac{\gamma \mu}{h} ((\mathbf{u}^n - \mathbf{u}_h^n) - (\dot{\mathbf{d}}^n - \dot{\mathbf{d}}_h^{n-\frac{1}{2}}), \mathbf{v}_h - \mathbf{w}_h)_\Sigma \\ & = -\rho^f ((\partial_t - \partial_\tau) \mathbf{u}^n, \mathbf{v}_h)_\Omega - \rho^s \epsilon ((\partial_t - \partial_\tau) \dot{\mathbf{d}}^n, \mathbf{w}_h)_\Sigma + S_h((\mathbf{u}_h^n, p_h^n), (\mathbf{v}_h, q_h)) \end{aligned} \quad (54)$$

for all $(\mathbf{v}_h, q_h, \mathbf{w}_h) \in \mathbf{V}_h \times Q_h \times \mathbf{W}_h$. Hence, from (47)-(49), we infer the following equation for the discrete errors $\boldsymbol{\theta}_h^n$, y_h^n , $\boldsymbol{\xi}_h^n$, $\dot{\boldsymbol{\xi}}_h^n$ and $\boldsymbol{\chi}_h^n$:

$$\begin{aligned} & \rho^f (\partial_\tau \boldsymbol{\theta}_h^n, \mathbf{v}_h)_\Omega + a^f((\boldsymbol{\theta}_h^n, y_h^n), (\mathbf{v}_h, q_h)) + S_h((\boldsymbol{\theta}_h^n, y_h^n), (\mathbf{v}_h, q_h)) + \rho^s \epsilon (\partial_\tau \dot{\boldsymbol{\xi}}_h^n, \mathbf{w}_h)_\Sigma \\ & + a^s(\boldsymbol{\xi}_h^n, \mathbf{w}_h) - (\boldsymbol{\sigma}(\boldsymbol{\theta}_h^n, y_h^n) \mathbf{n}, \mathbf{v}_h - \mathbf{w}_h)_\Sigma - (\boldsymbol{\theta}_h^n - \boldsymbol{\chi}_h^n, \boldsymbol{\sigma}(\mathbf{v}_h, -q_h) \mathbf{n})_\Sigma \\ & + \frac{\gamma \mu}{h} (\boldsymbol{\theta}_h^n - \boldsymbol{\chi}_h^n, \mathbf{v}_h - \mathbf{w}_h)_\Sigma = -\rho^f ((\partial_t - \partial_\tau) \mathbf{u}^n, \mathbf{v}_h)_\Omega - \rho^f (\partial_\tau \boldsymbol{\theta}_\pi^n, \mathbf{v}_h)_\Omega \\ & - \rho^s \epsilon ((\partial_t - \partial_\tau) \dot{\mathbf{d}}^n, \mathbf{w}_h)_\Sigma - \rho^s \epsilon (\partial_\tau \dot{\boldsymbol{\xi}}_\pi^n, \mathbf{w}_h)_\Sigma - a^s(\boldsymbol{\xi}_\pi^n, \mathbf{w}_h) \\ & + S_h((i_{sz} E_2 \mathbf{u}^n, i_{sz} E_1 p^n), (\mathbf{v}_h, q_h)) - \frac{\gamma \mu}{h} (\boldsymbol{\theta}_\pi^n - \dot{\boldsymbol{\xi}}_\pi^n, \mathbf{v}_h - \mathbf{w}_h)_\Sigma \\ & - a^f((\boldsymbol{\theta}_\pi^n, y_\pi^n), (\mathbf{v}_h, q_h)) + (\boldsymbol{\sigma}(\boldsymbol{\theta}_\pi^n, y_\pi^n) \mathbf{n}, \mathbf{v}_h - \mathbf{w}_h)_\Sigma + (\boldsymbol{\theta}_\pi^n - \dot{\boldsymbol{\xi}}_\pi^n, \boldsymbol{\sigma}(\mathbf{v}_h, -q_h) \mathbf{n})_\Sigma \quad (55) \end{aligned}$$

for all $(\mathbf{v}_h, q_h, \mathbf{w}_h) \in \mathbf{V}_h \times Q_h \times \mathbf{W}_h$ and $n > r$. Note that $a^s(\boldsymbol{\xi}_\pi^n, \mathbf{w}_h) = 0$ due to the definition of the solid projection operator $\boldsymbol{\pi}_h^s$. Taking $(\mathbf{v}_h, q_h, \mathbf{w}_h) = \tau(\boldsymbol{\theta}_h^n, y_h^n, \boldsymbol{\chi}_h^n)$ in (55), using Lemma 3.2, (50) and (51), yields the following energy inequality for the discrete errors:

$$\begin{aligned} & \frac{\rho^f}{2} (\tau \partial_\tau \|\boldsymbol{\theta}_h^n\|_{0,\Omega}^2 + \tau^2 \|\partial_\tau \boldsymbol{\theta}_h^n\|_{0,\Omega}^2) + \frac{\rho^s \epsilon}{2} (\tau \partial_\tau \|\dot{\boldsymbol{\xi}}_h^n\|_{0,\Sigma}^2 + \tau^2 \|\partial_\tau \dot{\boldsymbol{\xi}}_h^n\|_{0,\Sigma}^2) \\ & + c_g \tau (\mu \|\nabla \boldsymbol{\theta}_h^n\|_{0,\Omega_h}^2 + \gamma \mu \|\boldsymbol{\theta}_h^n - \boldsymbol{\chi}_h^n\|_{\frac{1}{2},h,\Sigma}^2 + |(\boldsymbol{\theta}_h^n, y_h^n)|_S^2) \\ & + \frac{1}{2} (\tau \partial_\tau \|\boldsymbol{\xi}_h^n\|_s^2 + \tau^2 \|\partial_\tau \boldsymbol{\xi}_h^n\|_s^2) \lesssim \underbrace{-\rho^f \tau ((\partial_t - \partial_\tau) \mathbf{u}^n, \boldsymbol{\theta}_h^n)_\Omega - \rho^f \tau (\partial_\tau \boldsymbol{\theta}_\pi^n, \boldsymbol{\theta}_h^n)_\Omega}_{T_1} \\ & \underbrace{-\rho^s \epsilon \tau ((\partial_t - \partial_\tau) \dot{\mathbf{d}}^n, \boldsymbol{\chi}_h^n)_\Sigma - \rho^s \epsilon \tau (\partial_\tau \dot{\boldsymbol{\xi}}_\pi^n, \boldsymbol{\chi}_h^n)_\Sigma}_{T_2} \underbrace{-\tau a^s(\boldsymbol{\xi}_h^n, \mathbf{z}_h^n)}_{T_3} \\ & \underbrace{+\tau S_h((i_{sz} E_2 \mathbf{u}^n, i_{sz} E_1 p^n), (\boldsymbol{\theta}_h^n, y_h^n))}_{T_4} \underbrace{-\tau \frac{\gamma \mu}{h} (\boldsymbol{\theta}_\pi^n - \dot{\boldsymbol{\xi}}_\pi^n, \boldsymbol{\theta}_h^n - \boldsymbol{\chi}_h^n)_\Sigma}_{T_5} \quad (56) \\ & \underbrace{+\tau (\boldsymbol{\sigma}(\boldsymbol{\theta}_\pi^n, y_\pi^n) \mathbf{n}, \boldsymbol{\theta}_h^n - \boldsymbol{\chi}_h^n)_\Sigma}_{T_6} \underbrace{-\tau a^f((\boldsymbol{\theta}_\pi^n, y_\pi^n), (\boldsymbol{\theta}_h^n, y_h^n)) + \tau (\boldsymbol{\theta}_\pi^n - \dot{\boldsymbol{\xi}}_\pi^n, \boldsymbol{\sigma}(\boldsymbol{\theta}_h^n, -y_h^n) \mathbf{n})_\Sigma}_{T_7} \\ & \underbrace{-\tau^2 (\partial_\tau \dot{\boldsymbol{\xi}}_h^n, \mathbf{L}_h(\boldsymbol{\xi}_h^n - \boldsymbol{\xi}_h^{n,*}))_\Sigma - \frac{\tau^2}{\rho^s \epsilon} (\mathbf{L}_h \boldsymbol{\xi}_h^n, \mathbf{L}_h(\boldsymbol{\xi}_h^n - \boldsymbol{\xi}_h^{n,*}))_\Sigma}_{T_8} \\ & \underbrace{+\tau^2 (\partial_\tau \dot{\boldsymbol{\xi}}_h^n, \mathbf{L}_h(\mathbf{d}^n - \mathbf{d}^{n,*}))_\Sigma}_{T_9} \underbrace{+\frac{\tau^2}{\rho^s \epsilon} (\mathbf{L}_h \boldsymbol{\xi}_h^n, \mathbf{L}_h(\mathbf{d}^n - \mathbf{d}^{n,*}))_\Sigma}_{T_{10}} \end{aligned}$$

for $n > r$. The terms $T_1 - T_4$ stem from the time-stepping and stabilization methods. The terms $T_5 - T_7$ come from Nitsche's method. Finally, terms $T_8 - T_{10}$ are due to the kinematic perturbation and depend on the extrapolation order. We proceed by treating each term separately.

Term T_1 can be bounded using a Taylor expansion, (42) and the Poincaré inequality with

constant C_P . This yields

$$\begin{aligned}
T_1 &\leq \rho^f \tau (\|\partial_t \mathbf{u}^n - \partial_\tau \mathbf{u}^n\|_{0,\Omega} + \|\partial_\tau \boldsymbol{\theta}_\pi^n\|_{0,\Omega}) \|\boldsymbol{\theta}_h^n\|_{0,\Omega} \\
&\leq \rho^f \tau \left(\tau^{\frac{1}{2}} \|\partial_{tt} \mathbf{u}\|_{L^2(t_{n-1}, t_n; L^2(\Omega))} + \tau^{-\frac{1}{2}} \|\partial_t \boldsymbol{\theta}_\pi\|_{L^2(t_{n-1}, t_n; L^2(\Omega))} \right) \|\boldsymbol{\theta}_h^n\|_{0,\Omega} \\
&\leq \frac{(\rho^f C_P)^2}{2\varepsilon_1 \mu} \left(\tau^2 \|\partial_{tt} \mathbf{u}\|_{L^2(t_{n-1}, t_n; L^2(\Omega))}^2 + \|\partial_t \boldsymbol{\theta}_\pi\|_{L^2(t_{n-1}, t_n; L^2(\Omega))}^2 \right) + \varepsilon_1 \tau \mu \|\nabla \boldsymbol{\theta}_h^n\|_{0,\Omega_h}^2 \\
&\lesssim \frac{(\rho^f C_P)^2}{2\varepsilon_1 \mu} \tau^2 \|\partial_{tt} \mathbf{u}\|_{L^2(t_{n-1}, t_n; L^2(\Omega))}^2 + \frac{(\rho^f C_P)^2}{2\varepsilon_1 \mu} h^2 \|\partial_t \mathbf{u}\|_{L^2(t_{n-1}, t_n; H^2(\Omega))}^2 \\
&\quad + \varepsilon_1 \tau \mu \|\nabla \boldsymbol{\theta}_h^n\|_{0,\Omega_h}^2,
\end{aligned} \tag{57}$$

with $\varepsilon_1 > 0$. Note that, by choosing ε_1 small enough, the last term of (57) can be absorbed by the left-hand side of (56).

For term T_2 , using again a Taylor expansion we have

$$\begin{aligned}
T_2 &\leq \rho^s \epsilon \tau (\|(\partial_t - \partial_\tau) \dot{\mathbf{d}}^n\|_{0,\Sigma} + \|\partial_\tau \dot{\boldsymbol{\xi}}_\pi^n\|_{0,\Sigma}) \|\boldsymbol{\chi}_h^n\|_{0,\Sigma} \\
&\leq \rho^s \epsilon \tau \left(\tau^{1/2} \|\partial_{tt} \mathbf{u}\|_{L^2(t_{n-1}, t_n; L^2(\Sigma))} + \tau^{-1/2} \|\partial_t \dot{\boldsymbol{\xi}}_\pi\|_{L^2(t_{n-1}, t_n; L^2(\Sigma))} \right) \|\boldsymbol{\chi}_h^n\|_{0,\Sigma} \\
&\lesssim \frac{\rho^s \epsilon T}{2\varepsilon_2} \left(\tau^2 \|\partial_{tt} \mathbf{u}\|_{L^2(t_{n-1}, t_n; L^2(\Sigma))}^2 + h^2 \|\partial_t \mathbf{u}\|_{L^2(t_{n-1}, t_n; H^2(\Sigma))}^2 \right) + \underbrace{\varepsilon_2 \tau \frac{\rho^s \epsilon}{T} \|\boldsymbol{\chi}_h^n\|_{0,\Sigma}^2}_{T_{2,r}}.
\end{aligned} \tag{58}$$

For the last term, using (51) and a triangular inequality, and since $\tau \leq T$, we have

$$\begin{aligned}
T_{2,r} &\leq \varepsilon_2 \tau \frac{\rho^s \epsilon}{T} \|\dot{\boldsymbol{\xi}}_h^n\|_{0,\Sigma}^2 + \varepsilon_2 \frac{\tau^3}{\rho^s \epsilon T} \|\mathbf{L}_h(\boldsymbol{\xi}_h^n - \boldsymbol{\xi}_h^{n,*})\|_{0,\Sigma}^2 + \varepsilon_2 \frac{\tau^3}{\rho^s \epsilon T} \|\mathbf{L}_h(\mathbf{d}^n - \mathbf{d}^{n,*})\|_{0,\Sigma}^2 \\
&\leq \varepsilon_2 \tau \frac{\rho^s \epsilon}{T} \|\dot{\boldsymbol{\xi}}_h^n\|_{0,\Sigma}^2 + \varepsilon_2 \frac{\tau^2}{\rho^s \epsilon} \|\mathbf{L}_h(\boldsymbol{\xi}_h^n - \boldsymbol{\xi}_h^{n,*})\|_{0,\Sigma}^2 + \varepsilon_2 \frac{\tau^2}{\rho^s \epsilon} \|\mathbf{L}_h(\mathbf{d}^n - \mathbf{d}^{n,*})\|_{0,\Sigma}^2.
\end{aligned} \tag{59}$$

The first term will be treated via Lemma 3.1 in (56). The remaining two terms will, respectively, be controlled below via the numerical dissipation provided by the fluid-solid splitting and a Taylor expansion. Since the bound depends on the extrapolation order, we postpone the analysis of $T_{2,r}$ to treat it together with the extrapolation-dependent terms $T_8 - T_{10}$.

For term T_3 using (39), (3), a triangular inequality, a Taylor expansion and approximation, we have

$$\begin{aligned}
T_3 &= -\tau a^s(\boldsymbol{\xi}_h^n, \mathcal{I}_h \dot{\mathbf{d}}^n - \partial_\tau \mathbf{d}^n) \leq \tau \|\boldsymbol{\xi}_h^n\|_s \|\mathcal{I}_h \dot{\mathbf{d}}^n - \partial_\tau \mathbf{d}^n\|_s \\
&\leq \tau T \left(\|\mathcal{I}_h \dot{\mathbf{d}}^n - \dot{\mathbf{d}}^n\|_s^2 + \|\dot{\mathbf{d}}^n - \partial_\tau \mathbf{d}^n\|_s^2 \right) + \frac{\tau}{2T} \|\boldsymbol{\xi}_h^n\|_s^2 \\
&\lesssim \tau h^2 \beta^s T \|\mathbf{u}^n\|_{2,\Sigma}^2 + \tau^2 \beta^s T \|\partial_t \mathbf{u}\|_{L^2(t_{n-1}, t_n; H^1(\Sigma))}^2 + \frac{\tau}{2T} \|\boldsymbol{\xi}_h^n\|_s^2,
\end{aligned} \tag{60}$$

where the last term can be controlled via Lemma 3.1 in (56).

For term T_4 , using the weak consistency of the stabilization operator (43), we observe that

$$T_4 \leq \tau \frac{1}{2\varepsilon_4} |(i_{sz} E_2 \mathbf{u}^n, i_{sz} E_1 p^n)|_S^2 + \tau \frac{\varepsilon_4}{2} |(\boldsymbol{\theta}_h^n, y_h^n)|_S^2 \lesssim \tau h^2 \frac{1}{\varepsilon_4 \mu} (\mu \|\mathbf{u}^n\|_{2,\Omega}^2 + \mu^{-1} \|p^n\|_{1,\Omega}^2) + \tau \frac{\varepsilon_4}{2} |(\boldsymbol{\theta}_h^n, y_h^n)|_S^2 \tag{61}$$

where the third term in the right hand side is absorbed in the left-hand side of (56), for $\varepsilon_4 > 0$ sufficiently small.

The boundary penalty term T_5 is handled using Cauchy-Schwarz inequality followed by (44),

$$T_5 \leq \tau \frac{1}{2\varepsilon_5} \gamma \mu \|\boldsymbol{\theta}_\pi^n - \dot{\boldsymbol{\xi}}_\pi^n\|_{\frac{1}{2},h,\Sigma}^2 + \tau \frac{\varepsilon_5}{2} \gamma \mu \|\boldsymbol{\theta}_h^n - \boldsymbol{\chi}_h^n\|_{\frac{1}{2},h,\Sigma}^2 \lesssim \tau h^2 \frac{\gamma \mu}{\varepsilon_5} (\|\mathbf{u}^n\|_{2,\Omega}^2 + h \|\dot{\mathbf{d}}^n\|_{2,\Sigma}^2) + \tau \frac{\varepsilon_5}{2} \gamma \mu \|\boldsymbol{\theta}_h^n - \boldsymbol{\chi}_h^n\|_{\frac{1}{2},h,\Sigma}^2. \quad (62)$$

Note that the second term can be absorbed in the left-hand side of (56), for $\varepsilon_5 > 0$ small enough.

Similarly, for the consistency term T_6 , using (42)₃, we have

$$\begin{aligned} T_6 &\leq \tau \frac{1}{2\varepsilon_6 \gamma \mu} \|\boldsymbol{\sigma}(\boldsymbol{\theta}_\pi^n, y_\pi^n) \mathbf{n}\|_{-\frac{1}{2},h,\Sigma}^2 + \tau \frac{\varepsilon_6}{2} \gamma \mu \|\boldsymbol{\theta}_h^n - \boldsymbol{\chi}_h^n\|_{\frac{1}{2},h,\Sigma}^2 \\ &\lesssim \tau h^2 \frac{1}{\varepsilon_6 \gamma \mu} (\|\mathbf{u}^n\|_{2,\Omega}^2 + \|p^n\|_{1,\Omega}^2) + \tau \frac{\varepsilon_6}{2} \gamma \mu \|\boldsymbol{\theta}_h^n - \boldsymbol{\chi}_h^n\|_{\frac{1}{2},h,\Sigma}^2. \end{aligned} \quad (63)$$

Note that the first term has the right convergence order and the second term can be absorbed in the left hand side of (56), for $\varepsilon_6 > 0$ small enough.

To estimate T_7 , we split it into two parts as in [13]. The velocity-velocity coupling part can be easily handled by using approximation and the robust trace inequality (25), as follows:

$$\begin{aligned} &-\tau a(\boldsymbol{\theta}_\pi^n, \boldsymbol{\theta}_h^n) + \tau(\boldsymbol{\sigma}(\boldsymbol{\theta}_h^n, 0) \mathbf{n}, \boldsymbol{\theta}_\pi^n - \dot{\boldsymbol{\xi}}_\pi^n)_\Sigma \\ &\leq -\tau a(\boldsymbol{\theta}_\pi^n, \boldsymbol{\theta}_h^n) + \tau \mu \varepsilon_7 \|\boldsymbol{\varepsilon}(\boldsymbol{\theta}_h^n) \mathbf{n}\|_{-\frac{1}{2},h,\Sigma}^2 + \tau \mu \frac{1}{\varepsilon_7} \|\boldsymbol{\theta}_\pi^n - \dot{\boldsymbol{\xi}}_\pi^n\|_{\frac{1}{2},h,\Sigma}^2 \\ &\lesssim \tau h^2 \frac{\mu}{\varepsilon_7 C_{\text{TI}}} \|\mathbf{u}^n\|_{2,\Omega}^2 + \tau \mu \frac{2}{\varepsilon_7} h^2 (\|\mathbf{u}^n\|_{2,\Omega}^2 + \|\dot{\mathbf{d}}^n\|_{2,\Sigma}^2) + 2\tau \varepsilon_7 \mu C_{\text{TI}} \|\nabla \boldsymbol{\theta}_h^n\|_{0,\Omega_h}^2. \end{aligned} \quad (64)$$

The last term can be, once again, absorbed in the left hand side of (56), for $\varepsilon_7 > 0$ sufficiently small. For the velocity-pressure coupling part we write, using integration by parts in the continuity equation,

$$\begin{aligned} &-\tau b(y_\pi^n, \boldsymbol{\theta}_h^n) + \tau b(y_h^n, \boldsymbol{\theta}_\pi^n) + \tau(\boldsymbol{\sigma}(0, -y_h^n) \mathbf{n}, \boldsymbol{\theta}_\pi^n - \dot{\boldsymbol{\xi}}_\pi^n)_\Sigma \\ &= \tau(y_\pi^n, \operatorname{div} \boldsymbol{\theta}_h^n)_\Omega - \tau(y_h^n, \operatorname{div} \boldsymbol{\theta}_\pi^n)_\Omega + \tau(\boldsymbol{\sigma}(0, -y_h^n) \mathbf{n}, \boldsymbol{\theta}_\pi^n - \dot{\boldsymbol{\xi}}_\pi^n)_\Sigma \\ &= \underbrace{\tau(y_\pi^n, \operatorname{div} \boldsymbol{\theta}_h^n)_\Omega}_{T_{7,1}} + \underbrace{\tau(\nabla y_h^n, \boldsymbol{\theta}_\pi^n)_\Omega}_{T_{7,2}} - \underbrace{\tau(y_h^n \mathbf{n}, \dot{\boldsymbol{\xi}}_\pi^n)_\Sigma}_{T_{7,3}}. \end{aligned}$$

For the terms $T_{7,1}$ and $T_{7,2}$, using the Cauchy-Schwarz inequality, (42) and (43), we have

$$T_{7,1} \lesssim \tau h^2 \frac{1}{2\varepsilon_{7,1} \mu} \|p^n\|_{1,\Omega}^2 + \tau \frac{\varepsilon_{7,1}}{2} \mu \|\nabla \boldsymbol{\theta}_h^n\|_{0,\Omega}^2, \quad T_{7,2} \lesssim \tau h^2 \frac{\mu}{2\varepsilon_{7,2}} \|\mathbf{u}^n\|_{2,\Omega}^2 + \tau \frac{\varepsilon_{7,2}}{2} |(0, y_h^n)|_S^2, \quad (65)$$

where the last terms of these inequalities can be absorbed in (56), for $\varepsilon_{7,1}, \varepsilon_{7,2} > 0$ small enough. For the third term $T_{7,3}$, denoting by $y_i^n \in \mathbb{R}$ the average of y_h^n over the interface patch P_i , using the property (40) of the operator \mathcal{I}_h and the standard orthogonal projection inequality

$$\|y_h^n - y_i^n\|_{0,P_i} \lesssim h \|\nabla y_h^n\|_{0,P_i},$$

together with the trace inequality (24) and (7), we get

$$\begin{aligned} T_{7,3} &= -\tau \sum_i (y_h^n - y_i^n, \dot{\boldsymbol{\xi}}_\pi^n \cdot \mathbf{n})_{P_i} \lesssim \tau \sum_i h \|\nabla y_h^n\|_{0,P_i} h^2 \|\dot{\boldsymbol{\xi}}_\pi^n\|_{2,P_i} \\ &\lesssim \tau h^3 \frac{\mu}{2\varepsilon_{7,3}} \|\dot{\mathbf{d}}^n\|_{2,\Sigma}^2 + \tau h^2 \frac{\varepsilon_{7,3}}{2\mu} \|\nabla y_h^n\|_{0,\Omega_h}^2, \\ &\lesssim \tau h^3 \frac{\mu}{2\varepsilon_{7,3}} \|\dot{\mathbf{d}}^n\|_{2,\Sigma}^2 + \tau \frac{\varepsilon_{7,3}}{2} |(0, y_h^n)|_S^2 \end{aligned} \quad (66)$$

Inria

the last terms of these inequality can be absorbed in (56), for $\varepsilon_{7,3} > 0$ small enough. The above estimations of $T_{7,1}$, $T_{7,2}$ and $T_{7,3}$ provide bounds which involve either terms with the right convergence order or contributions that can be absorbed by the left-hand side of (56).

We now proceed with the extrapolation-dependent terms $T_8 - T_{10}$ and the term $T_{2,r}$ from (58). We consider each case of extrapolation separately. Basically, the terms $T_8 - T_{10}$ are controlled as in [26, Theorem 2]. We include these estimates here for the sake of completeness.

Algorithm 2 with $r = 0$. We have the bound

$$T_8 \leq -\frac{\tau^2}{\rho^s \epsilon} \left(1 - \frac{1}{2\varepsilon_8}\right) \|\mathbf{L}_h \boldsymbol{\xi}_h^n\|_{0,\Sigma}^2 + \varepsilon_8 \frac{\rho^s \epsilon}{2} \|\dot{\boldsymbol{\xi}}_h^n - \dot{\boldsymbol{\xi}}_h^{n-1}\|_{0,\Sigma}^2,$$

with $\varepsilon_8 > 0$. On the other hand, we have

$$T_9 = \tau (\dot{\boldsymbol{\xi}}_h^n - \dot{\boldsymbol{\xi}}_h^{n-1}, \mathbf{L}_h \mathbf{d}^n)_\Sigma \leq \tau \|\dot{\boldsymbol{\xi}}_h^n - \dot{\boldsymbol{\xi}}_h^{n-1}\|_{0,\Sigma} \|\mathbf{L}_h \mathbf{d}^n\|_{0,\Sigma} \leq \frac{\varepsilon_9 \rho^s \epsilon}{2} \|\dot{\boldsymbol{\xi}}_h^n - \dot{\boldsymbol{\xi}}_h^{n-1}\|_{0,\Sigma}^2 + \frac{\tau^2}{2\varepsilon_9 \rho^s \epsilon} \|\mathbf{L}^e \mathbf{d}^n\|_{0,\Sigma}^2,$$

with $\varepsilon_9 > 0$, where we have used the h -uniform bound (20). For the last term, we have

$$T_{10} = \frac{\tau^2}{\rho^s \epsilon} (\mathbf{L}_h \boldsymbol{\xi}_h^n, \mathbf{L}_h \mathbf{d}^n)_\Sigma \leq \frac{\varepsilon_{10} \tau^2}{2\rho^s \epsilon} \|\mathbf{L}_h \boldsymbol{\xi}_h^n\|_{0,\Sigma}^2 + \frac{\tau^2}{2\varepsilon_{10} \rho^s \epsilon} \|\mathbf{L}^e \mathbf{d}^n\|_{0,\Sigma}^2,$$

with $\varepsilon_{10} > 0$. On the other hand, owing to (59), we have that for $r = 0$ it holds

$$T_{2,0} \leq \varepsilon_2 \tau \frac{\rho^s \epsilon}{T} \|\dot{\boldsymbol{\xi}}_h^n\|_{0,\Sigma}^2 + \varepsilon_2 \frac{\tau^2}{\rho^s \epsilon} \|\mathbf{L}_h \boldsymbol{\xi}_h^n\|_{0,\Sigma}^2 + \varepsilon_2 \frac{\tau^2}{\rho^s \epsilon} \|\mathbf{L}^e \mathbf{d}^n\|_{0,\Sigma}^2.$$

Thus, we get

$$\begin{aligned} T_8 + T_9 + T_{10} + T_{2,0} &\leq \varepsilon_2 \tau \frac{\rho^s \epsilon}{T} \|\dot{\boldsymbol{\xi}}_h^n\|_{0,\Sigma}^2 - \frac{\tau^2}{\rho^s \epsilon} \left(1 - \frac{1}{2\varepsilon_8} - \frac{\varepsilon_{10}}{2} - \varepsilon_2\right) \|\mathbf{L}_h \boldsymbol{\xi}_h^n\|_{0,\Sigma}^2 \\ &\quad + \frac{\tau^2}{2\rho^s \epsilon} \left(\frac{1}{\varepsilon_9} + \frac{1}{\varepsilon_{10}} + \varepsilon_2\right) \|\mathbf{L}^e \mathbf{d}^n\|_{0,\Sigma}^2 + \frac{\rho^s \epsilon}{2} (\varepsilon_8 + \varepsilon_9) \|\dot{\boldsymbol{\xi}}_h^n - \dot{\boldsymbol{\xi}}_h^{n-1}\|_{0,\Sigma}^2. \end{aligned} \quad (67)$$

Taking $\varepsilon_8 = \frac{3}{4}$, $\varepsilon_{10} = \frac{1}{3}$ and $\varepsilon_2 < \frac{1}{6}$, we have

$$1 - \frac{1}{2\varepsilon_8} - \frac{\varepsilon_{10}}{2} - \varepsilon_2 > 0$$

and the second term on the right-hand side of (67) is negative. The last term of (67) can be absorbed into the left-hand side of (56), for $\varepsilon_9 > 0$ small enough. In summary, the estimate (52) follows by inserting the above estimates into (56), summing over $m = 1, \dots, n$, and applying Lemma 3.1 with

$$a_m = \frac{\rho^f}{2} \|\boldsymbol{\theta}_h^m\|_{0,\Omega}^2 + \frac{\rho^s \epsilon}{2} \|\dot{\boldsymbol{\xi}}_h^m\|_{0,\Sigma}^2 + \frac{1}{2} \|\boldsymbol{\xi}_h^m\|_s^2, \quad \eta_m = \frac{1}{T}.$$

Note that, owing to the selection of the initial data, we have

$$\boldsymbol{\theta}_h^0 = \mathbf{0}, \quad \dot{\boldsymbol{\xi}}_h^0 = \boldsymbol{\xi}_h^0 = \mathbf{0}. \quad (68)$$

Algorithm 2 with $r = 1$. For the term T_8 , using (39), we have

$$\begin{aligned} T_8 &= -\frac{\tau^2}{2} \left(\|\dot{\boldsymbol{\xi}}_h^n\|_s^2 - \|\dot{\boldsymbol{\xi}}_h^{n-1}\|_s^2 + \|\dot{\boldsymbol{\xi}}_h^n - \dot{\boldsymbol{\xi}}_h^{n-1}\|_s^2 \right) + \underbrace{\tau^2 (\dot{\boldsymbol{\xi}}_h^n - \dot{\boldsymbol{\xi}}_h^{n-1}, \mathbf{L}_h (\mathcal{I}_h \mathbf{d}^n - \partial_\tau \mathbf{d}^n))_\Sigma}_{T_{8,1}} \\ &\quad - \frac{\tau^2}{2\rho^s \epsilon} \left(\|\mathbf{L}_h \boldsymbol{\xi}_h^n\|_{0,\Sigma}^2 - \|\mathbf{L}_h \boldsymbol{\xi}_h^{n-1}\|_{0,\Sigma}^2 + \|\mathbf{L}_h (\boldsymbol{\xi}_h^n - \boldsymbol{\xi}_h^{n-1})\|_{0,\Sigma}^2 \right). \end{aligned}$$

Similarly to (60), we get

$$T_{8,1} = \tau^2 d^s(\dot{\xi}_h^n - \dot{\xi}_h^{n-1}, \mathcal{I}_h \dot{\mathbf{d}}^n - \partial_\tau \mathbf{d}^n) \lesssim \frac{\tau^2}{4} \|\dot{\xi}_h^n - \dot{\xi}_h^{n-1}\|_s^2 + h^2 \beta^s \tau^2 \|\mathbf{u}^n\|_{2,\Sigma}^2 + \tau^3 \beta^s \|\partial_t \mathbf{u}\|_{L^2(t_{n-1}, t_n; H^1(\Sigma))}^2,$$

and, thus,

$$\begin{aligned} T_8 &\lesssim -\frac{\tau^2}{2} \left(\|\dot{\xi}_h^n\|_s^2 - \|\dot{\xi}_h^{n-1}\|_s^2 \right) - \frac{\tau^2}{4} \|\dot{\xi}_h^n - \dot{\xi}_h^{n-1}\|_s^2 \\ &\quad - \frac{\tau^2}{2\rho^s \epsilon} \left(\|\mathbf{L}_h \xi_h^n\|_{0,\Sigma}^2 - \|\mathbf{L}_h \xi_h^{n-1}\|_{0,\Sigma}^2 + \|\mathbf{L}_h(\xi_h^n - \xi_h^{n-1})\|_{0,\Sigma}^2 \right) \\ &\quad + h^2 \beta^s \tau^2 \|\mathbf{u}^n\|_{2,\Sigma}^2 + \tau^3 \beta^s \|\partial_t \mathbf{u}\|_{L^2(t_{n-1}, t_n; H^1(\Sigma))}^2. \end{aligned} \quad (69)$$

For T_9 , using (20) and a Taylor expansion, we get

$$\begin{aligned} T_9 &= \tau (\dot{\xi}_h^n - \dot{\xi}_h^{n-1}, \mathbf{L}_h(\mathbf{d}^n - \mathbf{d}^{n-1}))_\Sigma \leq \tau \|\dot{\xi}_h^n - \dot{\xi}_h^{n-1}\|_{0,\Sigma} \|\mathbf{L}_h(\mathbf{d}^n - \mathbf{d}^{n-1})\|_{0,\Sigma} \\ &\leq \tau \frac{\rho^s \epsilon}{4T} \left(\|\dot{\xi}_h^n\|_{0,\Sigma}^2 + \|\dot{\xi}_h^{n-1}\|_{0,\Sigma}^2 \right) + \frac{\tau T}{\rho^s \epsilon} \|\mathbf{L}^e(\mathbf{d}^n - \mathbf{d}^{n-1})\|_{0,\Sigma}^2 \\ &\leq \tau \frac{\rho^s \epsilon}{4T} \left(\|\dot{\xi}_h^n\|_{0,\Sigma}^2 + \|\dot{\xi}_h^{n-1}\|_{0,\Sigma}^2 \right) + \frac{\tau^2 T}{\rho^s \epsilon} \|\mathbf{L}^e \partial_t \mathbf{d}\|_{L^2(t_{n-1}, t_n; L^2(\Sigma))}^2. \end{aligned} \quad (70)$$

The first term of (70) is controlled by (56) via Lemma 3.1. Similarly, for term T_{10} , we obtain

$$\begin{aligned} T_{10} &= \frac{\tau^2}{\rho^s \epsilon} (\mathbf{L}_h \xi_h^n, \mathbf{L}_h(\mathbf{d}^n - \mathbf{d}^{n-1}))_\Sigma \leq \frac{\tau^3}{2T \rho^s \epsilon} \|\mathbf{L}_h \xi_h^n\|_{0,\Sigma}^2 + \frac{\tau T}{2\rho^s \epsilon} \|\mathbf{L}(\mathbf{d}^n - \mathbf{d}^{n-1})\|_{0,\Sigma}^2 \\ &\leq \frac{\tau^3}{2T \rho^s \epsilon} \|\mathbf{L}_h \xi_h^n\|_{0,\Sigma}^2 + \frac{\tau^2 T}{2\rho^s \epsilon} \|\mathbf{L}^e \partial_t \mathbf{d}\|_{L^2(t_{n-1}, t_n; L^2(\Sigma))}^2. \end{aligned} \quad (71)$$

The first term in the right-hand side of (71) is controlled by (69) and Lemma 3.1. On the other hand, from (59), we have

$$\begin{aligned} T_{2,1} &\leq \varepsilon_2 \tau \frac{\rho^s \epsilon}{T} \|\dot{\xi}_h^n\|_{0,\Sigma}^2 + \varepsilon_2 \frac{\tau^2}{\rho^s \epsilon} \|\mathbf{L}_h(\xi_h^n - \xi_h^{n-1})\|_{0,\Sigma}^2 + \varepsilon_2 \frac{\tau^2}{\rho^s \epsilon} \|\mathbf{L}^e(\mathbf{d}^n - \mathbf{d}^{n-1})\|_{0,\Sigma}^2 \\ &\leq \varepsilon_2 \tau \frac{\rho^s \epsilon}{T} \|\dot{\xi}_h^n\|_{0,\Sigma}^2 + \varepsilon_2 \frac{\tau^2}{\rho^s \epsilon} \|\mathbf{L}_h(\xi_h^n - \xi_h^{n-1})\|_{0,\Sigma}^2 + \varepsilon_2 \frac{\tau^3}{\rho^s \epsilon} \|\mathbf{L}^e \partial_t \mathbf{d}\|_{L^2(t_{n-1}, t_n; L^2(\Sigma))}^2. \end{aligned}$$

In summary, the estimate (52) follows by inserting the above estimates into (56), summing over $m = 2, \dots, n$, and applying Lemma 3.1 with

$$a_m = \frac{\rho^f}{2} \|\theta_h^m\|_{0,\Omega}^2 + \frac{\rho^s \epsilon}{2} \|\dot{\xi}_h^m\|_{0,\Sigma}^2 + \frac{1}{2} \|\xi_h^m\|_s^2 + \frac{\tau^2}{2\rho^s \epsilon} \|\mathbf{L}_h \xi_h^m\|_{0,\Sigma}^2, \quad \eta_m = \frac{1}{T}.$$

The right-hand side contributions obtained at time t_1 , can be controlled (due to the initialization procedure) by using (52) with $r = 0$, $T = \tau$ and $n = 1$.

Algorithm 2 with $r = 2$. Let us first consider the term T_9 . Using (20) followed by a Taylor expansion, we have

$$\begin{aligned} T_9 &= \tau^2 (\dot{\xi}_h^n - \dot{\xi}_h^{n-1}, \mathbf{L}_h(\partial_\tau \mathbf{d}^n - \dot{\mathbf{d}}^{n-1}))_\Sigma \leq \tau \frac{\rho^s \epsilon}{4T} \left(\|\dot{\xi}_h^n\|_{0,\Sigma}^2 + \|\dot{\xi}_h^{n-1}\|_{0,\Sigma}^2 \right) + \frac{\tau^3 T}{\rho^s \epsilon} \|\mathbf{L}^e(\partial_\tau \mathbf{d}^n - \dot{\mathbf{d}}^{n-1})\|_{0,\Sigma}^2 \\ &\leq \tau \frac{\rho^s \epsilon}{4T} \left(\|\dot{\xi}_h^n\|_{0,\Sigma}^2 + \|\dot{\xi}_h^{n-1}\|_{0,\Sigma}^2 \right) + \frac{\tau^4 T}{\rho^s \epsilon} \|\mathbf{L}^e \partial_{tt} \mathbf{d}\|_{L^2(t_{n-1}, t_n; L^2(\Sigma))}^2. \end{aligned} \quad (72)$$

The first term in the bound (72) is controlled via Lemma 3.1 and (56). For the term T_{10} , using the inverse estimate (23) and the $\frac{6}{5}$ -CFL condition (30), we have

$$\begin{aligned} T_{10} &= \frac{\tau^3}{\rho^s \epsilon} (\mathbf{L}_h \boldsymbol{\xi}_h^n, \mathbf{L}_h (\partial_\tau \mathbf{d}^n - \dot{\mathbf{d}}^{n-1}))_\Sigma \leq \frac{\tau^3}{2T \rho^s \epsilon} \|\mathbf{L}_h \boldsymbol{\xi}_h^n\|_{0,\Sigma}^2 + \frac{\tau^3 T}{2\rho^s \epsilon} \|\mathbf{L}(\partial_\tau \mathbf{d}^n - \dot{\mathbf{d}}^{n-1})\|_{0,\Sigma}^2 \\ &\leq \frac{\tau^3}{2T \rho^s \epsilon} \|\mathbf{L}_h \boldsymbol{\xi}_h^n\|_{0,\Sigma}^2 + \frac{\tau^4 T}{2\rho^s \epsilon} \|\partial_{tt} \mathbf{L}^e \mathbf{d}\|_{L^2(t_{n-1}, t_n; L^2(\Sigma))}^2 \leq \frac{\tau^3 (\omega^s C_1)^2}{2Th^2} \|\boldsymbol{\xi}_h^n\|_s^2 + \frac{\tau^4 T}{2\rho^s \epsilon} \|\partial_{tt} \mathbf{L}^e \mathbf{d}\|_{L^2(t_{n-1}, t_n; L^2(\Sigma))}^2 \\ &\leq \frac{\tau \alpha^{\frac{5}{3}} \tau^{\frac{1}{3}}}{2T} \|\boldsymbol{\xi}_h^n\|_s^2 + \frac{\tau^4 T}{2\rho^s \epsilon} \|\partial_{tt} \mathbf{L}^e \mathbf{d}\|_{L^2(t_{n-1}, t_n; L^2(\Sigma))}^2. \end{aligned} \quad (73)$$

The first term in the bound (73) is controlled via Lemma 3.1 and (56). Note that

$$\boldsymbol{\xi}_h^{n,*} = \boldsymbol{\xi}_h^{n-1} + \tau \dot{\boldsymbol{\xi}}_h^{n-1} + \tau (\pi_h^s \dot{\mathbf{d}}^{n-1} - \mathcal{I}_h \dot{\mathbf{d}}^{n-1}).$$

Hence, for the term T_8 , we get

$$\begin{aligned} T_8 &= -\tau^2 (\dot{\boldsymbol{\xi}}_h^n - \dot{\boldsymbol{\xi}}_h^{n-1}, \mathbf{L}_h (\dot{\boldsymbol{\xi}}_h^n - \dot{\boldsymbol{\xi}}_h^{n-1}))_\Sigma - \frac{\tau^3}{\rho^s \epsilon} (\mathbf{L}_h \boldsymbol{\xi}_h^n, \mathbf{L}_h (\dot{\boldsymbol{\xi}}_h^n - \dot{\boldsymbol{\xi}}_h^{n-1}))_\Sigma \\ &\quad + \underbrace{\tau^2 (\dot{\boldsymbol{\xi}}_h^n - \dot{\boldsymbol{\xi}}_h^{n-1}, \mathbf{L}_h (\mathcal{I}_h (\dot{\mathbf{d}}^n - \dot{\mathbf{d}}^{n-1}) - \partial_\tau \mathbf{d}^n + \dot{\mathbf{d}}^{n-1}))_\Sigma}_{T_{8,1}} \\ &\quad + \underbrace{\frac{\tau^3}{\rho^s \epsilon} (\mathbf{L}_h \boldsymbol{\xi}_h^n, \mathbf{L}_h (\mathcal{I}_h (\dot{\mathbf{d}}^n - \dot{\mathbf{d}}^{n-1}) - \partial_\tau \mathbf{d}^n + \dot{\mathbf{d}}^{n-1}))_\Sigma}_{T_{8,2}}. \end{aligned}$$

Under the $\frac{6}{5}$ -CFL condition (30), we proceed similarly to (35) and (37), and we have

$$T_8 \leq -\tau^2 \|\dot{\boldsymbol{\xi}}_h^n - \dot{\boldsymbol{\xi}}_h^{n-1}\|_s^2 + \frac{\rho^s}{4} \|\dot{\boldsymbol{\xi}}_h^n - \dot{\boldsymbol{\xi}}_h^{n-1}\|_{0,\Sigma}^2 + \tau \alpha^5 \|\boldsymbol{\xi}_h^n\|_s^2 + T_{8,1} + T_{8,2}. \quad (74)$$

We consider the terms $T_{8,1}$ and $T_{8,2}$ separately. Adding and subtracting $\dot{\mathbf{d}}^n$ in $T_{8,1}$ yields

$$T_{8,1} = \tau^2 a^s (\dot{\boldsymbol{\xi}}_h^n - \dot{\boldsymbol{\xi}}_h^{n-1}, \mathcal{I}_h (\dot{\mathbf{d}}^n - \dot{\mathbf{d}}^{n-1}) - (\dot{\mathbf{d}}^n - \dot{\mathbf{d}}^{n-1})) + \tau^2 (\dot{\boldsymbol{\xi}}_h^n - \dot{\boldsymbol{\xi}}_h^{n-1}, \mathbf{L}_h (\dot{\mathbf{d}}^n - \partial_\tau \mathbf{d}^n))_\Sigma.$$

Owing to (3) and the approximation properties, we have

$$\begin{aligned} T_{8,1} &\lesssim \frac{\tau^2}{2} \|\dot{\boldsymbol{\xi}}_h^n - \dot{\boldsymbol{\xi}}_h^{n-1}\|_s^2 + h^2 \beta^s \tau^2 \|\mathbf{u}^n - \mathbf{u}^{n-1}\|_{2,\Sigma}^2 \\ &\quad + \tau \frac{\rho^s \epsilon}{4T} (\|\dot{\boldsymbol{\xi}}_h^n\|_{0,\Sigma}^2 + \|\dot{\boldsymbol{\xi}}_h^{n-1}\|_{0,\Sigma}^2) + \frac{\tau^4 T}{\rho^s \epsilon} \|\mathbf{L}^e \partial_{tt} \mathbf{d}\|_{L^2(t_{n-1}, t_n; L^2(\Sigma))}^2. \end{aligned} \quad (75)$$

For the term $T_{8,2}$ we have

$$T_{8,2} = \frac{\tau^3}{\rho^s \epsilon} a^s (\mathbf{L}_h \boldsymbol{\xi}_h^n, \mathcal{I}_h (\dot{\mathbf{d}}^n - \dot{\mathbf{d}}^{n-1}) - (\dot{\mathbf{d}}^n - \dot{\mathbf{d}}^{n-1})) + \frac{\tau^3}{\rho^s \epsilon} (\mathbf{L}_h \boldsymbol{\xi}_h^n, \mathbf{L}_h (\dot{\mathbf{d}}^n - \partial_\tau \mathbf{d}^n))_\Sigma. \quad (76)$$

The second term in the right-hand side of (76) is treated similarly to (73). The estimate for the first term follow by the inverse estimates (22), (23) and the $\frac{6}{5}$ -CFL condition (30). We have

$$\begin{aligned} T_{8,2} &\leq \frac{\tau^5}{2T(\rho^s \epsilon)^2} \|\mathbf{L}_h \boldsymbol{\xi}_h^n\|_s^2 + \frac{\tau T}{2} \|\mathcal{I}_h (\dot{\mathbf{d}}^n - \dot{\mathbf{d}}^{n-1}) - (\dot{\mathbf{d}}^n - \dot{\mathbf{d}}^{n-1})\|_s^2 + \frac{\tau \alpha^{\frac{5}{3}} \tau^{\frac{1}{3}}}{2T} \|\boldsymbol{\xi}_h^n\|_s^2 + \frac{\tau^4 T}{2\rho^s \epsilon} \|\partial_{tt} \mathbf{L}^e \mathbf{d}\|_{L^2(t_{n-1}, t_n; L^2(\Sigma))}^2 \\ &\lesssim \left(\frac{\tau \alpha^{\frac{10}{3}} \tau^{\frac{2}{3}}}{2T} + \frac{\tau \alpha^{\frac{5}{3}} \tau^{\frac{1}{3}}}{2T} \right) \|\boldsymbol{\xi}_h^n\|_s^2 + h^2 \beta^s \tau T \|\mathbf{u}^n - \mathbf{u}^{n-1}\|_{2,\Sigma}^2 + \frac{\tau^4 T}{2\rho^s \epsilon} \|\partial_{tt} \mathbf{L}^e \mathbf{d}\|_{L^2(t_{n-1}, t_n; L^2(\Sigma))}^2. \end{aligned} \quad (77)$$

Substitution of (75) and (77) into (74), yields

$$\begin{aligned} T_8 \lesssim & -\frac{\tau^2}{2} \|\dot{\boldsymbol{\xi}}_h^n - \dot{\boldsymbol{\xi}}_h^{n-1}\|_s^2 + \frac{\rho^s}{4} \|\dot{\boldsymbol{\xi}}_h^n - \dot{\boldsymbol{\xi}}_h^{n-1}\|_{0,\Sigma}^2 + \tau \frac{\rho^s \epsilon}{4T} \left(\|\dot{\boldsymbol{\xi}}_h^n\|_{0,\Sigma}^2 + \|\dot{\boldsymbol{\xi}}_h^{n-1}\|_{0,\Sigma}^2 \right) \\ & + \tau \left(\alpha^5 + \frac{\alpha^{\frac{10}{3}} \tau^{\frac{2}{3}}}{2T} + \frac{\alpha^{\frac{5}{3}} \tau^{\frac{1}{3}}}{2T} \right) \|\boldsymbol{\xi}_h^n\|_s^2 + \frac{\tau^4 T}{\rho^s \epsilon} \|\mathbf{L}^e \partial_{tt} \mathbf{d}\|_{L^2(t_{n-1}, t_n; L^2(\Sigma))}^2 \\ & + h^2 \beta^s (T + \tau) \tau \|\mathbf{u}^n - \mathbf{u}^{n-1}\|_{2,\Sigma}^2. \end{aligned} \quad (78)$$

The first term on the right hand side is absorbed into the left-hand side of (56) and, the following two are treated via Lemma 3.1.

On the other hand, regarding the term $T_{2,2}$ from (59), we get

$$\begin{aligned} T_{2,2} & \leq \varepsilon_2 \tau \frac{\rho^s \epsilon}{T} \|\dot{\boldsymbol{\xi}}_h^n\|_{0,\Sigma}^2 + \varepsilon_2 \frac{\tau^2}{\rho^s \epsilon} \|\mathbf{L}_h(\boldsymbol{\xi}_h^n - \boldsymbol{\xi}_h^{n,*})\|_{0,\Sigma}^2 + \varepsilon_2 \frac{\tau^4}{\rho^s \epsilon} \|\mathbf{L}^e(\partial_\tau \mathbf{d}^n - \dot{\mathbf{d}}^{n-1})\|_{0,\Sigma}^2 \\ & \leq \varepsilon_2 \tau \frac{\rho^s \epsilon}{T} \|\dot{\boldsymbol{\xi}}_h^n\|_{0,\Sigma}^2 + \underbrace{\varepsilon_2 \frac{\tau^2}{\rho^s \epsilon} \|\mathbf{L}_h(\boldsymbol{\xi}_h^n - \boldsymbol{\xi}_h^{n,*})\|_{0,\Sigma}^2}_{T_{2,2,1}} + \varepsilon_2 \frac{\tau^5}{\rho^s \epsilon} \|\mathbf{L}^e \partial_{tt} \mathbf{d}\|_{L^2(t_{n-1}, t_n; L^2(\Sigma))}^2. \end{aligned}$$

Moreover, we have

$$\begin{aligned} T_{2,2,1} & \leq \varepsilon_2 \frac{\tau^4}{\rho^s \epsilon} \|\mathbf{L}_h(\dot{\boldsymbol{\xi}}_h^n - \dot{\boldsymbol{\xi}}_h^{n-1}) + \mathbf{L}_h(\mathbf{z}_h^n - \mathbf{z}_h^{n-1})\|_{0,\Sigma}^2 \leq 2\varepsilon_2 \frac{\tau^4 \beta^s}{h^2 \rho^s \epsilon} (\|\dot{\boldsymbol{\xi}}_h^n - \dot{\boldsymbol{\xi}}_h^{n-1}\|_s^2 + \|\mathbf{z}_h^n - \mathbf{z}_h^{n-1}\|_s^2) \\ & \leq 2\varepsilon_2 (\gamma \tau)^{\frac{1}{3}} \tau^2 (\|\dot{\boldsymbol{\xi}}_h^n - \dot{\boldsymbol{\xi}}_h^{n-1}\|_s^2 + \|\mathbf{z}_h^n - \mathbf{z}_h^{n-1}\|_s^2). \end{aligned}$$

The first term can be controlled with the numerical dissipation of (78) and the second term can be estimated as in the previous estimations. The estimate (52) then follows by inserting the above estimates into (56), summing over $m = 3, \dots, n$, using (68) and applying Lemma 3.1 with

$$a_m = \frac{\rho^f}{2} \|\boldsymbol{\theta}_h^m\|_{0,\Omega}^2 + \frac{\rho^s \epsilon}{2} \|\dot{\boldsymbol{\xi}}_h^m\|_{0,\Sigma}^2 + \frac{1}{2} \|\boldsymbol{\xi}_h^m\|_s^2, \quad \gamma_m = \max \left\{ \frac{1}{T}, 2\alpha^5, \frac{\alpha^{\frac{10}{3}} \tau^{\frac{2}{3}} + \alpha^{\frac{5}{3}} \tau^{\frac{1}{3}}}{T} \right\}.$$

The right-hand side contributions obtained at time t_2 , can be controlled (due to the initialization procedure) by using (52) with $r = 1$, $T = 2\tau$ and $n = 2$. Hence, the proof is complete. \square

We define the energy-norm of the error at time step t_n , as

$$\begin{aligned} \mathcal{Z}_h^n & \stackrel{\text{def}}{=} (\rho^f)^{\frac{1}{2}} \|\mathbf{u}^n - \mathbf{u}_h^n\|_{0,\Omega} + (\rho^s \epsilon)^{\frac{1}{2}} \|\dot{\mathbf{d}}^n - \dot{\mathbf{d}}_h^n\|_{0,\Sigma} + \|\mathbf{d}^n - \mathbf{d}_h^n\|_s + \left(\sum_{m=r+1}^n c_g \tau |(\mathbf{u}_h^m, \mathbf{p}_h^m)|_S^2 \right)^{\frac{1}{2}} \\ & + \left(\sum_{m=r+1}^n c_g \tau \mu \|\nabla(\mathbf{u}^m - \mathbf{u}_h^m)\|_{0,\Omega}^2 \right)^{\frac{1}{2}} + \left(\sum_{m=r+1}^n c_g \tau \gamma \mu \|\mathbf{u}_h^m - \dot{\mathbf{d}}_h^{m-\frac{1}{2}}\|_{\frac{1}{2},h,\Sigma}^2 \right)^{\frac{1}{2}} \end{aligned}$$

for $n > r$. As a corollary of Theorem 3.2, we have the following a priori estimate.

Corollary 3.1. *Under the assumptions of Theorem 3.2, we have the following error estimate, for $n > r$ and $n\tau < T$:*

$$\mathcal{Z}_h^n \lesssim c_1 h + c_2 \tau + c_3 \tau^{2^{r-1}}.$$

Here, the symbols $\{c_i\}_{i=1}^3$ denote positive constants independent of h and τ , but which depend on the physical parameters and on the regularity of $(\mathbf{u}, p, \mathbf{d}, \dot{\mathbf{d}})$.

Proof. The proof follows directly as a consequence of a triangle inequality, Theorem 3.2 and the optimal approximation properties of the interpolation operators. \square

We then observe that the scheme displays optimal accuracy for the extrapolated variants ($r = 1, 2$) whereas a suboptimal convergence rate is obtained without extrapolation ($r = 0$). Thus, we retrieve the same convergence behavior as in the fitted case for the original Robin-Neumann schemes (see [26, Corollary 1]). From the proofs of Theorem 3.2 and Corollary 3.1, we can readily obtain the following optimal error estimate for Algorithm 1.

Corollary 3.2. *Let $(\mathbf{u}, p, \mathbf{d}, \dot{\mathbf{d}})$ be the solution of the coupled problem (1)-(2) and $\{(\mathbf{u}_h^n, p_h^n, \mathbf{d}_h^n, \dot{\mathbf{d}}_h^n)\}_{n>r}$ be the approximation given by Algorithm 1 with initial data $(\mathbf{u}_h^0, \mathbf{d}_h^0, \dot{\mathbf{d}}_h^0) = (i_{\text{sz}} E_2 \mathbf{u}^0, \pi_h^s \mathbf{d}^0, \mathcal{I}_h \dot{\mathbf{d}}^0)$. Suppose that the exact solution has the regularity (45)-(46). Then, we have the following error estimates, for $n > 0$ and $n\tau < T$:*

$$\mathcal{Z}_h^n \lesssim c_1 h + c_2 \tau$$

with c_1 and c_2 positive constants independent of h and τ , but depending on the physical parameters and on the regularity of $(\mathbf{u}, p, \mathbf{d}, \dot{\mathbf{d}})$.

Proof. Taking $(\mathbf{v}_h, q_h, \mathbf{w}_h) = \tau(\boldsymbol{\theta}_h^n, y_h^n, \dot{\boldsymbol{\xi}}_h^n)$ in (55), the energy inequality (56) holds with $\chi_h^n = \dot{\boldsymbol{\xi}}_h^n$ and $T_8 = T_9 = T_{10} = 0$. The terms T_5 and T_6 are treated similarly to (62) and (63). Note that the Nitsche's dissipation on the interface is given in this case by

$$c_g \tau \gamma \mu \|\boldsymbol{\theta}_h^n - \dot{\boldsymbol{\xi}}_h^n\|_{\frac{2}{2}, h, \Sigma}^2.$$

Similarly to (58), for the term T_2 , we have

$$T_2 \lesssim \frac{\rho^s \epsilon T}{2\varepsilon_2} (\tau^2 \|\partial_{tt} \mathbf{u}\|_{L^2(t_{n-1}, t_n; L^2(\Sigma))}^2 + h^2 \|\partial_t \mathbf{u}\|_{L^2(t_{n-1}, t_n; H^2(\Sigma))}^2) + \varepsilon_2 \tau \frac{\rho^s \epsilon}{T} \|\dot{\boldsymbol{\xi}}_h^n\|_{0, \Sigma}^2.$$

The last term may be controlled by Lemma 3.1. The remaining terms T_1, T_3, T_4 and T_7 are treated exactly as above. We obtain thus an optimal a priori estimate for the discrete errors. We conclude as in Corollary 3.1. \square

4 First discretize in time and then in space: explicit schemes

Step (16) of Algorithm 2 is more computationally demanding than a single fluid problem due to the presence of the additional unknown $\dot{\mathbf{d}}_h^{n-\frac{1}{2}}$. In this section, a new explicit coupling scheme is presented which overcomes this issue without compromising stability and accuracy. The main idea consists in performing the space and time discretization reversely.

4.1 Robin-Neumann explicit coupling schemes

The starting point of the methods is the time semi-discrete explicit coupling schemes introduced in [26, 30]. Note that these schemes may be derived by applying first the fractional-step splitting of Section 3.2 to the continuous problem (1)-(2) and then eliminating, contrarily to Algorithm 2, the intermediate solid velocity $\dot{\mathbf{d}}_h^{n-\frac{1}{2}}$ (see Remark 3.3). Applied to the continuous problem (1)-(2), these schemes read: for $n > r$

1. Fluid substep: find $\mathbf{u}^n : \Omega \times \mathbb{R}^+ \rightarrow \mathbb{R}^d$ and $p^n : \Omega \times \mathbb{R}^+ \rightarrow \mathbb{R}$ such that

$$\begin{cases} \rho^f \partial_\tau \mathbf{u}^n - \operatorname{div} \boldsymbol{\sigma}(\mathbf{u}^n, p^n) = \mathbf{0} & \text{in } \Omega, \\ \operatorname{div} \mathbf{u}^n = 0 & \text{in } \Omega, \\ \mathbf{u}^n = \mathbf{0} & \text{on } \Gamma^f, \\ \boldsymbol{\sigma}(\mathbf{u}^n, p^n) \mathbf{n} + \kappa \mathbf{u}^n = \kappa \dot{\mathbf{d}}^{n-1} + \mathbf{g}^{n,*} & \text{on } \Sigma, \end{cases} \quad (79)$$

with the notations:

$$\kappa \stackrel{\text{def}}{=} \frac{\rho^s \epsilon}{\tau}, \quad \mathbf{g}^{n,*} \stackrel{\text{def}}{=} \rho^s \epsilon \partial_\tau \dot{\mathbf{d}}^{n,*} + \boldsymbol{\sigma}(\mathbf{u}^{n,*}, p^{n,*}) \mathbf{n}.$$

2. Solid substep: find $\mathbf{d}^n : \Sigma \times \mathbb{R}^+ \rightarrow \mathbb{R}^d$ and $\dot{\mathbf{d}}^n : \Sigma \times \mathbb{R}^+ \rightarrow \mathbb{R}^d$ such that $\dot{\mathbf{d}}^n = \partial_\tau \mathbf{d}^n$ and

$$\begin{cases} \rho^s \epsilon \partial_\tau \dot{\mathbf{d}}^n + \mathbf{L}^e \mathbf{d}^n = -\boldsymbol{\sigma}(\mathbf{u}^n, p^n) \mathbf{n} & \text{on } \Sigma, \\ \mathbf{d}^n = \mathbf{0} & \text{on } \partial \Sigma. \end{cases} \quad (80)$$

4.2 Fully discrete formulation: explicit coupling scheme with unfitted meshes

The fundamental idea consists in performing directly an unfitted interface treatment (à la Nitsche) of the time splitting (79)-(80). This is achieved by extending the arguments introduced in [13] and [15, 38] to the present Robin-Neumann framework, in such a way that robustness with respect to the Robin coefficient κ is guaranteed. The proposed numerical methods build on the following consistency result.

Lemma 4.1 (Consistency). *Let $\{(\mathbf{u}^n, p^n, \dot{\mathbf{d}}^n, \mathbf{d}^n)\}_{n>r}$ be given by (79)-(80). Then, there holds*

$$\begin{cases} \rho^f (\partial_\tau \mathbf{u}^n, \mathbf{v}_h)_\Omega + a^f((\mathbf{u}^n, p^n), (\mathbf{v}_h, q_h)) + \rho^s \epsilon (\partial_\tau \dot{\mathbf{d}}^n, \mathbf{w}_h)_\Sigma + a^s(\mathbf{d}^n, \mathbf{w}_h) \\ + \frac{\gamma \kappa \mu}{\gamma \mu + \kappa h} (\mathbf{u}^n - \dot{\mathbf{d}}^{n-1}, \mathbf{v}_h - \mathbf{w}_h)_\Sigma - \frac{\gamma \mu}{\gamma \mu + \kappa h} (\mathbf{g}^{n,*}, \mathbf{v}_h - \mathbf{w}_h)_\Sigma \\ - \frac{\kappa h}{\gamma \mu + \kappa h} \left[(\boldsymbol{\sigma}(\mathbf{u}^n, p^n) \mathbf{n}, \mathbf{v}_h - \mathbf{w}_h)_\Sigma + (\mathbf{u}^n - \dot{\mathbf{d}}^{n-1}, \boldsymbol{\sigma}(\mathbf{v}_h, -q_h) \mathbf{n})_\Sigma \right] \\ - \frac{h}{\gamma \mu + \kappa h} (\boldsymbol{\sigma}(\mathbf{u}^n, p^n) \mathbf{n}, \boldsymbol{\sigma}(\mathbf{v}_h, -q_h) \mathbf{n})_\Sigma + \frac{h}{\gamma \mu + \kappa h} (\mathbf{g}^{n,*}, \boldsymbol{\sigma}(\mathbf{v}_h, -q_h) \mathbf{n})_\Sigma = 0 \end{cases} \quad (81)$$

for all $(\mathbf{v}_h, q_h, \mathbf{w}_h) \in \mathbf{V}_h \times Q_h \times \mathbf{W}_h$.

Proof. Multiplying (79)₁ and (79)₂ by \mathbf{v}_h and q_h respectively, integrating by parts over Ω and adding both equations we get

$$\rho^f (\partial_\tau \mathbf{u}^n, \mathbf{v}_h)_\Omega + a^f((\mathbf{u}^n, p^n), (\mathbf{v}_h, q_h)) - (\boldsymbol{\sigma}(\mathbf{u}^n, p^n) \mathbf{n}, \mathbf{v}_h)_\Sigma = 0. \quad (82)$$

On the other hand, multiplying (80)₁ by \mathbf{w}_h and integrating over Σ we get

$$\rho^s \epsilon (\partial_\tau \dot{\mathbf{d}}^n, \mathbf{w}_h)_\Sigma + a^s(\mathbf{d}^n, \mathbf{w}_h) + (\boldsymbol{\sigma}(\mathbf{u}^n, p^n) \mathbf{n}, \mathbf{w}_h)_\Sigma = 0. \quad (83)$$

Adding (82) and (83), we obtain

$$\rho^f (\partial_\tau \mathbf{u}^n, \mathbf{v}_h)_\Omega + a^f((\mathbf{u}^n, p^n), (\mathbf{v}_h, q_h)) + \rho^s \epsilon (\partial_\tau \dot{\mathbf{d}}^n, \mathbf{w}_h)_\Sigma + a^s(\mathbf{d}^n, \mathbf{w}_h) - (\boldsymbol{\sigma}(\mathbf{u}^n, p^n) \mathbf{n}, \mathbf{v}_h - \mathbf{w}_h)_\Sigma = 0. \quad (84)$$

Multiplying the interface condition (79)₄ by $\frac{\gamma\mu}{\gamma\mu + \kappa h}(\mathbf{v}_h - \mathbf{w}_h)$ and integrating over Σ , we get

$$\frac{\gamma\kappa\mu}{\gamma\mu + \kappa h}(\mathbf{u}^n - \dot{\mathbf{d}}^{n-1}, \mathbf{v}_h - \mathbf{w}_h)_\Sigma + \frac{\gamma\mu}{\gamma\mu + \kappa h}(\boldsymbol{\sigma}(\mathbf{u}^n, p^n)\mathbf{n}, \mathbf{v}_h - \mathbf{w}_h)_\Sigma - \frac{\gamma\mu}{\gamma\mu + \kappa h}(\mathbf{g}^{n,*}, \mathbf{v}_h - \mathbf{w}_h)_\Sigma = 0. \quad (85)$$

Multiplying the interface condition (79)₄ by $-\frac{h}{\gamma\mu + \kappa h}\boldsymbol{\sigma}(\mathbf{v}_h, -q_h)\mathbf{n}$ and integrating over Σ , we get

$$\begin{aligned} -\frac{\kappa h}{\gamma\mu + \kappa h}(\mathbf{u}^n - \dot{\mathbf{d}}^{n-1}, \boldsymbol{\sigma}(\mathbf{v}_h, -q_h)\mathbf{n})_\Sigma - \frac{h}{\gamma\mu + \kappa h}(\boldsymbol{\sigma}(\mathbf{u}^n, p^n)\mathbf{n}, \boldsymbol{\sigma}(\mathbf{v}_h, -q_h)\mathbf{n})_\Sigma \\ + \frac{h}{\gamma\mu + \kappa h}(\mathbf{g}^{n,*}, \boldsymbol{\sigma}(\mathbf{v}_h, -q_h)\mathbf{n})_\Sigma = 0. \end{aligned} \quad (86)$$

Finally, by adding (84)-(86) we recover (81), which completes the proof. \square

The key feature of (81) is the fact that for $\kappa \rightarrow \infty$ (i.e., whenever $\tau \rightarrow 0$) we formally retrieve the unfitted formulation (5). Alternatively, if $h \rightarrow 0$ we formally retrieve the the weak formulation of the Robin-Neumann splitting (79)-(80).

Taking successively $\mathbf{w}_h = \mathbf{0}$ and $(\mathbf{v}_h, q_h) = (\mathbf{0}, 0)$ in (81) we obtain the following partitioned formulation of (81):

- Fluid:

$$\left\{ \begin{aligned} &\rho^f(\partial_\tau \mathbf{u}^n, \mathbf{v}_h)_\Omega + a^f((\mathbf{u}^n, p^n), (\mathbf{v}_h, q_h)) + \frac{\gamma\kappa\mu}{\gamma\mu + \kappa h}(\mathbf{u}^n - \dot{\mathbf{d}}^{n-1}, \mathbf{v}_h)_\Sigma \\ &- \frac{\gamma\mu}{\gamma\mu + \kappa h}(\mathbf{g}^{n,*}, \mathbf{v}_h)_\Sigma - \frac{h}{\gamma\mu + \kappa h}(\boldsymbol{\sigma}(\mathbf{u}^n, p^n)\mathbf{n}, \boldsymbol{\sigma}(\mathbf{v}_h, -q_h)\mathbf{n})_\Sigma \\ &- \frac{\kappa h}{\gamma\mu + \kappa h}[(\boldsymbol{\sigma}(\mathbf{u}^n, p^n)\mathbf{n}, \mathbf{v}_h)_\Sigma + (\mathbf{u}^n - \dot{\mathbf{d}}^{n-1}, \boldsymbol{\sigma}(\mathbf{v}_h, -q_h)\mathbf{n})_\Sigma] \\ &+ \frac{h}{\gamma\mu + \kappa h}(\mathbf{g}^{n,*}, \boldsymbol{\sigma}(\mathbf{v}_h, -q_h)\mathbf{n})_\Sigma = 0 \end{aligned} \right.$$

for all $(\mathbf{v}_h, q_h) \in \mathbf{V}_h \times Q_h$.

- Solid:

$$\left\{ \begin{aligned} &\rho^s \epsilon(\partial_\tau \dot{\mathbf{d}}^n, \mathbf{w}_h)_\Sigma + a^s(\dot{\mathbf{d}}^n, \mathbf{w}_h) = -\frac{\kappa h}{\gamma\mu + \kappa h}(\boldsymbol{\sigma}(\mathbf{u}^n, p^n)\mathbf{n}, \mathbf{w}_h)_\Sigma \\ &+ \frac{\gamma\kappa\mu}{\gamma\mu + \kappa h}(\mathbf{u}^n - \dot{\mathbf{d}}^{n-1}, \mathbf{w}_h)_\Sigma - \frac{\gamma\mu}{\gamma\mu + \kappa h}(\mathbf{g}^{n,*}, \mathbf{w}_h)_\Sigma \end{aligned} \right.$$

for all $\mathbf{w}_h \in \mathbf{W}_h$.

This motivates the fully discrete method reported in Algorithm 3. Note that the resulting coupling scheme is explicit.

4.3 Stability and convergence analysis for $r = 0$

We present in this section an energy-based stability and a priori error analysis for Algorithm 3 with $r = 0$. The stability and convergence properties of Algorithm 3 with $r = 1, 2$ are investigated in Section 5 via numerical experiments.

Algorithm 3 Explicit coupling schemes.

For $n > r$:

1. Fluid substep: find $(\mathbf{u}_h^n, p_h^n) \in \mathbf{V}_h \times Q_h$ such that

$$\begin{cases} r\rho^f(\partial_\tau \mathbf{u}_h^n, \mathbf{v}_h)_\Omega + a_h^f((\mathbf{u}_h^n, p_h^n), (\mathbf{v}_h, q_h)) + \frac{\gamma\kappa\mu}{\gamma\mu + \kappa h}(\mathbf{u}_h^n - \dot{\mathbf{d}}_h^{n-1}, \mathbf{v}_h)_\Sigma \\ - \frac{\gamma\mu}{\gamma\mu + \kappa h}(\mathbf{g}_h^{n,*}, \mathbf{v}_h)_\Sigma - \frac{h}{\gamma\mu + \kappa h}(\boldsymbol{\sigma}(\mathbf{u}_h^n, p_h^n)\mathbf{n}, \boldsymbol{\sigma}(\mathbf{v}_h, -q_h)\mathbf{n})_\Sigma \\ - \frac{\kappa h}{\gamma\mu + \kappa h}[(\boldsymbol{\sigma}(\mathbf{u}_h^n, p_h^n)\mathbf{n}, \mathbf{v}_h)_\Sigma + (\mathbf{u}_h^n - \dot{\mathbf{d}}_h^{n-1}, \boldsymbol{\sigma}(\mathbf{v}_h, -q_h)\mathbf{n})_\Sigma] \\ + \frac{h}{\gamma\mu + \kappa h}(\mathbf{g}_h^{n,*}, \boldsymbol{\sigma}(\mathbf{v}_h, -q_h)\mathbf{n})_\Sigma = 0 \end{cases} \quad (87)$$

for all $(\mathbf{v}_h, q_h) \in \mathbf{V}_h \times Q_h$.

2. Solid substep: find $(\dot{\mathbf{d}}_h^n, \mathbf{d}_h^n) \in \mathbf{W}_h \times \mathbf{W}_h$ such that $\dot{\mathbf{d}}_h^n = \partial_\tau \mathbf{d}_h^n$ and

$$\begin{cases} \rho^s \epsilon (\partial_\tau \dot{\mathbf{d}}_h^n, \mathbf{w}_h)_\Sigma + a^s(\mathbf{d}_h^n, \mathbf{w}_h) = -\frac{\kappa h}{\gamma\mu + \kappa h}(\boldsymbol{\sigma}(\mathbf{u}_h^n, p_h^n)\mathbf{n}, \mathbf{w}_h)_\Sigma \\ + \frac{\gamma\kappa\mu}{\gamma\mu + \kappa h}(\mathbf{u}_h^n - \dot{\mathbf{d}}_h^{n-1}, \mathbf{w}_h)_\Sigma - \frac{\gamma\mu}{\gamma\mu + \kappa h}(\mathbf{g}_h^{n,*}, \mathbf{w}_h)_\Sigma \end{cases} \quad (88)$$

for all $\mathbf{w}_h \in \mathbf{W}_h$.

4.3.1 Stability analysis

We consider the discrete energy E_h^n given by (27) at time-step t_n . The dissipation is given in this case by

$$\begin{aligned} \tilde{D}_h^n &\stackrel{\text{def}}{=} \frac{\rho^f}{\tau} \|\mathbf{u}_h^n - \mathbf{u}_h^{n-1}\|_{0,\Omega}^2 + c_g \mu \|\nabla \mathbf{u}_h^n\|_{0,\Omega_h}^2 + \frac{\gamma\kappa\mu}{\gamma\mu + \kappa h} \|\mathbf{u}_h^n - \dot{\mathbf{d}}_h^n\|_{0,\Sigma}^2 + |(\mathbf{u}_h^n, p_h^n)|_S^2 \\ &+ \frac{\rho^s \epsilon}{\tau} \frac{\kappa h}{\gamma\mu + \kappa h} \|\dot{\mathbf{d}}_h^n - \dot{\mathbf{d}}_h^{n-1}\|_{0,\Sigma}^2 + \frac{1}{\tau} \|\mathbf{d}_h^n - \mathbf{d}_h^{n-1}\|_s^2 + \frac{h}{\gamma\mu + \kappa h} \|p_h^n\|_{0,\Sigma}^2. \end{aligned}$$

The following result establishes the unconditional energy stability of Algorithm 3 with $r = 0$.

Theorem 4.1. *Let $\{(\mathbf{u}_h^n, p_h^n, \dot{\mathbf{d}}_h^n, \mathbf{d}_h^n)\}_{n \geq 1}$ be given by Algorithm 3 with $r = 0$. For $\gamma > 12C_{\text{TI}}/\tilde{c}_g$, we have*

$$E_h^n + \tau \sum_{m=1}^n \tilde{D}_h^m \lesssim E_h^0. \quad (89)$$

Proof. We first note that in the case $r = 0$ we have $\mathbf{g}_h^{n,*} = \mathbf{0}$. Thus, by taking $(\mathbf{v}_h, q_h) = \tau(\mathbf{u}_h^n, p_h^n)$ in (87) and $\mathbf{w}_h = \tau \dot{\mathbf{d}}_h^n$ in (88), adding the resulting equations and applying (9), we get the

following discrete energy inequality

$$\begin{aligned}
& \frac{\rho^f}{2} (\tau \partial_\tau \|\mathbf{u}_h^n\|_{0,\Omega}^2 + \|\mathbf{u}_h^n - \mathbf{u}_h^{n-1}\|_{0,\Omega}^2) + \tilde{c}_g \tau (\mu \|\boldsymbol{\varepsilon}(\mathbf{u}_h^n)\|_{0,\Omega_h}^2 + g_h(\mathbf{u}_h^n, \mathbf{u}_h^n)) \\
& \quad + \tau s_h(p_h^n, p_h^n) + \frac{1}{2} (\tau \partial_\tau \|\mathbf{d}_h^n\|_s^2 + \|\mathbf{d}_h^n - \mathbf{d}_h^{n-1}\|_s^2) \\
& \quad - \underbrace{\frac{\kappa h}{\gamma\mu + \kappa h} \tau \left[(\boldsymbol{\sigma}(\mathbf{u}_h^n, p_h^n) \mathbf{n}, \mathbf{u}_h^n - \dot{\mathbf{d}}_h^n)_\Sigma + (\mathbf{u}_h^n - \dot{\mathbf{d}}_h^{n-1}, \boldsymbol{\sigma}(\mathbf{u}_h^n, -p_h^n) \mathbf{n})_\Sigma \right]}_{T_1} \\
& \quad + \underbrace{\tau \kappa (\dot{\mathbf{d}}_h^n - \dot{\mathbf{d}}_h^{n-1}, \dot{\mathbf{d}}_h^n)_\Sigma + \frac{\gamma\kappa\mu}{\gamma\mu + \kappa h} \tau (\mathbf{u}_h^n - \dot{\mathbf{d}}_h^{n-1}, \mathbf{u}_h^n - \dot{\mathbf{d}}_h^n)_\Sigma}_{T_2} \\
& \quad - \underbrace{\frac{h}{\gamma\mu + \kappa h} \tau (\boldsymbol{\sigma}(\mathbf{u}_h^n, p_h^n) \mathbf{n}, \boldsymbol{\sigma}(\mathbf{u}_h^n, -p_h^n) \mathbf{n})_\Sigma}_{T_3} \leq 0. \quad (90)
\end{aligned}$$

Note that the solid inertia term is included in term T_2 . We now proceed by estimating separately the terms T_1 , T_2 and T_3 . For the first, we have

$$\begin{aligned}
T_1 &= - \underbrace{\frac{\kappa h}{\gamma\mu + \kappa h} 2\tau (\boldsymbol{\sigma}(\mathbf{u}_h^n, 0) \mathbf{n}, \mathbf{u}_h^n - \dot{\mathbf{d}}_h^n)_\Sigma}_{T_{1,1}} - \underbrace{\frac{\kappa h}{\gamma\mu + \kappa h} \tau (\boldsymbol{\sigma}(\mathbf{u}_h^n, 0) \mathbf{n}, \dot{\mathbf{d}}_h^n - \dot{\mathbf{d}}_h^{n-1})_\Sigma}_{T_{1,2}} \\
& \quad + \underbrace{\frac{\kappa h}{\gamma\mu + \kappa h} \tau (\boldsymbol{\sigma}(\mathbf{0}, p_h^n) \mathbf{n}, \dot{\mathbf{d}}_h^n - \dot{\mathbf{d}}_h^{n-1})_\Sigma}_{T_{1,3}}.
\end{aligned}$$

By combining the Cauchy-Schwarz and Young inequalities with the robust trace inequality (25), we obtain the following estimates:

$$\begin{aligned}
T_{1,1} &\geq - \frac{\kappa h}{\gamma(\gamma\mu + \kappa h)} 4\mu\tau \|\boldsymbol{\varepsilon}(\mathbf{u}_h^n)\|_{0,\Sigma} \|\mathbf{u}_h^n - \dot{\mathbf{d}}_h^n\|_{0,\Sigma} \\
&\geq - \frac{1}{2\varepsilon_1} \frac{\kappa h}{\gamma(\gamma\mu + \kappa h)} 16\mu C_{\text{TI}} \tau \|\boldsymbol{\varepsilon}(\mathbf{u}_h^n)\|_{0,\Omega_h}^2 - \frac{\varepsilon_1}{2} \frac{\gamma\kappa\mu\tau}{\gamma\mu + \kappa h} \|\mathbf{u}_h^n - \dot{\mathbf{d}}_h^n\|_{0,\Sigma}^2, \\
T_{1,2} &\geq - \frac{\kappa h}{\gamma\mu + \kappa h} 2\mu\tau \|\boldsymbol{\varepsilon}(\mathbf{u}_h^n)\|_{0,\Sigma} \|\dot{\mathbf{d}}_h^n - \dot{\mathbf{d}}_h^{n-1}\|_{0,\Sigma} \\
&\geq - \frac{1}{2\varepsilon_2} \frac{\mu}{\gamma\mu + \kappa h} 4\mu C_{\text{TI}} \tau \|\boldsymbol{\varepsilon}(\mathbf{u}_h^n)\|_{0,\Omega_h}^2 - \frac{\varepsilon_2}{2} \frac{\kappa^2 h \tau}{\gamma\mu + \kappa h} \|\dot{\mathbf{d}}_h^n - \dot{\mathbf{d}}_h^{n-1}\|_{0,\Sigma}^2, \\
T_{1,3} &\geq - \frac{\kappa h}{\gamma\mu + \kappa h} \tau \|p_h^n\|_{0,\Sigma} \|\dot{\mathbf{d}}_h^n - \dot{\mathbf{d}}_h^{n-1}\|_{0,\Sigma} \\
&\geq - \frac{1}{2\varepsilon_3} \frac{h}{\gamma\mu + \kappa h} \tau \|p_h^n\|_{0,\Sigma}^2 - \frac{\varepsilon_3}{2} \frac{\kappa^2 h \tau}{\gamma\mu + \kappa h} \|\dot{\mathbf{d}}_h^n - \dot{\mathbf{d}}_h^{n-1}\|_{0,\Sigma}^2.
\end{aligned}$$

On the other hand, by adding and subtracting suitable terms, for the second term we have

$$\begin{aligned} T_2 &= \tau \kappa (\dot{\mathbf{d}}_h^n - \dot{\mathbf{d}}_h^{n-1}, \dot{\mathbf{d}}_h^n)_\Sigma + \frac{\gamma \kappa \mu \tau}{\gamma \mu + \kappa h} (\mathbf{u}_h^n - \dot{\mathbf{d}}_h^{n-1}, \mathbf{u}_h^n - \dot{\mathbf{d}}_h^n)_\Sigma \\ &= \tau \kappa (\dot{\mathbf{d}}_h^n - \dot{\mathbf{d}}_h^{n-1}, \dot{\mathbf{d}}_h^n)_\Sigma + \frac{\gamma \kappa \mu \tau}{\gamma \mu + \kappa h} (\mathbf{u}_h^n - \dot{\mathbf{d}}_h^n + \dot{\mathbf{d}}_h^n - \dot{\mathbf{d}}_h^{n-1}, \mathbf{u}_h^n - \dot{\mathbf{d}}_h^n)_\Sigma \\ &= \tau \kappa (\dot{\mathbf{d}}_h^n - \dot{\mathbf{d}}_h^{n-1}, \dot{\mathbf{d}}_h^n)_\Sigma + \frac{\gamma \kappa \mu \tau}{\gamma \mu + \kappa h} (\dot{\mathbf{d}}_h^n - \dot{\mathbf{d}}_h^{n-1}, \mathbf{u}_h^n - \dot{\mathbf{d}}_h^n)_\Sigma + \frac{\gamma \kappa \mu \tau}{\gamma \mu + \kappa h} \|\mathbf{u}_h^n - \dot{\mathbf{d}}_h^n\|_{0,\Sigma}^2. \end{aligned}$$

Hence, using the Cauchy-Schwarz inequality, we infer the following fundamental lower bound

$$T_2 \geq \frac{\rho^s \epsilon}{2} \tau \partial_\tau \|\dot{\mathbf{d}}_h^n\|_{0,\Sigma}^2 + \frac{1}{2} \frac{\kappa^2 h \tau}{\gamma \mu + \kappa h} \|\dot{\mathbf{d}}_h^n - \dot{\mathbf{d}}_h^{n-1}\|_{0,\Sigma}^2 + \frac{1}{2} \frac{\gamma \kappa \mu \tau}{\gamma \mu + \kappa h} \|\mathbf{u}_h^n - \dot{\mathbf{d}}_h^n\|_{0,\Sigma}^2.$$

Finally, for the last term, using once more the Cauchy-Schwarz and Young inequalities, we get

$$T_3 \geq -\frac{\mu}{\gamma \mu + \kappa h} 4\mu C_{\text{TI}} \tau \|\boldsymbol{\varepsilon}(\mathbf{u}_h^n)\|_{0,\Omega_h}^2 + \frac{h \tau}{\gamma \mu + \kappa h} \|p_h^n\|_{0,\Sigma}^2.$$

By collecting the above bounds for T_1 , T_2 and T_3 and inserting them into (90), we obtain

$$\begin{aligned} & \frac{\rho^f}{2} (\tau \partial_\tau \|\mathbf{u}_h^n\|_{0,\Omega}^2 + \|\mathbf{u}_h^n - \mathbf{u}_h^{n-1}\|_{0,\Omega}^2) + \tilde{c}_g \tau g_h(\mathbf{u}_h^n, \mathbf{u}_h^n) + \tau s_h(p_h^n, p_h^n) + \frac{\rho^s \epsilon}{2} \tau \partial_\tau \|\dot{\mathbf{d}}_h^n\|_{0,\Sigma}^2 \\ & + \frac{1}{2} (\tau \partial_\tau \|\mathbf{d}_h^n\|_s^2 + \|\mathbf{d}_h^n - \mathbf{d}_h^{n-1}\|_s^2) + \tau \mu \left[\tilde{c}_g - \frac{4C_{\text{TI}}}{\gamma} \frac{(1 + \frac{1}{2\varepsilon_2}) \gamma \mu + \frac{2}{\varepsilon_1} \kappa h}{\gamma \mu + \kappa h} \right] \|\boldsymbol{\varepsilon}(\mathbf{u}_h^n)\|_{0,\Omega_h}^2 \\ & + \frac{1}{2} \frac{\gamma \kappa \mu}{\gamma \mu + \kappa h} \tau (1 - \varepsilon_1) \|\mathbf{u}_h^n - \dot{\mathbf{d}}_h^n\|_{0,\Sigma}^2 + \frac{1}{2} \kappa \frac{\kappa h}{\gamma \mu + \kappa h} \tau (1 - (\varepsilon_2 + \varepsilon_3)) \|\dot{\mathbf{d}}_h^n - \dot{\mathbf{d}}_h^{n-1}\|_{0,\Sigma}^2 \\ & + \frac{h}{\gamma \mu + \kappa h} \tau \left(1 - \frac{1}{2\varepsilon_3} \right) \|p_h^n\|_{0,\Sigma}^2 \leq 0. \end{aligned}$$

The estimate (89) then follows by choosing

$$\varepsilon_1 = \frac{2}{3}, \quad \varepsilon_2 = \frac{1}{4}, \quad \varepsilon_3 = \frac{5}{8}, \quad \gamma > \frac{12C_{\text{TI}}}{\tilde{c}_g},$$

using Korn's inequality and summing over $m = 1, \dots, n$. This completes the proof. \square

4.3.2 Convergence analysis

In the sequel we assume that the interface Σ is flat and that the exact solution of problem (1)-(2) has the regularity given by (45) and (46) for a given final time $T \geq \tau$. For the derivation of the error estimate, we also build on the decomposition of the error given by (47)-(48). Let us first estimate the discrete errors $(\boldsymbol{\theta}_h^n, y_h^n, \boldsymbol{\xi}_h^n, \dot{\boldsymbol{\xi}}_h^n)$. An a priori bound is stated in Theorem 4.2 below, with the energy-norm of the discrete error being defined, at time step t_n , as

$$\begin{aligned} \tilde{\mathcal{E}}_h^n &\stackrel{\text{def}}{=} (\rho^f)^{\frac{1}{2}} \|\boldsymbol{\theta}_h^n\|_{0,\Omega} + (\rho^s \epsilon)^{\frac{1}{2}} \|\dot{\boldsymbol{\xi}}_h^n\|_{0,\Sigma} + \|\boldsymbol{\xi}_h^n\|_s + \left(\sum_{m=1}^n c_g \tau \mu \|\nabla \boldsymbol{\theta}_h^m\|_{0,\Omega}^2 \right)^{\frac{1}{2}} \\ &+ \left(\sum_{m=1}^n c_g \tau |(\boldsymbol{\theta}_h^m, y_h^m)|_S^2 \right)^{\frac{1}{2}} + \left(\sum_{m=1}^n \frac{\gamma \kappa \mu}{\gamma \mu + \kappa h} \tau \|\boldsymbol{\theta}_h^m - \dot{\boldsymbol{\xi}}_h^m\|_{0,\Sigma}^2 \right)^{\frac{1}{2}} + \left(\sum_{m=1}^n \frac{h}{\gamma \mu + \kappa h} \tau \|y_h^m\|_{0,\Sigma}^2 \right)^{\frac{1}{2}} \end{aligned}$$

for $n > 0$.

Theorem 4.2. Let $(\mathbf{u}, p, \mathbf{d}, \dot{\mathbf{d}})$ be the solution of the coupled problem (1)-(2) and $\{(\mathbf{u}_h^n, p_h^n, \mathbf{d}_h^n, \dot{\mathbf{d}}_h^n)\}_{n>r}$ be the approximation given by Algorithm 3 with initial data $(\mathbf{u}_h^0, \mathbf{d}_h^0, \dot{\mathbf{d}}_h^0) = (i_{sz}E_2\mathbf{u}^0, \pi_h^s\mathbf{d}^0, \mathcal{I}_h\dot{\mathbf{d}}^0)$ and $r = 0$. We assume that the exact solution has the regularity (45)-(46). Assume that $\gamma > 0$ is given by Theorem 4.1. Then, we have the following error estimates, for $n > r$ and $n\tau < T$:

$$\tilde{\mathcal{E}}_h^n \lesssim c_1 h + c_2 \tau + c_3 \tau^{\frac{1}{2}}. \quad (91)$$

Here, the symbols $\{c_i\}_{i=1}^3$ denote positive constants independent of h and τ , but which depend on the physical parameters and on the regularity of $(\mathbf{u}, p, \mathbf{d}, \dot{\mathbf{d}})$.

Proof. At time t_n , the exact solution $(\mathbf{u}, p, \mathbf{d}, \dot{\mathbf{d}})$ of the coupled problem (1)-(2) satisfies

$$\left\{ \begin{array}{ll} \rho^f \partial_t \mathbf{u}^n - \operatorname{div} \boldsymbol{\sigma}(\mathbf{u}^n, p^n) = \mathbf{0} & \text{in } \Omega, \\ \operatorname{div} \mathbf{u}^n = 0 & \text{in } \Omega, \\ \mathbf{u}^n = \mathbf{0} & \text{on } \Gamma^f, \\ \boldsymbol{\sigma}(\mathbf{u}^n, p^n) \mathbf{n} + \kappa \mathbf{u}^n = \kappa \dot{\mathbf{d}}^{n-1} - \mathbf{L} \mathbf{d}^n - \rho^s \epsilon (\partial_t - \partial_\tau) \dot{\mathbf{d}}^n & \text{on } \Sigma, \end{array} \right. \quad \left\{ \begin{array}{ll} \mathbf{u}^n = \dot{\mathbf{d}}^n & \text{on } \Sigma, \\ \rho^s \epsilon \partial_t \dot{\mathbf{d}}^n + \mathbf{L}^e \mathbf{d}^n = -\boldsymbol{\sigma}(\mathbf{u}^n, p^n) \mathbf{n} & \text{on } \Sigma, \\ \dot{\mathbf{d}}^n = \partial_t \mathbf{d}^n & \text{on } \Sigma, \\ \mathbf{d}^n = \mathbf{0} & \text{on } \partial \Sigma. \end{array} \right.$$

Then, similarly to Lemma 4.1, we can show that the exact solution, at time t_n , of the coupled problem (1)-(2) satisfies

$$\begin{aligned} & \rho^f (\partial_t \mathbf{u}^n, \mathbf{v}_h)_\Omega + a^f((\mathbf{u}^n, p^n), (\mathbf{v}_h, q_h)) + \rho^s \epsilon (\partial_t \dot{\mathbf{d}}^n, \mathbf{w}_h)_\Sigma + a^s(\mathbf{d}^n, \mathbf{w}_h) \\ & + \frac{\gamma \kappa \mu}{\gamma \mu + \kappa h} (\mathbf{u}^n - \dot{\mathbf{d}}^{n-1}, \mathbf{v}_h - \mathbf{w}_h)_\Sigma + \frac{\gamma \mu}{\gamma \mu + \kappa h} (\mathbf{L} \mathbf{d}^n + \rho^s \epsilon (\partial_t - \partial_\tau) \dot{\mathbf{d}}^n, \mathbf{v}_h - \mathbf{w}_h)_\Sigma \\ & - \frac{\kappa h}{\gamma \mu + \kappa h} \left[(\boldsymbol{\sigma}(\mathbf{u}^n, p^n) \mathbf{n}, \mathbf{v}_h - \mathbf{w}_h)_\Sigma + (\mathbf{u}^n - \dot{\mathbf{d}}^{n-1}, \boldsymbol{\sigma}(\mathbf{v}_h, -q_h) \mathbf{n})_\Sigma \right] \\ & - \frac{h}{\gamma \mu + \kappa h} (\mathbf{L} \mathbf{d}^n + \rho^s \epsilon (\partial_t - \partial_\tau) \dot{\mathbf{d}}^n, \boldsymbol{\sigma}(\mathbf{v}_h, -q_h) \mathbf{n})_\Sigma - \frac{h}{\gamma \mu + \kappa h} (\boldsymbol{\sigma}(\mathbf{u}^n, p^n) \mathbf{n}, \boldsymbol{\sigma}(\mathbf{v}_h, -q_h) \mathbf{n})_\Sigma = 0 \end{aligned} \quad (92)$$

for all $\mathbf{v}_h, q_h, \mathbf{w}_h \in \mathbf{V}_h \times Q_h \times \mathbf{W}_h$. Subtracting (87) and (88) to the continuous problem (92) we obtain, after adding and subtracting $\partial_\tau \mathbf{u}^n$ and $\partial_\tau \dot{\mathbf{d}}^n$, the following modified Galerkin

orthogonality:

$$\begin{aligned}
& \rho^f (\partial_\tau (\mathbf{u}^n - \mathbf{u}_h^n), \mathbf{v}_h)_\Omega + a^f((\mathbf{u}^n - \mathbf{u}_h^n, p^n - p_h^n), (\mathbf{v}_h, q_h)) + \rho^s \epsilon (\partial_\tau (\dot{\mathbf{d}}^n - \dot{\mathbf{d}}_h^n), \mathbf{w}_h)_\Sigma + a^s(\mathbf{d}^n - \mathbf{d}_h^n, \mathbf{w}_h) \\
& - \frac{\kappa h}{\gamma\mu + \kappa h} \left[(\boldsymbol{\sigma}(\mathbf{u}^n - \mathbf{u}_h^n, p^n - p_h^n) \mathbf{n}, \mathbf{v}_h - \mathbf{w}_h)_\Sigma + ((\mathbf{u}^n - \mathbf{u}_h^n) - (\dot{\mathbf{d}}^{n-1} - \dot{\mathbf{d}}_h^{n-1}), \boldsymbol{\sigma}(\mathbf{v}_h, -q_h) \mathbf{n})_\Sigma \right] \\
& + \frac{\gamma\kappa\mu}{\gamma\mu + \kappa h} ((\mathbf{u}^n - \mathbf{u}_h^n) - (\dot{\mathbf{d}}^{n-1} - \dot{\mathbf{d}}_h^{n-1}), \mathbf{v}_h - \mathbf{w}_h)_\Sigma - \frac{h}{\gamma\mu + \kappa h} (\boldsymbol{\sigma}(\mathbf{u}^n - \mathbf{u}_h^n, p^n - p_h^n) \mathbf{n}, \boldsymbol{\sigma}(\mathbf{v}_h, -q_h) \mathbf{n})_\Sigma \\
& = -\rho^f ((\partial_t - \partial_\tau) \mathbf{u}^n, \mathbf{v}_h)_\Omega - \rho^s \epsilon ((\partial_t - \partial_\tau) \dot{\mathbf{d}}^n, \mathbf{w}_h)_\Sigma + S_h((\mathbf{u}_h^n, p_h^n), (\mathbf{v}_h, q_h)) \\
& - \frac{\gamma\mu}{\gamma\mu + \kappa h} (\mathbf{L} \mathbf{d}^n + \rho^s \epsilon (\partial_t - \partial_\tau) \dot{\mathbf{d}}^n, \mathbf{v}_h - \mathbf{w}_h)_\Sigma + \frac{h}{\gamma\mu + \kappa h} (\mathbf{L} \mathbf{d}^n + \rho^s \epsilon (\partial_t - \partial_\tau) \dot{\mathbf{d}}^n, \boldsymbol{\sigma}(\mathbf{v}_h, -q_h) \mathbf{n})_\Sigma
\end{aligned} \tag{93}$$

for all $(\mathbf{v}_h, q_h, \mathbf{w}_h) \in \mathbf{V}_h \times Q_h \times \mathbf{W}_h$. Hence, from (47)-(48), we infer the following equation for the discrete errors $\boldsymbol{\theta}_h^n$, y_h^n , $\boldsymbol{\xi}_h^n$ and $\dot{\boldsymbol{\xi}}_h^n$:

$$\begin{aligned}
& \rho^f (\partial_\tau \boldsymbol{\theta}_h^n, \mathbf{v}_h)_\Omega + a^f((\boldsymbol{\theta}_h^n, y_h^n), (\mathbf{v}_h, q_h)) + S_h((\boldsymbol{\theta}_h^n, y_h^n), (\mathbf{v}_h, q_h)) + \rho^s \epsilon (\partial_\tau \dot{\boldsymbol{\xi}}_h^n, \mathbf{w}_h)_\Sigma + a^s(\boldsymbol{\xi}_h^n, \mathbf{w}_h) \\
& - \frac{\kappa h}{\gamma\mu + \kappa h} \left[(\boldsymbol{\sigma}(\boldsymbol{\theta}_h^n, y_h^n) \mathbf{n}, \mathbf{v}_h - \mathbf{w}_h)_\Sigma + (\boldsymbol{\theta}_h^n - \dot{\boldsymbol{\xi}}_h^{n-1}, \boldsymbol{\sigma}(\mathbf{v}_h, -q_h) \mathbf{n})_\Sigma \right] \\
& + \frac{\gamma\kappa\mu}{\gamma\mu + \kappa h} (\boldsymbol{\theta}_h^n - \dot{\boldsymbol{\xi}}_h^{n-1}, \mathbf{v}_h - \mathbf{w}_h)_\Sigma - \frac{h}{\gamma\mu + \kappa h} (\boldsymbol{\sigma}(\boldsymbol{\theta}_h^n, y_h^n) \mathbf{n}, \boldsymbol{\sigma}(\mathbf{v}_h, -q_h) \mathbf{n})_\Sigma \\
& = -\rho^f ((\partial_t - \partial_\tau) \mathbf{u}^n, \mathbf{v}_h)_\Omega - \rho^f (\partial_\tau \boldsymbol{\theta}_\pi^n, \mathbf{v}_h)_\Omega - \rho^s \epsilon ((\partial_t - \partial_\tau) \dot{\mathbf{d}}^n, \mathbf{w}_h)_\Sigma - \rho^s \epsilon (\partial_\tau \dot{\boldsymbol{\xi}}_\pi^n, \mathbf{w}_h)_\Sigma \\
& - a^s(\boldsymbol{\xi}_\pi^n, \mathbf{w}_h) + S_h((i_{sz} E_2 \mathbf{u}^n, i_{sz} E_1 p^n), (\mathbf{v}_h, q_h)) - a^f((\boldsymbol{\theta}_\pi^n, y_\pi^n), (\mathbf{v}_h, q_h)) \\
& + \frac{\kappa h}{\gamma\mu + \kappa h} \left[(\boldsymbol{\sigma}(\boldsymbol{\theta}_\pi^n, y_\pi^n) \mathbf{n}, \mathbf{v}_h - \mathbf{w}_h)_\Sigma + (\boldsymbol{\theta}_\pi^n - \dot{\boldsymbol{\xi}}_\pi^{n-1}, \boldsymbol{\sigma}(\mathbf{v}_h, -q_h) \mathbf{n})_\Sigma \right] \\
& - \frac{\gamma\kappa\mu}{\gamma\mu + \kappa h} (\boldsymbol{\theta}_\pi^n - \dot{\boldsymbol{\xi}}_\pi^{n-1}, \mathbf{v}_h - \mathbf{w}_h)_\Sigma + \frac{h}{\gamma\mu + \kappa h} (\boldsymbol{\sigma}(\boldsymbol{\theta}_\pi^n, y_\pi^n) \mathbf{n}, \boldsymbol{\sigma}(\mathbf{v}_h, -q_h) \mathbf{n})_\Sigma \\
& - \frac{\gamma\mu}{\gamma\mu + \kappa h} (\mathbf{L} \mathbf{d}^n + \rho^s \epsilon (\partial_t - \partial_\tau) \dot{\mathbf{d}}^n, \mathbf{v}_h - \mathbf{w}_h)_\Sigma + \frac{h}{\gamma\mu + \kappa h} (\mathbf{L} \mathbf{d}^n + \rho^s \epsilon (\partial_t - \partial_\tau) \dot{\mathbf{d}}^n, \boldsymbol{\sigma}(\mathbf{v}_h, -q_h) \mathbf{n})_\Sigma
\end{aligned} \tag{94}$$

for all $(\mathbf{v}_h, q_h, \mathbf{w}_h) \in \mathbf{V}_h \times Q_h \times \mathbf{W}_h$ and $n > r$. Note that $a^s(\boldsymbol{\xi}_\pi^n, \mathbf{w}_h) = 0$ due to the definition of the solid projection operator $\boldsymbol{\pi}_h^s$. Taking $(\mathbf{v}_h, q_h, \mathbf{w}_h) = \tau(\boldsymbol{\theta}_h^n, y_h^n, \dot{\boldsymbol{\xi}}_h^n)$ in (94), using the stability estimate reported in Theorem 4.1 and (50), yields the following energy inequality for the discrete

errors:

$$\begin{aligned}
& \frac{\rho^f}{2} (\tau \partial_\tau \|\boldsymbol{\theta}_h^n\|_{0,\Omega}^2 + \tau^2 \|\partial_\tau \boldsymbol{\theta}_h^n\|_{0,\Omega}^2) + \tilde{c}_g \tau (\mu \|\nabla \boldsymbol{\theta}_h^n\|_{0,\Omega_h}^2 + |(\boldsymbol{\theta}_h^n, \mathbf{y}_h^n)|_S^2) \\
& + \frac{1}{2} (\tau \partial_\tau \|\boldsymbol{\xi}_h^n\|_s^2 + \tau^2 \|\partial_\tau \boldsymbol{\xi}_h^n\|_s^2) + \frac{1}{6} \frac{\gamma \kappa \mu}{\gamma \mu + \kappa h} \tau \|\boldsymbol{\theta}_h^n - \dot{\boldsymbol{\xi}}_h^n\|_{0,\Sigma}^2 \\
& + \frac{1}{5} \frac{h}{\gamma \mu + \kappa h} \tau \|\mathbf{y}_h^n\|_{0,\Sigma}^2 + \frac{\rho^s \epsilon}{2} \left(\tau \partial_\tau \|\dot{\boldsymbol{\xi}}_h^n\|_{0,\Sigma}^2 + \frac{1}{8} \frac{\kappa h}{\gamma \mu + \kappa h} \tau^2 \|\partial_\tau \dot{\boldsymbol{\xi}}_h^n\|_{0,\Sigma}^2 \right) \\
& \leq \underbrace{-\rho^f \tau ((\partial_t - \partial_\tau) \mathbf{u}^n, \boldsymbol{\theta}_h^n)_\Omega - \rho^f \tau (\partial_\tau \boldsymbol{\theta}_\pi^n, \boldsymbol{\theta}_h^n)_\Omega}_{T_1} \\
& \quad \underbrace{-\rho^s \epsilon \tau ((\partial_t - \partial_\tau) \dot{\mathbf{d}}^n, \dot{\boldsymbol{\xi}}_h^n)_\Sigma - \rho^s \epsilon \tau (\partial_\tau \dot{\boldsymbol{\xi}}_\pi^n, \dot{\boldsymbol{\xi}}_h^n)_\Sigma}_{T_2} \underbrace{-\tau a^s(\boldsymbol{\xi}_h^n, \mathbf{z}_h^n)}_{T_3} \\
& \quad \underbrace{+\tau S_h((i_{sz} E_2 \mathbf{u}(t), i_{sz} E_1 p(t)), (\boldsymbol{\theta}_h^n, \mathbf{y}_h^n))}_{T_4} \underbrace{-\tau \frac{\gamma \kappa \mu}{\gamma \mu + \kappa h} (\boldsymbol{\theta}_\pi^n - \dot{\boldsymbol{\xi}}_\pi^n, \boldsymbol{\theta}_h^n - \dot{\boldsymbol{\xi}}_h^n)_\Sigma}_{T_5} \\
& \quad \underbrace{+\tau \frac{\kappa h}{\gamma \mu + \kappa h} (\boldsymbol{\sigma}(\boldsymbol{\theta}_\pi^n, \mathbf{y}_\pi^n) \mathbf{n}, \boldsymbol{\theta}_h^n - \dot{\boldsymbol{\xi}}_h^n)_\Sigma}_{T_6} \\
& \quad \underbrace{-\tau a^f((\boldsymbol{\theta}_\pi^n, \mathbf{y}_\pi^n), (\boldsymbol{\theta}_h^n, \mathbf{y}_h^n)) + \tau \frac{\kappa h}{\gamma \mu + \kappa h} (\boldsymbol{\theta}_\pi^n - \dot{\boldsymbol{\xi}}_\pi^n, \boldsymbol{\sigma}(\boldsymbol{\theta}_h^n, -\mathbf{y}_h^n) \mathbf{n})_\Sigma}_{T_7} \\
& \quad \underbrace{+\tau \frac{h}{\gamma \mu + \kappa h} (\boldsymbol{\sigma}(\boldsymbol{\theta}_\pi^n, \mathbf{y}_\pi^n) \mathbf{n}, \boldsymbol{\sigma}(\boldsymbol{\theta}_h^n, -\mathbf{y}_h^n) \mathbf{n})_\Sigma}_{T_8} \underbrace{-\tau \frac{\gamma \kappa \mu}{\gamma \mu + \kappa h} (\dot{\boldsymbol{\xi}}_\pi^n - \dot{\boldsymbol{\xi}}_\pi^{n-1}, \boldsymbol{\theta}_h^n - \dot{\boldsymbol{\xi}}_h^n)_\Sigma}_{T_9} \\
& \quad \underbrace{+\tau \frac{\kappa h}{\gamma \mu + \kappa h} (\dot{\boldsymbol{\xi}}_\pi^n - \dot{\boldsymbol{\xi}}_\pi^{n-1}, \boldsymbol{\sigma}(\boldsymbol{\theta}_h^n, -\mathbf{y}_h^n) \mathbf{n})_\Sigma}_{T_{10}} \\
& \quad \underbrace{-\frac{\gamma \mu}{\gamma \mu + \kappa h} (\mathbf{L} \mathbf{d}^n + \rho^s \epsilon (\partial_t - \partial_\tau) \dot{\mathbf{d}}^n, \boldsymbol{\theta}_h^n - \dot{\boldsymbol{\xi}}_h^n)_\Sigma}_{T_{11}} \\
& \quad \underbrace{+\frac{h}{\gamma \mu + \kappa h} (\mathbf{L} \mathbf{d}^n + \rho^s \epsilon (\partial_t - \partial_\tau) \dot{\mathbf{d}}^n, \boldsymbol{\sigma}(\boldsymbol{\theta}_h^n, -\mathbf{y}_h^n) \mathbf{n})_\Sigma}_{T_{12}}
\end{aligned} \tag{95}$$

with $\tilde{c}_g > 0$. The terms $T_1 - T_4$ stem from the time-stepping and the stabilization methods. The terms $T_5 - T_8$ come from the generalized Nitsche's method. Finally, terms $T_9 - T_{12}$ are due to the kinematic perturbation and, hence, are inherent to the fluid-solid time-splitting scheme.

Note that terms T_1 , T_3 and T_4 can be bounded exactly as in (57), (60) and (61). For term T_2 we can proceed in a similar manner to (58) to get

$$T_2 \lesssim \frac{\rho^s \epsilon T}{2\varepsilon_2} (\tau^2 \|\partial_{tt} \mathbf{u}\|_{L^2(t_{n-1}, t_n; L^2(\Sigma))}^2 + h^2 \|\partial_t \dot{\mathbf{d}}\|_{L^2(t_{n-1}, t_n; H^2(\Sigma))}^2) + \varepsilon_2 \tau \frac{\rho^s \epsilon}{T} \|\dot{\boldsymbol{\xi}}_h^n\|_{0,\Sigma}^2. \tag{96}$$

The last term will be treated using Lemma 3.1.

The boundary penalty term T_5 can be handled in a similar manner to (62) yielding

$$T_5 \lesssim \tau h^2 \frac{\gamma\mu}{\varepsilon_5} (\|\mathbf{u}^n\|_{2,\Omega}^2 + h\|\dot{\mathbf{d}}^n\|_{2,\Sigma}^2) + \tau \frac{\varepsilon_5}{2} \frac{\gamma\kappa\mu}{\gamma\mu + \kappa h} \|\boldsymbol{\theta}_h^n - \dot{\boldsymbol{\xi}}_\pi^n\|_{0,\Sigma}^2,$$

where we have used that

$$0 < \frac{\kappa h}{\gamma\mu + \kappa h} < 1.$$

Note that the second term can be absorbed in the left-hand side of (95), for $\varepsilon_5 > 0$ small enough.

Similarly, for the consistency term T_6 , we have, using (42)

$$T_6 \lesssim \tau h^2 \frac{1}{\varepsilon_6 \gamma\mu} (\|\mathbf{u}^n\|_{2,\Omega}^2 + \|p^n\|_{1,\Omega}^2) + \tau \frac{\varepsilon_6}{2} \frac{\gamma\kappa\mu}{\gamma\mu + \kappa h} \|\boldsymbol{\theta}_h^n - \dot{\boldsymbol{\xi}}_\pi^n\|_{0,\Sigma}^2.$$

Note that the first term has the right convergence order and the second term can be absorbed in the left hand side of (95), for $\varepsilon_6 > 0$ sufficiently small.

As in the proof of Theorem 3.2, we split T_7 into two parts. The velocity-velocity coupling contribution can be easily handled as in (64), viz.,

$$\begin{aligned} & -\tau a(\boldsymbol{\theta}_\pi^n, \boldsymbol{\theta}_h^n) + \tau \frac{\kappa h}{\gamma\mu + \kappa h} (\boldsymbol{\sigma}(\boldsymbol{\theta}_h^n, 0)\mathbf{n}, \boldsymbol{\theta}_\pi^n - \dot{\boldsymbol{\xi}}_\pi^n)_\Sigma \\ & \lesssim \tau h^2 \frac{\mu}{\varepsilon_7 C_{\text{TI}}} \|\mathbf{u}^n\|_{2,\Omega}^2 + \tau \mu \frac{2}{\varepsilon_7} h^2 (\|\mathbf{u}^n\|_{2,\Omega}^2 + \|\dot{\mathbf{d}}^n\|_{2,\Sigma}^2) + 2\tau \varepsilon_7 \mu C_{\text{TI}} \|\nabla \boldsymbol{\theta}_h^n\|_{0,\Omega_h}^2. \end{aligned}$$

The last term can be, once again, absorbed in the left hand side of (95), for $\varepsilon_7 > 0$ sufficiently small. For the velocity-pressure coupling part we write, using integration by parts in the continuity equation,

$$\begin{aligned} & -\tau b(y_\pi^n, \boldsymbol{\theta}_h^n) + \tau b(y_h^n, \boldsymbol{\theta}_\pi^n) + \tau \frac{\kappa h}{\gamma\mu + \kappa h} (\boldsymbol{\sigma}(0, -y_h^n)\mathbf{n}, \boldsymbol{\theta}_\pi^n - \dot{\boldsymbol{\xi}}_\pi^n)_\Sigma \\ & = \underbrace{\tau(y_\pi^n, \text{div} \boldsymbol{\theta}_h^n)_\Omega}_{T_{7,1}} + \underbrace{\tau(\nabla y_h^n, \boldsymbol{\theta}_\pi^n)_\Omega}_{T_{7,2}} - \underbrace{\tau \frac{\kappa h}{\gamma\mu + \kappa h} (y_h^n \mathbf{n}, \dot{\boldsymbol{\xi}}_\pi^n)_\Sigma}_{T_{7,3}} - \underbrace{\tau \frac{\gamma\mu}{\gamma\mu + \kappa h} (y_h^n \mathbf{n}, \boldsymbol{\theta}_\pi^n)_\Sigma}_{T_{7,4}}. \end{aligned}$$

Terms $T_{7,1}$ and $T_{7,2}$ can be bounded as in (65). The control for $T_{7,3}$ follows as in (66). For $T_{7,4}$, using (44), we have

$$\begin{aligned} T_{7,4} & \leq \tau \frac{1}{2\varepsilon_{7,4}} \gamma\mu \|\boldsymbol{\theta}_\pi^n\|_{\frac{1}{2},h,\Sigma}^2 + \tau \frac{\varepsilon_{7,4}}{2} \frac{h}{\gamma\mu + \kappa h} \|y_h^n\|_{0,\Sigma}^2 \\ & \lesssim \tau h^2 \frac{\gamma\mu}{\varepsilon_{7,4}} \|\mathbf{u}^n\|_{2,\Omega}^2 + \tau \frac{\varepsilon_{7,4}}{2} \frac{h}{\gamma\mu + \kappa h} \|y_h^n\|_{0,\Sigma}^2, \end{aligned}$$

the last term can be absorbed in the left hand side of (95), for $\varepsilon_{7,4} > 0$ small enough. The above estimations of $T_{7,1}$, $T_{7,2}$, $T_{7,3}$ and $T_{7,4}$ provide bounds which involve either terms with the right convergence order or contributions that can be absorbed by the left-hand side of (95).

For the term T_8 we have

$$\begin{aligned} T_8 & = \tau \frac{h}{\gamma\mu + \kappa h} (\boldsymbol{\sigma}(\boldsymbol{\theta}_\pi^n, y_\pi^n)\mathbf{n}, \boldsymbol{\sigma}(\boldsymbol{\theta}_h^n, 0)\mathbf{n})_\Sigma + \tau \frac{h}{\gamma\mu + \kappa h} (\boldsymbol{\sigma}(\boldsymbol{\theta}_\pi^n, y_\pi^n)\mathbf{n}, y_h^n \mathbf{n})_\Sigma \\ & \leq \tau \frac{1}{\varepsilon_8} \frac{1}{\gamma\mu + \kappa h} \|\boldsymbol{\sigma}(\boldsymbol{\theta}_\pi^n, y_\pi^n)\mathbf{n}\|_{-\frac{1}{2},h,\Sigma}^2 + 2\tau \varepsilon_8 \frac{\mu}{\gamma\mu + \kappa h} \|\varepsilon(\boldsymbol{\theta}_h^n)\mathbf{n}\|_{-\frac{1}{2},h,\Sigma}^2 \\ & \quad + \tau \frac{\varepsilon_8}{2} \frac{h}{\gamma\mu + \kappa h} \|y_h^n\|_{0,\Sigma}^2, \\ & \lesssim \tau h^2 \frac{1}{\varepsilon_8 \gamma\mu} (\|\mathbf{u}^n\|_{2,\Omega}^2 + \|p^n\|_{1,\Omega}^2) + 2\tau \varepsilon_8 \frac{1}{\gamma} \mu C_{\text{TI}} \|\nabla \boldsymbol{\theta}_h^n\|_{0,\Omega_h}^2 + \tau \frac{\varepsilon_8}{2} \frac{h}{\gamma\mu + \kappa h} \|y_h^n\|_{0,\Sigma}^2, \end{aligned} \quad \text{Inria}$$

and the last two terms can be absorbed by the left-hand side of (95), for $\varepsilon_8 > 0$ small enough.

The boundary penalty term T_9 can be controlled using a Taylor expansion

$$\begin{aligned} T_9 &\leq \tau \frac{1}{2\varepsilon_9} \frac{\gamma\kappa\mu}{\gamma\mu + \kappa h} \|\tau \partial_\tau \dot{\boldsymbol{\xi}}_\pi^n\|_{0,\Sigma}^2 + \tau \frac{\varepsilon_9}{2} \frac{\gamma\kappa\mu}{\gamma\mu + \kappa h} \|\boldsymbol{\theta}_h^n - \dot{\boldsymbol{\xi}}_h^n\|_{0,\Sigma}^2 \\ &\lesssim \tau^2 \frac{1}{2\varepsilon_9} \frac{\gamma\kappa\mu}{\gamma\mu + \kappa h} \|\partial_t \dot{\boldsymbol{\xi}}_\pi^n\|_{L^2(t_{n-1}, t_n; L^2(\Sigma))}^2 + \tau \frac{\varepsilon_9}{2} \frac{\gamma\kappa\mu}{\gamma\mu + \kappa h} \|\boldsymbol{\theta}_h^n - \dot{\boldsymbol{\xi}}_h^n\|_{0,\Sigma}^2 \\ &\lesssim \tau \frac{1}{2\varepsilon_9} h^2 \rho^s \epsilon \|\partial_t \mathbf{u}\|_{L^2(t_{n-1}, t_n; H^2(\Sigma))}^2 + \tau \frac{\varepsilon_9}{2} \frac{\gamma\kappa\mu}{\gamma\mu + \kappa h} \|\boldsymbol{\theta}_h^n - \dot{\boldsymbol{\xi}}_h^n\|_{0,\Sigma}^2. \end{aligned}$$

Note that the second term can be absorbed in the left-hand side of (95), for $\varepsilon_9 > 0$ small enough.

Similarly, the boundary penalty term T_{10} is bounded by

$$\begin{aligned} T_{10} &= \tau \frac{\kappa h}{\gamma\mu + \kappa h} (\dot{\boldsymbol{\xi}}_\pi^n - \dot{\boldsymbol{\xi}}_\pi^{n-1}, \boldsymbol{\sigma}(\boldsymbol{\theta}_h^n, 0)\mathbf{n})_\Sigma + \tau \frac{\kappa h}{\gamma\mu + \kappa h} (\dot{\boldsymbol{\xi}}_\pi^n - \dot{\boldsymbol{\xi}}_\pi^{n-1}, y_h^n \mathbf{n})_\Sigma \\ &\lesssim \tau \frac{1}{2\varepsilon_{10}} h^2 \rho^s \epsilon \|\partial_t \dot{\mathbf{d}}\|_{L^2(t_{n-1}, t_n; H^2(\Sigma))}^2 + 2\tau \varepsilon_{10} \mu C_{\text{TI}} \|\nabla \boldsymbol{\theta}_h^n\|_{0,\Omega_h}^2 + \tau \frac{\varepsilon_{10}}{2} \frac{h}{\gamma\mu + \kappa h} \|y_h^n\|_{0,\Sigma}^2, \end{aligned}$$

Note that the second term can be absorbed in the left-hand side of (95), for $\varepsilon_{10} > 0$ small enough.

Similarly, the boundary penalty term T_{11} is bounded by

$$T_{11} \lesssim \tau \frac{1}{2\varepsilon_{11}} \rho^s \epsilon \tau^2 \|\partial_{tt} \mathbf{u}\|_{L^2(t_{n-1}, t_n; L^2(\Sigma))}^2 + \tau \frac{1}{2\varepsilon_{11}} \frac{\tau}{\rho^s \epsilon} \|\mathbf{L}^e \mathbf{d}^n\|_{0,\Sigma}^2 + \tau \frac{\varepsilon_{11}}{2} \frac{\gamma\kappa\mu}{\gamma\mu + \kappa h} \|\boldsymbol{\theta}_h^n - \dot{\boldsymbol{\xi}}_h^n\|_{0,\Sigma}^2.$$

The last term can be absorbed in the left-hand side of (95), for $\varepsilon_{11} > 0$ sufficiently small.

Similarly, the boundary penalty term T_{12} is bounded by

$$T_{12} \lesssim \tau \frac{1}{\varepsilon_{12}} \rho^s \epsilon \tau^2 \|\partial_{tt} \mathbf{u}\|_{L^2(t_{n-1}, t_n; L^2(\Sigma))}^2 + \tau \frac{1}{\varepsilon_{12}} \frac{\tau}{\rho^s \epsilon} \|\mathbf{L}^e \mathbf{d}^n\|_{0,\Sigma}^2 + \tau \varepsilon_{12} C_{\text{TI}} \mu \|\nabla \boldsymbol{\theta}_h^n\|_{0,\Omega_h}^2 + \tau \varepsilon_{12} \frac{h}{\gamma\mu + \kappa h} \|y_h^n\|_{0,\Sigma}^2,$$

The last term can be absorbed in the left-hand side of (95), for $\varepsilon_{12} > 0$ small enough.

The estimate (91) follows by inserting the above estimates into (95), summing over $m = 1, \dots, n$, and applying Lemma 3.1 with

$$a_m = \frac{\rho^f}{2} \|\boldsymbol{\theta}_h^m\|_{0,\Omega}^2 + \frac{\rho^s \epsilon}{2} \|\dot{\boldsymbol{\xi}}_h^m\|_{0,\Sigma}^2 + \frac{1}{2} \|\boldsymbol{\xi}_h^m\|_s^2, \quad \eta_m = \frac{1}{T}.$$

Note in particular that, owing to the selection of the initial data, we have

$$\boldsymbol{\theta}_h^0 = \mathbf{0}, \quad \dot{\boldsymbol{\xi}}_h^0 = \boldsymbol{\xi}_h^0 = \mathbf{0}.$$

□

We define the energy-norm of the error and dissipation error, at time step t_n , as

$$\begin{aligned} \tilde{\mathcal{Z}}_h^n &\stackrel{\text{def}}{=} (\rho^f)^{\frac{1}{2}} \|\mathbf{u}^n - \mathbf{u}_h^n\|_{0,\Omega} + (\rho^s \epsilon)^{\frac{1}{2}} \|\dot{\mathbf{d}}^n - \dot{\mathbf{d}}_h^n\|_{0,\Sigma} + \|\mathbf{d}^n - \mathbf{d}_h^n\|_s, \\ &\quad \left(\sum_{m=1}^n c_g \tau \mu \|\nabla(\mathbf{u}^m - \mathbf{u}_h^m)\|_{0,\Omega} \right)^{\frac{1}{2}} + \left(\sum_{m=1}^n c_g \tau |(u_h^m, p_h^m)|_S^2 \right)^{\frac{1}{2}} + \left(\sum_{m=1}^n c_g \tau \frac{\gamma\kappa\mu}{\gamma\mu + \kappa h} \|\mathbf{u}_h^m - \dot{\mathbf{d}}_h^m\|_{0,\Sigma}^2 \right)^{\frac{1}{2}} \end{aligned}$$

for $n > 0$. We have the following a priori estimate as a corollary of Theorem 4.2.

Corollary 4.1. *Under the assumptions of Theorem 4.2, we have the following error estimates, for $n > r$ and $n\tau < T$:*

$$\tilde{\mathcal{Z}}_h^n \lesssim c_1 h + c_2 \tau + c_3 \tau^{\frac{1}{2}}.$$

Here, the symbols $\{c_i\}_{i=1}^3$ denote positive constants independent of h and τ , but which depend on the physical parameters and on the regularity of $(\mathbf{u}, p, \mathbf{d}, \dot{\mathbf{d}})$.

Proof. The proof follows directly as a consequence of a triangle inequality, Theorem 4.2 and the optimal approximation properties of the interpolation operators. \square

The error estimate provided by Corollary 4.1 predicts a suboptimal $\mathcal{O}(\tau^{\frac{1}{2}})$ accuracy in time and an optimal $\mathcal{O}(h)$ error contribution in space for Algorithm 3 with $r = 0$. It is worth noting that a similar error estimate has been derived in Corollary 3.1 for Algorithm 2 with $r = 0$. This indicates that, at least for the case $r = 0$, the semi-implicit or explicit nature of the splitting does not affect the overall accuracy of the methods. Numerical evidence that this also holds for $r = 1, 2$ is given in the next section.

5 Numerical experiments

In order to illustrate the stability and the accuracy of the proposed schemes, we consider the problem of a pressure-wave propagation within a straight elastic tube (see, e.g., [13]). The solid is modeled as a 1D string model, hence in (2) we have

$$\mathbf{d} = \begin{pmatrix} 0 \\ \eta \end{pmatrix}, \quad \mathbf{L}\mathbf{d} = \begin{pmatrix} 0 \\ -\lambda_1 \partial_{xx} \eta + \lambda_0 \eta \end{pmatrix}, \quad \lambda_1 \stackrel{\text{def}}{=} \frac{E\epsilon}{2(1+\nu)}, \quad \lambda_0 \stackrel{\text{def}}{=} \frac{E\epsilon}{R^2(1-\nu^2)}.$$

In the sequel, all the units are given in the CGS (Centimetre-Gram-Second) system. The fluid domain is given by the rectangle $\Omega = (0, L) \times (0, R)$ and the interface by the segment $\Sigma = [0, L] \times \{R\}$ with $L = 6$ and $R = 0.5$. At $x = 0$ we impose a sinusoidal normal traction of maximal amplitude 2×10^4 during 5×10^{-3} seconds, corresponding to half a period. Zero traction is enforced at $x = 6$ and a symmetry condition is applied on the lower wall $y = 0$. The fluid physical parameters are given by $\rho^f = 1.0$, $\mu = 0.035$. For the solid we have $\rho^s = 1.1$ and $\epsilon = 0.1$ with Young's modulus $E = 0.75 \times 10^6$ and Poisson's ratio $\nu = 0.5$.

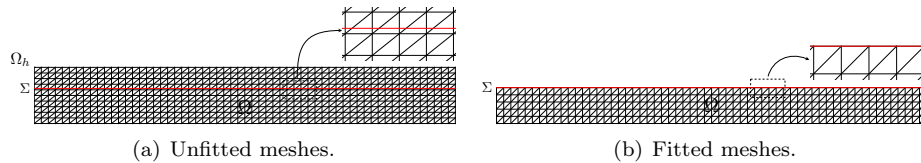


Figure 2: Example of unfitted and fitted mesh configurations.

We compare the results obtained with the unfitted mesh methods given by Algorithms 1–3 and a first-order fully implicit scheme with fitted meshes. An example of the fitted and unfitted mesh configurations considered in this study is given in Figure 2. In the unfitted case, we have $\Omega_h = (0, L) \times (0, R + 0.3)$ so that we are in the framework of Remark 3.2. In Algorithms 1–3, the Nitsche's parameter is set to $\gamma = 10^3$ and the pressure and ghost-penalty stabilization terms in (6) are given by (8) and (11) with $\gamma_p = 10^{-3}$ and $\gamma_g = 1$, respectively. All the computations have been performed with FreeFem++ [35].

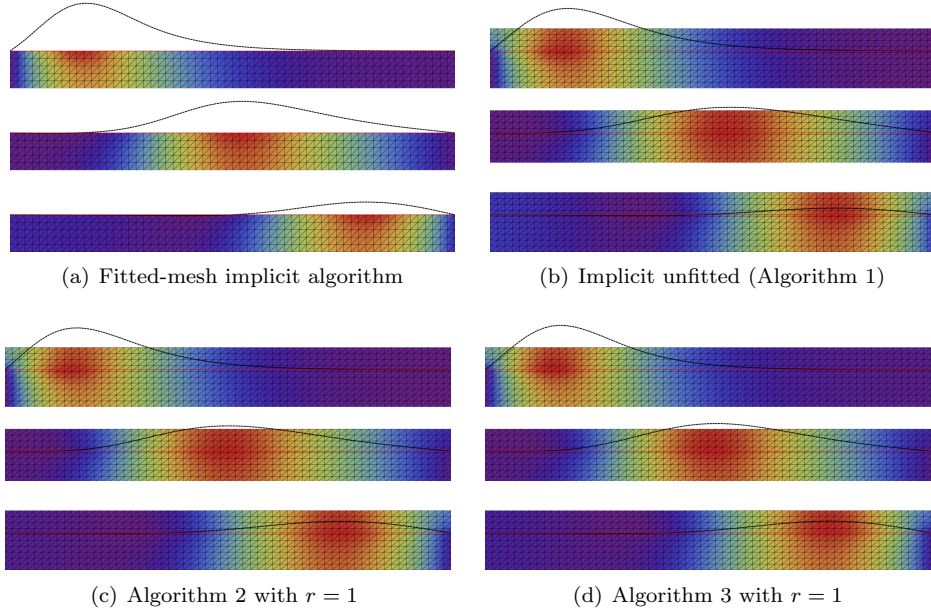


Figure 3: Snapshots of the fluid pressure and (exaggerated) solid displacement at time instants $t = 0.005, 0.01, 0.015$. The discretization parameters are given by $\tau = 2 \cdot 10^{-4}$ and $h = 0.01$

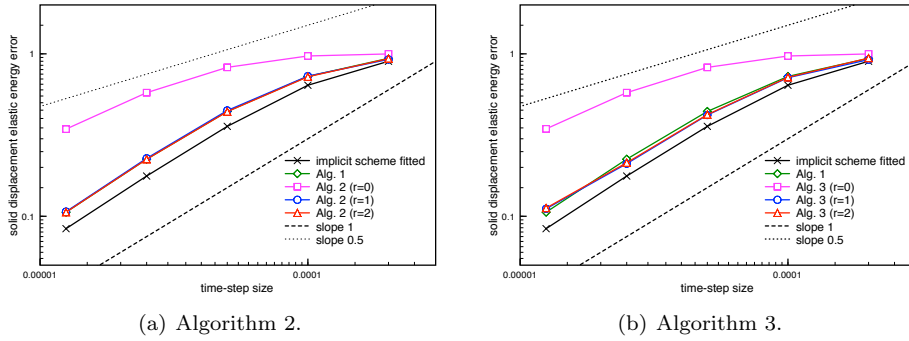


Figure 4: Time convergence history of the solid displacement in the relative elastic energy norm with $\tau = \mathcal{O}(h)$.

Figure 3 presents the snapshots of the pressure field and the solid displacement (amplified by a factor 5) at the time instants $t = 0.005, 0.01$ and 0.015 , obtained with $\tau = 2 \cdot 10^{-4}$ and $h = 0.1$ using the fitted-mesh implicit method (Figure 3(a)), Algorithm 1 (Figure 3(b)), Algorithm 2 with $r = 1$ (Figure 3(c)) and Algorithm 3 with $r = 1$ (Figure 3(d)). The schemes reproduce a stable pressure-wave propagation. Note that this stable behavior was predicted for Algorithms 2 and 1 by Theorem 3.1 and Remark 3.6, respectively.

In order to assess the overall convergence rate of Algorithms 1–3, we have uniformly refined in time and in space according to

$$(\tau, h) = \{2 \cdot 10^{-4}/2^i, 10^{-1}/2^i\}_{i=0}^4. \quad (97)$$

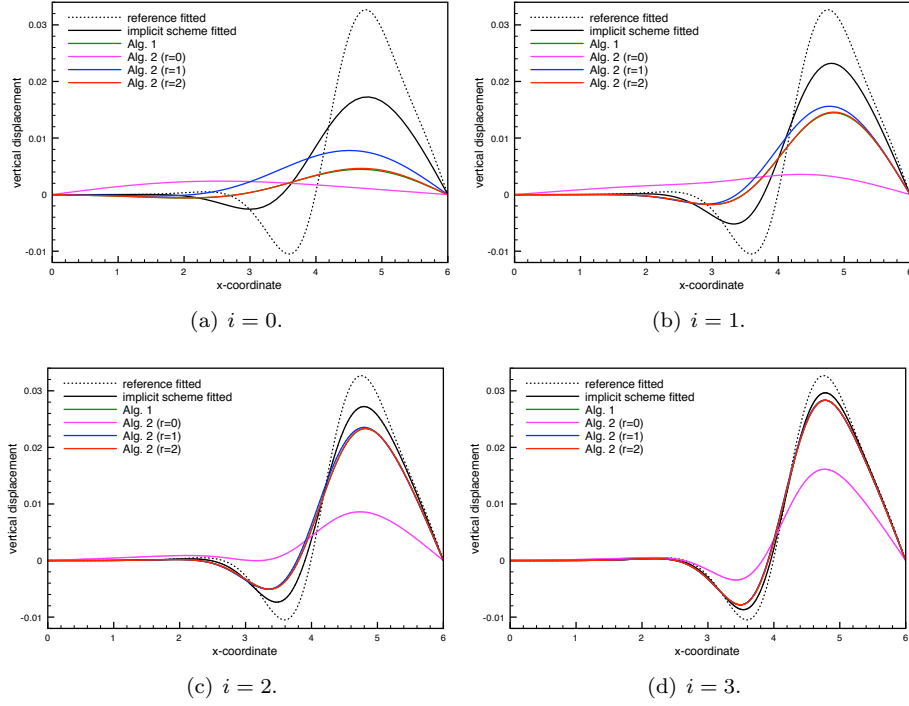


Figure 5: Algorithm 2. Comparison of the solid displacements at $t = 0.015$ for different levels of (τ, h) -refinement (97).

Note that $\tau = \mathcal{O}(h)$. Figure 4 reports the relative elastic energy-norm error of the solid displacement, at time $t = 0.015$, obtained with all the different variants of Algorithm 2 (Alg. 2 in Figure 4(a)) and Algorithm 3 (Alg. 3 in Figure 4(b)). For comparison purposes, the results obtained with both the fitted-mesh and the unfitted-mesh implicit schemes (Algorithm 1) are also included in Figures 4(a) and 4(b). The reference solution has been computed using the fitted-mesh implicit method, with a high space-time resolution: $h = 3.125 \cdot 10^{-3}$ and $\tau = 10^{-6}$.

The results of Figure 4(a) show an overall $\mathcal{O}(\tau)$ optimal accuracy for Algorithm 2 with $r = 1, 2$, while a sub-optimal $\mathcal{O}(\tau^{\frac{1}{2}})$ is obtained with $r = 0$. This is in agreement with the error estimates stated in Corollary 3.1. Very similar results are observed for Algorithm 3 in Figure 4(b): an optimal $\mathcal{O}(\tau)$ convergence is obtained with $r = 1, 2$ and a sub-optimal $\mathcal{O}(\tau^{\frac{1}{2}})$ convergence is retrieved with $r = 0$. We recall that the sub-optimality in Algorithm 3 with $r = 0$ was predicted by Corollary 4.1. The first-order convergence rate $\mathcal{O}(\tau)$ predicted by Corollary 3.2 for Algorithm 1 is also clearly visible.

Further numerical evidence of the above observations is given in Figures 5–6, where we have displayed the displacements at $t = 0.015$ obtained with Algorithms 2 and 3, respectively, for different levels of space-time refinement. For illustration purposes, the displacements obtained with the implicit schemes, both in the fitted and unfitted frameworks, are also shown in both figures.

Finally, Figure 7 compares the results obtained with the first-order extrapolated variants of Algorithms 2 and 3 ($r = 1$) and with the stabilized explicit scheme of [13] (without correction iterations). These results demonstrate that Algorithms 2 and 3 with $r = 1$ overcome the $\mathcal{O}(\tau/h)$ non-uniformity in space of the splitting error induced by the stabilized explicit scheme (which

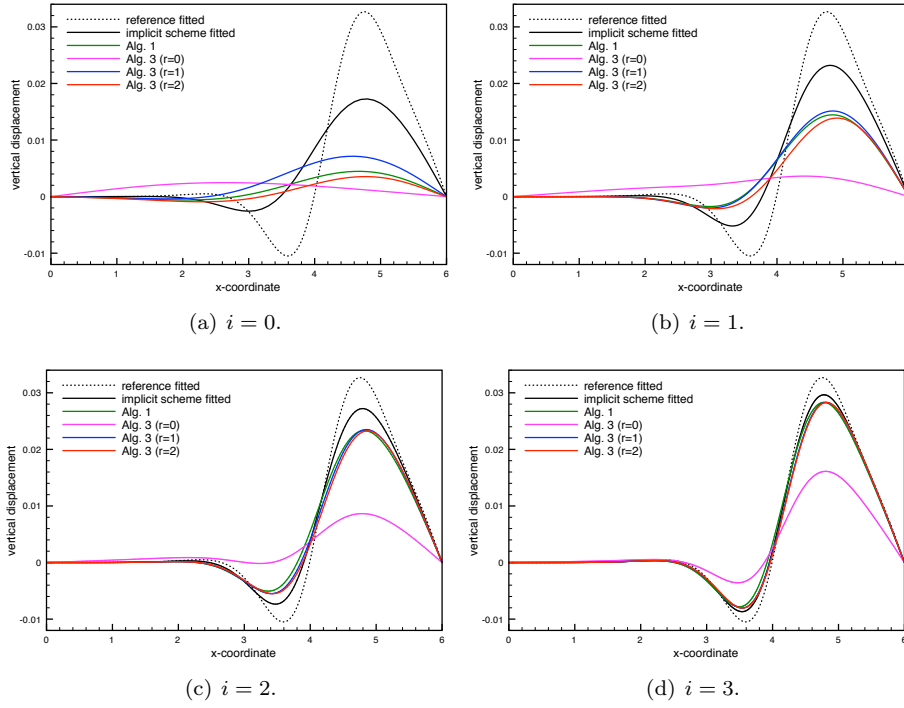


Figure 6: Algorithm 3. Comparison of the solid displacements at $t = 0.015$ for different levels of (τ, h) -refinement (97).

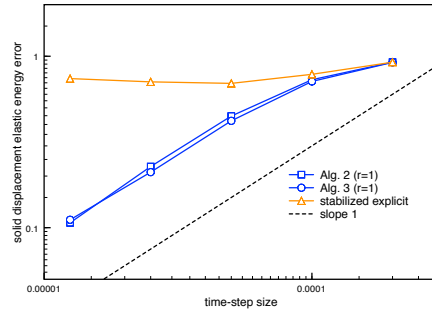


Figure 7: Time convergence history of the solid displacement in the relative elastic energy norm using Algorithm 2 ($r = 1$), Algorithm 3 ($r = 1$) and the stabilized explicit scheme of [13] with $\tau = \mathcal{O}(h)$.

clearly prevents convergence under $\tau = \mathcal{O}(h)$.

6 Conclusion

In this paper, we have introduced two new numerical methods for incompressible fluid/thin-walled structure interaction using unfitted meshes. Their semi-implicit or explicit nature depends

on the order in which the space and time discretizations are performed:

- discretizing first in space using the unfitted formulation (5) and then in time via (14)-(15) led to the semi-implicit schemes reported in Algorithm 2;
- discretizing first in time using (79)-(80) and then in space using a variant of Nitsche's method for Robin boundary conditions led to the explicit schemes reported in Algorithm 3.

For all the semi-implicit schemes ($r = 0, 1, 2$), a complete numerical analysis has been performed in Section 3.3. The analysis retrieves the $\mathcal{O}(\tau + h + \tau^{2^{r-1}})$ convergence rate obtained in [26] for fitted mesh case. These theoretical findings have been confirmed by the numerical evidence of Section 5 which shows, in particular, that the semi-implicit scheme with $r = 1$: (i) delivers superior stability and/or accuracy with respect to explicit methods reported in [7, 13] and (ii) avoids the strong coupling of alternative methods (see, e.g., [47, 8]), without compromising stability and accuracy.

For the explicit scheme with $r = 0$, the stability and convergence results (Section 4.3) are similar to those obtained for the same variant of the semi-implicit scheme. We retrieve, in particular, the same $\mathcal{O}(h + \tau^{\frac{1}{2}})$ sub-optimal convergence rate. The analysis of the explicit schemes with $r = 1, 2$ is open. Yet, the numerical evidence of Section 5 suggests that, in spite of their different semi-implicit and explicit nature, Algorithms 2 and 3 deliver practically the same behavior.

Acknowledgement

Work funded by the french National Research Agency (ANR) through the EXIFSI project (ANR-12-JS01-0004).

References

- [1] F. Alauzet, B. Fabrèges, and M. Fernández, M.A. and Landajuela. Nitsche-XFEM for the coupling of an incompressible fluid with immersed thin-walled structures. *Comput. Methods Appl. Mech. Engrg.*, 301:300–335, 2016.
- [2] M. Astorino, J.-F. Gerbeau, O. Pantz, and K.-F. Traoré. Fluid-structure interaction and multi-body contact: Application to aortic valves. *Comput. Methods Appl. Mech. Engrg.*, 198(45-46):3603–3612, 2009.
- [3] M. Astorino and C. Grandmont. Convergence analysis of a projection semi-implicit coupling scheme for fluid-structure interaction problems. *Numer. Math.*, 116:721–767, 2010.
- [4] S. Badia, A. Quaini, and A. Quarteroni. Splitting methods based on algebraic factorization for fluid-structure interaction. *SIAM J. Sci. Comput.*, 30(4):1778–1805, 2008.
- [5] J.W. Banks, W.D. Henshaw, and D.W. Schwendeman. An analysis of a new stable partitioned algorithm for FSI problems. Part II: Incompressible flow and structural shells. *J. Comput. Phys.*, 268:399–416, 2014.
- [6] R. Becker, E. Burman, and P. Hansbo. A Nitsche extended finite element method for incompressible elasticity with discontinuous modulus of elasticity. *Comput. Methods Appl. Mech. Engrg.*, 198(41-44):3352–3360, 2009.

- [7] D. Boffi, N. Cavallini, and L. Gastaldi. Finite element approach to immersed boundary method with different fluid and solid densities. *Math. Models Methods Appl. Sci.*, 21(12):2523–2550, 2011.
- [8] D. Boffi, N. Cavallini, and L. Gastaldi. The finite element immersed boundary method with distributed Lagrange multiplier. *SIAM J. Numer. Anal.*, 53(6):2584–2604, 2015.
- [9] D. Boffi and L. Gastaldi. A fictitious domain approach with distributed Lagrange multiplier for fluid-structure interactions. <http://arxiv.org/abs/1510.06856v1>, 2015.
- [10] F. Brezzi and J. Pitkäranta. On the stabilization of finite element approximations of the Stokes equations. In *Efficient solutions of elliptic systems (Kiel, 1984)*, volume 10 of *Notes Numer. Fluid Mech.*, pages 11–19. Vieweg, 1984.
- [11] M. Bukac, C. Canic, R. Glowinski, T. Tambaca, and A. Quaini. Fluid-structure interaction in blood flow capturing non-zero longitudinal structure displacement. *J. Comp. Phys.*, 235(0):515–541, 2013.
- [12] E. Burman and M.A. Fernández. Stabilization of explicit coupling in fluid-structure interaction involving fluid incompressibility. *Comput. Methods Appl. Mech. Engrg.*, 198(5-8):766–784, 2009.
- [13] E. Burman and M.A. Fernández. An unfitted Nitsche method for incompressible fluid-structure interaction using overlapping meshes. *Comput. Methods Appl. Mech. Engrg.*, 279:497–514, 2014.
- [14] E. Burman and P. Hansbo. Fictitious domain finite element methods using cut elements: II. A stabilized Nitsche method. *Applied Numerical Mathematics*, 62(4):328–341, 2012.
- [15] A. Caiazzo, M.A. Fernández, J.-F. Gerbeau, and V. Martin. Projection schemes for fluid flows through a porous interface. *SIAM J. Sci. Comput.*, 33(2):541–564, 2011.
- [16] P. Causin, J.-F. Gerbeau, and F. Nobile. Added-mass effect in the design of partitioned algorithms for fluid-structure problems. *Comput. Methods Appl. Mech. Engrg.*, 194(42–44):4506–4527, 2005.
- [17] D. Chapelle and K.J. Bathe. *The Finite Element Analysis of Shells - Fundamentals*. Springer, 2011.
- [18] N. Diniz dos Santos, J.-F. Gerbeau, and J.-F. Bourgat. A partitioned fluid-structure algorithm for elastic thin valves with contact. *Comput. Methods Appl. Mech. Engrg.*, 197(19–20):1750–1761, 2008.
- [19] Q. Du, M. D. Gunzburger, L. S. Hou, and J. Lee. Analysis of a linear fluid-structure interaction problem. *Discrete Contin. Dyn. Syst.*, 9(3):633–650, 2003.
- [20] Q. Du, M. D. Gunzburger, L. S. Hou, and J. Lee. Semidiscrete finite element approximations of a linear fluid-structure interaction problem. *SIAM J. Numer. Anal.*, 42(1):1–29 (electronic), 2004.
- [21] A. Ern and J.-L. Guermond. *Theory and practice of finite elements*. Springer, 2004.
- [22] M. Eswaran, U.K. Saha, and D. Maity. Effect of baffles on a partially filled cubic tank: Numerical simulation and experimental validation. *Computers & Structures*, 87(3–4):198–205, 2009.

- [23] L.C. Evans. *Partial Differential Equations*. Graduate studies in mathematics. American Mathematical Society, 2010.
- [24] J. Fernández, M.A. and Mullaert. Convergence and error analysis for a class of splitting schemes in incompressible fluid-structure interaction. *IMA J. Numer. Anal.*, 2015. DOI: 10.1093/imanum/drv055.
- [25] J. Fernández, M.A. and Mullaert and M. Vidrascu. Generalized Robin-Neumann explicit coupling schemes for incompressible fluid-structure interaction: stability analysis and numerics. *Internat. J. Numer. Methods Engrg.*, 101(3):199–229, 2015.
- [26] M.A. Fernández. Incremental displacement-correction schemes for incompressible fluid-structure interaction: stability and convergence analysis. *Numer. Math.*, 123(1):21–65, 2013.
- [27] M.A. Fernández, J.F. Gerbeau, and C. Grandmont. A projection semi-implicit scheme for the coupling of an elastic structure with an incompressible fluid. *Int. J. Num. Meth. Engrg.*, 69(4):794–821, 2007.
- [28] M.A. Fernández and M. Landajuela. Splitting schemes for incompressible fluid/thin-walled structure interaction with unfitted meshes. *Comptes Rendus Mathematique*, 353(7):647–652, 2015.
- [29] M.A. Fernández, M. Landajuela, and M. Vidrascu. Fully decoupled time-marching schemes for incompressible fluid/thin-walled structure interaction. *Journal of Computational Physics*, 297:156–181, 2015.
- [30] M.A. Fernández, J. Mullaert, and M. Vidrascu. Explicit Robin-Neumann schemes for the coupling of incompressible fluids with thin-walled structures. *Comput. Methods Appl. Mech. Engrg.*, 267:566–593, 2013.
- [31] C. Förster, W.A. Wall, and E. Ramm. Artificial added mass instabilities in sequential staggered coupling of nonlinear structures and incompressible viscous flows. *Comput. Methods Appl. Mech. Engrg.*, 196(7):1278–1293, 2007.
- [32] A. Gerstenberger and W.A. Wall. An extended finite element method/Lagrange multiplier based approach for fluid-structure interaction. *Comput. Methods Appl. Mech. Engrg.*, 197(19-20):1699–1714, 2008.
- [33] G. Guidoboni, R. Glowinski, N. Cavallini, and S. Canic. Stable loosely-coupled-type algorithm for fluid-structure interaction in blood flow. *J. Comp. Phys.*, 228(18):6916–6937, 2009.
- [34] A. Hansbo and P. Hansbo. An unfitted finite element method, based on nitsche’s method, for elliptic interface problems. *Computer Methods in Applied Mechanics and Engineering*, 191(47–48):5537 – 5552, 2002.
- [35] F. Hecht. New development in FreeFem++. *J. Numer. Math.*, 20(3-4):251–265, 2012.
- [36] M. Heil and A.L. Hazel. Fluid-structure interaction in internal physiological flows. In *Annual review of fluid mechanics. Volume 43, 2011*, volume 43 of *Annu. Rev. Fluid Mech.*, pages 141–162. Annual Reviews, 2011.
- [37] J.G. Heywood and R. Rannacher. Finite-element approximation of the nonstationary Navier-Stokes problem. IV. Error analysis for second-order time discretization. *SIAM J. Numer. Anal.*, 27(2):353–384, 1990.

- [38] M. Juntunen and R. Stenberg. Nitsche's method for general boundary conditions. *Math. Comp.*, 78(267):1353–1374, 2009.
- [39] D. Kamensky, M.-C. Hsu, D. Schillinger, J.A. Evans, A. Aggarwal, Y. Bazilevs, M.S. Sacks, and T.J.R. Hughes. An immersogeometric variational framework for fluid–structure interaction: Application to bioprosthetic heart valves. *Comput. Methods Appl. Mech. Engrg.*, 284:1005–1053, 2015.
- [40] M. Landajuela, M. Vidrascu, D. Chapelle, and M.A. Fernández. Coupling schemes for the FSI forward prediction challenge: comparative study and validation. Research Report RR-8824, Inria, 2015. <https://hal.inria.fr/hal-01239931>.
- [41] P. Le Tallec and S. Mani. Numerical analysis of a linearised fluid-structure interaction problem. *Numer. Math.*, 87(2):317–354, 2000.
- [42] P. Le Tallec and J. Mouro. Fluid structure interaction with large structural displacements. *Comput. Meth. Appl. Mech. Engrg.*, 190:3039–3067, 2001.
- [43] A. Legay, J. Chessa, and T. Belytschko. An Eulerian-Lagrangian method for fluid-structure interaction based on level sets. *Comput. Methods Appl. Mech. Engrg.*, 195(17-18):2070–2087, 2006.
- [44] M. Lombardi, N. Parolini, A. Quarteroni, and G. Rozza. Numerical simulation of sailing boats: Dynamics, FSI, and shape optimization. In G. Buttazzo and A. Frediani, editors, *Variational Analysis and Aerospace Engineering: Mathematical Challenges for Aerospace Design*, Springer Optimization and Its Applications, pages 339–377. Springer, 2012.
- [45] M. Lukacova-Medvid'ovaa, G. Rusnakovaa, and A. Hundertmark-Zauskovaa. Kinematic splitting algorithm for fluid-structure interaction in hemodynamics. *Comput. Methods Appl. Mech. Engrg.*, 265(1):83–106, 2013.
- [46] A. Massing, M. G. Larson, and A. Logg. Efficient implementation of finite element methods on nonmatching and overlapping meshes in three dimensions. *SIAM Journal on Scientific Computing*, 35(1):C23–C47, 2013.
- [47] E.P. Newren, A.L. Fogelson, R.D. Guy, and R.M. Kirby. Unconditionally stable discretizations of the immersed boundary equations. *J. Comput. Phys.*, 222(2):702–719, 2007.
- [48] M.P. Paidoussis, S.J. Price, and E. de Langre. *Fluid-structure interactions: cross-flow-induced instabilities*. Cambridge University Press, 2011.
- [49] C.S. Peskin. The immersed boundary method. *Acta Numer.*, 11:479–517, 2002.
- [50] C. Pozrikidis. *Computational hydrodynamics of capsules and biological cells*. Chapman & Hall/CRC Mathematical and Computational Biology. CRC Press, 2010.
- [51] A. Quaini and A. Quarteroni. A semi-implicit approach for fluid-structure interaction based on an algebraic fractional step method. *Math. Models Methods Appl. Sci.*, 17(6):957–983, 2007.
- [52] T. Sawada and A. Tezuka. LLM and X-FEM based interface modeling of fluid-thin structure interactions on a non-interface-fitted mesh. *Comput. Mech.*, 48(3):319–332, 2011.
- [53] K. Takizawa and T.E. Tezduyar. Computational methods for parachute fluid-structure interactions. *Arch. Comput. Methods Eng.*, 19:125–169, 2012.

- [54] E.H. van Brummelen. Added mass effects of compressible and incompressible flows in fluid-structure interaction. *J. Appl. Mech.*, 76(2):021206–7, 2009.
- [55] A. Zilian and A. Legay. The enriched space-time finite element method (EST) for simultaneous solution of fluid-structure interaction. *Internat. J. Numer. Methods Engrg.*, 75(3):305–334, 2008.

Contents

1	Introduction	3
2	Linear model problem	4
3	First discretize in space and then in time: semi-implicit schemes	5
3.1	Unfitted mesh spatial semi-discretization	5
3.1.1	The stabilization operator S_h	6
3.2	Fully discrete formulation: semi-implicit coupling scheme with unfitted meshes	7
3.2.1	Kinematic perturbation of implicit coupling.	10
3.3	Stability and convergence analysis	10
3.3.1	Stability analysis	12
3.3.2	Convergence analysis	14
4	First discretize in time and then in space: explicit schemes	25
4.1	Robin-Neumann explicit coupling schemes	25
4.2	Fully discrete formulation: explicit coupling scheme with unfitted meshes	26
4.3	Stability and convergence analysis for $r = 0$	27
4.3.1	Stability analysis	28
4.3.2	Convergence analysis	30
5	Numerical experiments	36
6	Conclusion	39



**RESEARCH CENTRE
PARIS – ROCQUENCOURT**

Domaine de Voluceau, - Rocquencourt
B.P. 105 - 78153 Le Chesnay Cedex

Publisher
Inria
Domaine de Voluceau - Rocquencourt
BP 105 - 78153 Le Chesnay Cedex
inria.fr

ISSN 0249-6399